ABSTRACT

STUDY OF Si/SiO_2 INTERFACE PASSIVATION AND SiO_2 RELIABILITY ON DEUTERIUM IMPLANTED SILICON

by
Tias Kundu

One of the major defects that contribute to the interface states in the silicon band gap is the dangling bond, which degrades performance of MOS devices. Passivation of these bonds with hydrogen had been found to diminish their effect but the improvement degrades the operation due to hot electron effect. Passivation with deuterium annealing has proven to improve the lifetime of the metal oxide semiconductor devices but this technique is not very effective for a multi-level metal-dielectric structure. This work investigates and optimizes incorporation of deuterium by ion implantation into the silicon substrate before the growth of 6.5 nm thin oxides. Different implantation conditions were used for optimization of passivation in the silicon dangling bonds effectively. The interface states density and reliability of deuterium-implanted capacitors was investigated by extensive electrical characterization. Deuterium and hydrogen implanted capacitors showed identical interface passivation effect. Secondary Ion Mass Spectroscopy (SIMS) study supported the electrically measured data and showed the presence of deuterium both at the interface and in the oxide. The optimum passivation was obtained for deuterium implantation at 20keV with dose of $1x10^{14}$atoms/cm^2. For higher dose of implantation, $1x10^{15}$/cm^2, the reduced passivation and oxide quality has been observed and attributed to implantation induced damage not being completely annealed during oxidation.

Deuterium distribution in silicon/silicon oxide systems was further investigated by subjecting the MOS capacitors to annealing conditions at 600°C and 700°C. Interface quality and oxide reliability degraded in annealed devices with lower dose of implantation, $1x10^{14}/cm^2$ while improved for higher dose of implantation at $1x10^{15}/cm^2$. The out diffusion of deuterium ions during annealing governed the interface and oxide degradation for lower dose. The improvement in case of higher dose is due to the partial recovery of the damage, which is not completely removed during oxidation. Also, diffusion of deuterium during annealing from damage sites lead to the incorporation of deuterium ions at the interface and in the oxide.

For comparison, hydrogen implantation was carried out at similar conditions. Hydrogen-implanted devices exhibited more charge trapping (increased Stress Induced Leakage Current and Flat Band voltage shift), larger generation of interface states, and a smaller charge to breakdown under electrical stress, compared to the deuterium devices confirming the isotope effect.

STUDY OF Si/SiO_2 INTERFACE PASSIVATION AND SiO_2 RELIABILITY ON DEUTERIUM IMPLANTED SILICON

by
Tias Kundu

A Dissertation
Submitted to the Faculty of
New Jersey Institute of Technology
in Partial Fulfillment of the Requirements for the Degree of
Doctor of Philosophy in Electrical Engineering

Department of Electrical and Computer Engineering

August 2005

APPROVAL PAGE

STUDY OF Si/SiO_2 INTERFACE PASSIVATION AND SiO_2 RELIABILITY ON DEUTERIUM IMPLANTED SILICON

Tias Kundu

Dr. Durgamadhab Misra, Dissertation Advisor — Date
Professor of Electrical and Computer Engineering, NJIT

Dr. Marek Sosnowski, Committee Member — Date
Professor of Electrical and Computer Engineering, NJIT

Dr. Leonid Tsybeskov, Committee Member — Date
Associate Professor of Electrical and Computer Engineering, NJIT

Dr. Roland Levy, Committee Member — Date
Distinguished Professor of Physics, NJIT

Dr. Anthony Fiory, Committee Member — Date
Research Professor of Physics, NJIT

BIOGRAPHICAL SKETCH

Author: Tias Kundu

Degree: Doctor of Philosophy

Date: August 2005

Undergraduate and Graduate Education:

- Doctor of Philosophy in Electrical Engineering,
  New Jersey Institute of Technology, Newark, NJ, 2005

- Master of Science in Electronics,
  University of Hyderabad, Hyderabad, India, 2000

- Bachelor of Science in Maths, Physics and Computers,
  Osmania University, Hyderabad, India, 1998

Major: Electrical Engineering

Presentations and Publications:

T. Kundu and D. Misra,
"Si-SiO_2 Passivation using Deuterium and Hydrogen Implantation"
Electrochemical and Solid-State Letters,
vol. 8, No.2, pp. G35-G37, 2005.

T. Kundu and D. Misra,
"Electron Transit Model in Photodetectors for High Speed Imaging"
Semiconductor Science and Technology,
(Submitted).

T. Kundu and D. Misra,
"Enhanced SiO_2 Reliability of Deuterium Implanted Si"
IEEE Transactions on Device and Materials Reliability,
(Submitted).

T. Kundu and D. Misra,
"Annealing Effect on the Distribution of Deuterium on Deuterium-Implanted Silicon"
Journal of Applied Physics,
(In Preparation).

T. Kundu and D. Misra,

"A Model for Implanted Deuterium Diffusion and its Effect on the Si/SiO_2 Interface Passivation"
Physical Review Letters,
(In Preparation).

T. Kundu and D. Misra,

"Annealing Effect on Reliability Study for Deuterium Implanted Silicon,"
Proceedings of the Fifth International Symposium on the Physics and Chemistry of SiO_2 and the $Si-SiO_2$ interface, 208^{th} meeting of Electrochemical Society meeting, Los Angeles, California, October 2005.

T. Kundu and D. Misra,

"Electrical Techniques for the Characterization of Dielectric Films,"
Interface of the 208^{th} meeting of Electrochemical Society, vol. 14, pp. 9-10, Los Angeles, California, October 2005.

T. Kundu and D. Misra,

"Hydrogen/Deuterium Implantation for Si-Dielectric interface in Nanoscale devices"
Proceedings of International Symposium on 206^{th} meeting of Electrochemical Society, Honolulu, Hawaii,
vol. PV. 2004-04, pp. 346-355, October 2004.

T. Kundu and D. Misra,

"Interface Passivation by deuterium for Nanoscale Devices"
Proceedings of 7^{th} International Conference on Solid-State and IC Technology, Beijing, China,
vol. II, pp. 792-797, November 2004.

T. Kundu and D. Misra,

"Interface Passivation by Hydrogen and Deuterium Implantation,"
Proceedings of 204^{th} meeting of Electrochemical Society, Orlando, Florida,
Abstract. 643, October 2003.

T. Kundu, R.K. Jarwal and D. Misra,

"Enhanced Electron Transit Time in Pinned-Buried Photo Detector"
Proceedings of 1st International Symposium on Integrated OptoElectronics of Electrochemical Society, Philadelphia,
vol. PV 2002-4, pp. 253-259, May 2002.

Dedicated To My Mom and Dad

ACKNOWLEDGMENT

I would like to express my sincere gratitude to Dr. Durgamadhab Misra for agreeing to be my dissertation advisor. I am thankful to him for his constant support, encouragement, and reassurance during the entire course of my graduate study. I also express my sincere thanks to Dr. Marek Sosnowski, Dr. Leonid Tsybeskov, Dr. Roland Levy and Dr. Anthony Fiory for actively participating in my dissertation committee.

I would like to acknowledge the financial support from National Science Foundation, grant ECS-0140584.

I would like to thank my sister, Tania Kundu, for her constant words of encouragement during the course of my graduate study. I would also like to thank my husband, Sanjeeb Pal, for his patience and encouragement.

Finally, I thank my parents for their encouragement and support through out my graduate study, giving me the strength to finish this dissertation.

TABLE OF CONTENTS

TABLE OF CONTENTS
(Continued)

Chapter **Page**

TABLE OF CONTENTS
(Continued)

Chapter **Page**

TABLE OF CONTENTS
(Continued)

LIST OF TABLES

LIST OF FIGURES

LIST OF FIGURES
(Continued)

Figure **Page**

LIST OF FIGURES
(Continued)

Figure **Page**

LIST OF FIGURES
(Continued)

Figure **Page**

LIST OF FIGURES
(Continued)

Figure **Page**

LIST OF FIGURES
(Continued)

Figure **Page**

CHAPTER 1

INTRODUCTION MOTIVATION AND OBJECTIVE

1.1 Introduction

1.1.1 Si – SiO_2 Interface and Dangling Bonds

The Si-SiO_2 structure is the basic component in the metal oxide semiconductor Field Effect Transistors (MOSFET). The Si-SiO_2 interface has been most widely studied, but reliability of the interface still remains a major concern today. With the trend to even smaller devices with thin gate oxides (<7nm region) in VLSI technology, it faces an ever-growing relative importance of the nanoscale Si-SiO_2 regions.

One of the major areas of vulnerability of MOS devices results from the interface region. The device performance is strongly degraded by defect generation as a result of electrical stressing of thin oxides and Si-SiO_2 interface regions during device operation [1]. The defects at the interface lead to electrical interface states (D_{it}) in the silicon band gap, which behave as trapping sites and recombination centers. These defects are responsible for the high mean value and variation of the threshold voltage and reduced channel mobility. High levels of interface trap density are unacceptable for complementary MOS (CMOS) circuit operation and stability. This has evoked an intense research in to the structural identification of these defects ever since the incorporation of the Si- SiO_2 entity as a major constituent of successful devices [2, 3, 4, 5]. Information on the nature of a defect is important, as they lead to ultimate failure of the chip. The most useful information about the structure of defects in Si-SiO_2 has come from the analysis [3, 4] supplied by the electron spin resonance (ESR). The ESR active defects are referred to as P_b centers [5-11]. These dangling bonds were analyzed using capacitance-

voltage (C-V) as well as electron spin resonance (ESR) techniques [12, 13]. There are two species of P_b defects. The first, P_{b0} center, which is triply, bonded silicon with the dangling orbital protruding in to the oxide along two tetrahedral Si bond directions denoted as $\cdot Si \equiv Si_3$. The second (100) defect specie is P_{b1}, which has geometry similar to P_{b0} but is chemically and paramagnetically different. P_{b1} is partially oxidized center $\cdot Si \equiv Si_2O$. These defects give rise to interface states in the Si band gap [3, 9]. P_{b0} has its ($0 \rightarrow 1$) electron transition approximately at 0.3 eV and ($1 \rightarrow 2$) transition at 0.85eV above the valance band edge, while P_{b1} has its ($0 \rightarrow 1$) electron transition approximately at 0.45 eV and ($1 \rightarrow 2$) transition at 0.8eV above the valance band edge. The structure of P_{b1} is still unknown and is under investigation.

1.1.2 Passivation of Dangling Bonds

Silicon-dangling bonds at the Si-SiO_2 interface are electrically active and lead to the reduction of channel conductance and also result in deviations from the ideal capacitance-voltage (C-V) characteristics. The high mean value and variation of the threshold voltage and reduced channel mobility is a clear indication of the unacceptable levels of interface trap density for CMOS circuit operation and stability. Since the dangling bonds at the interface of the Si-SiO_2 give rise to states in the Si band gap and also contribute to the ultimate breakdown of the oxide, reduction of these states would lead to improvement in the Si-SiO_2 interface and also the extension of ultimate life time of the oxide.

1.1.2.1 Reduced Interface Trap Density by H_2 Passivation. It has been found that hydrogen contributes to the passivation of the dangling bond orbital [8, 14]. Intense research had been carried out and the passivation effect of the hydrogen at the interface of Si-SiO_2. Hydrogen is introduced during several device-processing steps, for example,

during the annealing of the wafers at elevated temperature in hydrogen ambient [15]. Low-temperature post metal anneals (350-450°C) in forming gas (10% H_2) have been successfully used in MOS fabrication technologies to passivate silicon dangling bonds and consequently, to reduce Si/SiO_2 interface trap charge density [16]. Electron spin resonance (ESR) measurements [7] performed in conjunction with deep-level transient spectroscopy (DLTS) and C-V measurements have elucidated the role of hydrogen in this passivation process [8,14] which is described as $P_b + H_2 \rightarrow Pb_H + H$, where P_bH is the passivated dangling bond.

The importance of hydrogen in the electrical degradation process for the Si/SiO_2 system was demonstrated by Nicollian *et al.* [17] by using a series of experiments performed on MOS capacitors. Nicollian *et al.* showed that there was a one-to-one correspondence between the hydrogen lost (*i.e.*, reduced activity) and negative charge produced in a hydrated SiO_2 layer in the presence of electron currents. The n-MOSFET threshold voltage and transconductance distributions on a wafer annealed in forming gas (10% H_2) showed significant improvement compared with an untreated wafer. These measurements indicated that for the oxides grown on Si (111) the density of the interface trap states in the middle of the forbidden gap decreases from 10^{11}-10^{12} cm^{-2} eV^{-1} to about 10^{10} cm^{-2} eV^{-1}after post metal anneal process step. The Si (100) material system, which is technologically more significant, exhibits the same qualitative behavior.

1.1.2.2 Hot Electron Effect. In a MOS transistor when electron travels from the source to the drain along the channel, it gains kinetic energy at the expense of electrostatic potential energy in the pinch-off region, and becomes a "hot" electron. Some of these injected hot electrons can go through the gate oxide and be collected as gate current

thereby reducing the input impedance. Some of these electrons can be trapped in the gate oxide as fixed oxide charges. This increases the flatband voltage and therefore the threshold voltage. These energetic hot carriers can also break Si-H bonds that exist at the Si-SiO_2 interface, creating fast interface states that degrade MOSFET parameters such as transconductance and the subthreshold slope. The result of hot carrier degradation is an increase of threshold voltage and decrease of transconductance of MOS transistor.

It has been suggested that the generation of the interface trap states is due to hot carrier stimulated hydrogen desorption and depassivation of the silicon dangling bonds [18]. The existence of degradation, at low voltages, indicates multiple vibrational excitation mechanism of H desorption at the Si/SiO_2 interface and a dependence of desorption mechanism on both voltage (electric field) and current density.

Hot carrier reliability concerns are further exacerbated by ongoing scaling efforts and complexity in device processing. The time-dependent degradation of metal oxide semiconductor transistor performance resulting from hot (energetic) electron effects has been an area of considerable study over the past 25 years. According to the established theory, this aging process is thought to occur in part as the result of hot electrons stimulating desorption of hydrogen from the Si-SiO_2 interface region [19,20].

1.1.2.3 Replacement of Hydrogen by Deuterium. By passivating defects at the silicon/silicon dioxide interface with deuterium instead of hydrogen, Lyding *et al.* [16-23] found the hot-electron degradation of metal–oxide–semiconductor (MOS) transistors was spectacularly reduced by factors of 10–50. The giant isotope effect implied that deuterium (D) depassivation is substantially slower than hydrogen (H) depassivation. The idea of using deuterium instead of hydrogen was inspired by experiments in which a

scanning tunneling microscope was used to stimulate the desorption of hydrogen from Si (100) surfaces under ultrahigh vacuum (UHV) conditions [22-24]. From these experiments it was discovered that it is much more difficult to remove deuterium than to desorb hydrogen. The activation energies for desorption of hydrogen and deuterium are 1.94eV and 2.5eV, respectively. The D desorption yield was 50 times lower than that of H from scanning tunneling microscope (STM) measurements [24-27]. Since the chemistry of deuterium and hydrogen is virtually identical, either atom is equally suitable for passivating the dangling bonds at interfaces. Hot electrons, or nonradiative electron–hole recombination following illumination, can excite a Si–H bond to a highly excited vibrational state [28]. If the highly excited Si–H oscillation can be sustained, the H can be emitted over the barrier to a mobile transport state, leaving behind a silicon-dangling bond. Deuterium bonds are more difficult to break compared to the hydrogen due to the heavier isotope effect [22, 23].

1.2 Motivation

The effects of passivation with deuterium in thin SiO_2 films [20] and in CMOS devices [29] were studied in the past. Even though there was noticeable improvement observed in hot carrier lifetime, the devices were unstable and returned to initial unpassivated condition when the samples are subjected to further processing [30]. Also, when CMOS technologies incorporate multiple metal and dielectric layers, the improvement due to deuterium diffusion was reduced further [31]. In addition, undoped polycrystalline silicon [32] and SiN, used as a sidewall spacer, limit the transport of deuterium to the Si–SiO_2 interface during annealing by serving as a diffusion barrier for deuterium [33]. In

some processes, these limitations were overcome by extended time and increased temperature anneals at higher deuterium concentration [34] but these anneals had detrimental effects on the long-term device performance requiring exploration of possible alternative methods for deuterium incorporation at the Si–SiO_2 interface.

To overcome these problems, this research investigates ion implantation before the growth of gate oxides as an alternate technique for incorporation of deuterium to obtain effective passivation of the interface states. This approach may also streamline process integration and reduce cycle time.

1.3 Objective

The objective of this work is to investigate the incorporation of deuterium ions at the semiconductor-oxide interface in MOS device using the technique of ion implantation before the growth of the gate oxide. Ion implantation of deuterium in bare silicon and silicon oxide systems has been studied by Park and Helms [37]. In the same study while evaluating the effect of annealing on the distribution of deuterium, it was shown that the release of deuterium from bare silicon is possible at 600 °C whereas deuterium could diffuse out completely from Si–SiO_2 system at 900 °C. It is therefore, important to investigate oxide/interface quality when the oxide was grown on deuterium-implanted silicon substrate. Selection of the appropriate ion implantation conditions is critical. If not selected appropriately, implantation can cause irreparable substrate damage and thereby deteriorate device performance. Electrical characterization of MOS devices on deuterium implanted Si substrate has been carried out by earlier work [38]. The purpose of this study is to (i) optimize the implantation conditions to effectively passivate the Si-

SiO_2 interface with minimum damage; (ii) to investigate the effect of diffusion of the implanted ions at high processing temperatures and their corresponding effect at the interface and (iii) to compare the reliability of SiO_2 on deuterium and hydrogen implanted silicon substrates. The additional objective is to confirm the isotope effect i.e. the difference between the effect of hydrogen and deuterium implantation.

To realize these objectives wares of (100) Si were implanted with Deuterium and hydrogen ions at energies of implantation 15keV, 20keV, 25keV, 30keV, 35keV with doses $1x10^{13}/cm^2$, $1x10^{14}/cm^2$, $1x10^{15}/cm^2$. Ion implantation in to the Si substrate has been simulated using Stopping Range of Ions in Matter (SRIM). The physical characterization to detect the presence and retention of deuterium has been conducted using the Secondary Ion Mass Spectroscopy (SIMS).

The electrical characterization techniques involved the high frequency (HF) CV measurements and the quasistatic C-V techniques in order to evaluate the density of the interface states. In order to evaluate the device characteristics under stress conditions the devices were exposed to voltage stress and the interface state and the SILC measurements have been conducted to study the effect of stress. The TDDB (Time Dependent Dielectric Breakdown) measurements were conducted and the break down characteristics of the implanted samples at various conditions has also been investigated.

1.4 Dissertation Organization

Chapter 2 discusses the overview of the present status of the techniques involved in deuterium passivation. Techniques described in this chapter for deuterium incorporation involves the discussion of deuterium annealing, growth of gate oxide in presence of D_2O

atmosphere, annealing in ND_3 atmosphere, deuterium pyrogenic oxidation and deuterated poly-Si deposition, deuterium prebake and post oxidation anneal and hydrogen implantation.

The steps involved in the fabrication of MOS capacitors are outlined in Chapter 3. Also described in this chapter is the setup of electrical characterization, conducted to test the interface passivation and reliability of the fabricated deuterium and hydrogen implanted MOS devices.

Chapter 4 discusses the simulation results carried out using Stopping Range of Ions in Matter (SRIM) to obtain an initial estimate of the implantation depth and damage distribution within the Si substrate for various cases of deuterium and hydrogen implantation. The physical characterization technique conducted using Secondary Ion Mass Spectroscopy (SIMS) to detect the presence and retention of deuterium is also described in this chapter.

Passivation of the dangling bonds at the $Si\text{-}SiO_2$ interface can be evaluated by estimating interface state density, D_{it}. Chapter 5 discusses the experimental results and the derived interface state density from high frequency-low frequency (HF-LF) C-V method for all conditions of deuterium and hydrogen implantation. This chapter also describes the estimate of the deuterium diffusivity obtained in the silicon substrate during oxidation both from the electrical and physical characterization results. Also described in this chapter is the effect of interface state density on further annealing of the samples at higher temperatures in nitrogen atmosphere.

Chapter 6 discusses the reliability study conducted for the MOS devices with deuterium implantation. Also discussed in this chapter is the detailed analysis of the

isotope effect. Leakage current measurements and reliability study of the annealed samples has also been discussed in this chapter.

Chapter 7 describes the conclusions of this research. Also described in this chapter are the proposed suggestions for future work.

CHAPTER 2

DEUTERIUM PASSIVATION: CURRENT STATUS

2.1 Deuterium Annealing

Hydrogen is known to passivate the silicon dangling bonds at the interface. Hydrogen incorporation during several device-processing steps was found to improve the device function but it sets stage for subsequent hot electron degradation [23, 39]. The time dependent degradation in MOS transistors has been known to occur as a result of the hot electrons stimulating the desorption of hydrogen from the SiO_2 interface region. Threshold voltage instability and channel tranconductance degradation have been observed in MOS transistors because of hot carriers generated by source-drain electric filed [40, 41].

In a complementary study, the characteristics of deuterium passivation as a function of thermal annealing were examined in thin SiO_2 films [20] for CMOS devices [29]. Transistors annealed in deuterium atmosphere have been found to yield better results compared to the hydrogen counterpart due to a lower sensitivity of Si-H bond to hot electron effect. Improvement in the lifetime and reduced variation in threshold voltage were also observed. This isotope effect has been found to improve the transistor lifetime by factors of 10-50 as shown in Figure (2.1). Deuterium incorporation has been carried out at various processing steps of the device. After the first steps of metal processing, uncapped wafers as well as wafers capped with SiN were subjected to deuterium anneal process. Smaller improvements were observed under circumstance of large background hydrogen concentration or reduced deuterium diffusion (nitride spacers) [23]. The noticeable improvement in hot carrier lifetime in deuterium-annealed

samples however could be unstable and relaxed when the samples are subjected to further processing [30]. Also, when CMOS technologies incorporate multiple metal and dielectric layers, the improvement due to deuterium sintering was reduced further [31]. In addition, undoped polycrystalline silicon [32] and SiN, used as a sidewall spacer, could limit the transportation of deuterium to the Si–SiO_2 interface during annealing by serving as a diffusion barrier for deuterium [33]. In some processes, these limitations were overcome by extended time and temperature anneals at higher deuterium concentration [34] but cycle time associated with extended anneals had detrimental effects at higher temperatures on the long-term metal properties, requiring to explore possible alternatives for deuterium incorporation at the Si–SiO_2 interface.

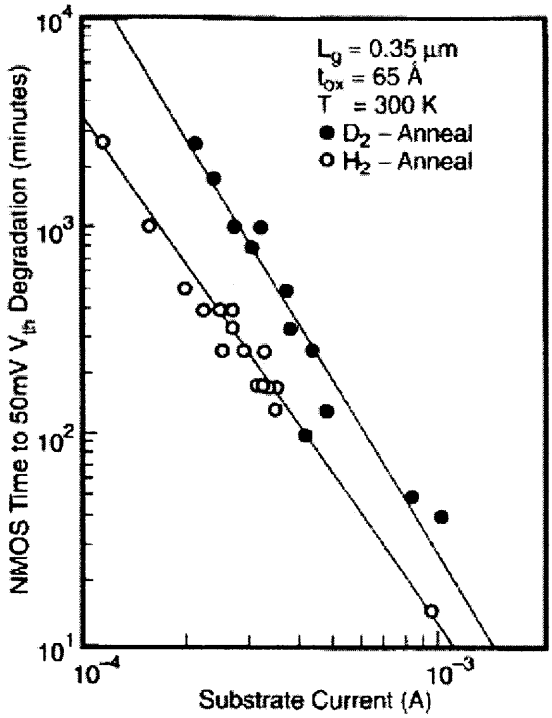

Figure 2.1 Hot electron degradation Vs substrate current- Improvement in the transistor Lifetime in case of deuterium compared to hydrogen annealing.
Source: [42]

2.2 High Pressure Deuterium Annealing

As discussed earlier, metal layers and nitride sidewall spacers were found to be a diffusion barrier for the incorporation of deuterium during deuterium annealing. Increased deuterium incorporation and greater hot carrier lifetime, using high pressure deuterium annealing was detected in comparison to deuterium annealing at atmospheric pressure [43]. The MOS devices were typically subjected to sintering at 450 ^{0}C at pressures (2 and 6 atmospheres). The annealing time was varied from 10 minutes to 3 hours. With higher-pressure processing, shorter annealing times were found to achieve the same magnitude of improvement and also higher pressure increased the incorporation of deuterium at the interface. Annealing condition at 6 atmospheres and 3 hours yielded the best improvement in the transistor hot carrier lifetime. With increased pressure, an improvement of the fully processed wafers with (four metal layers) with nitride sidewall spacers and SiON cap layers has been observed. Results demonstrated improvement in the transistor lifetime in comparison to ambient pressure anneals. High pressure processing was found to be effective and also the annealing time considerably reduced [43].

2.3 Oxidation in D_2O Atmosphere

An investigation of gate oxidation process to incorporate deuterium at the Si/SiO_2 interface using D_2O as an oxidizing gas was carried out [41]. This process showed an improvement of the interface. Electrical characteristics yielded less interface state generation, less electron trapping, lower SILC, and very large charge to breakdown under constant current stress conditions. Figure 2.2 shows the effect of constant current stress

(CCS) on the quasistatic capacitance versus voltage plots for the MOS devices where oxides grown by D_2O and H_2O are compared. The initial C-V curves obtained for both the samples were same but the D_2O grown oxide showed fewer interface states under the same electrical stress conditions. The increase in the low frequency capacitance and distortions shown in Figure 2.2 indicate the generation of interface states (Discussed in Section 3.3.1). Reduction in gate voltage indicates an improvement in quality [44].

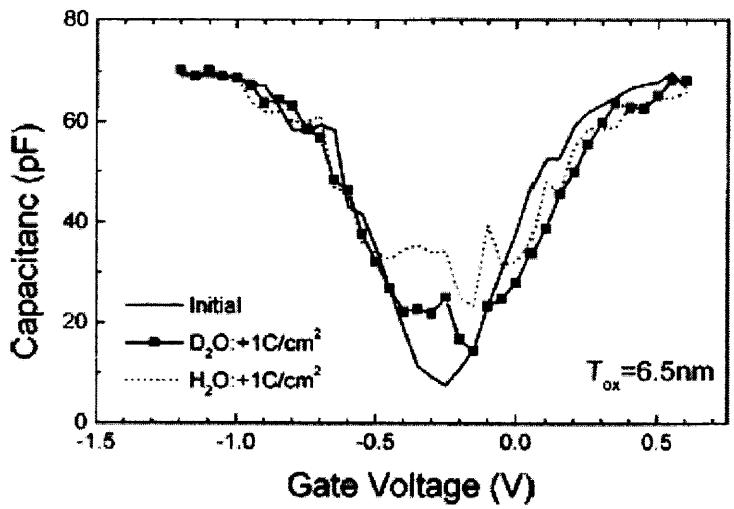

Figure 2.2 Quasistatic curves for D_2O and H_2O grown oxides both before stress and after $+1C/cm^2$ stress. Compared to control oxide the distortion of the C-V curve after electrical stress was less for oxides grown in D_2O ambient.
Source: [44]

2.4 Post Oxidation Annealing in ND_3 Atmosphere

To incorporate both N_2 and D_2 at the interface, post oxidation annealing was carried out in ND_3 atmosphere. N_2 is known to relieve stress at the interface [45]. Nitridation in a ND_3 ambient was performed at 800 °C for 30 min. Gate oxides, which had been annealed in a ND_3 ambient, exhibited less charge trapping, less generation of interface states, and a larger charge to breakdown under electrical stress. The fact that Si–D bonds are more difficult to break than Si–H bonds due to the heavy mass of deuterium, explained the improvement in the gate oxide annealed in ND_3. Figure 2.3 shows the gate voltage shift under stress for ND_3 and NH_3 annealed samples. Compared to the ND_3 annealed samples the NH_3 cases exhibit more voltage shift indicating more trapping of the electrons in the oxide (Section 3.3.1).

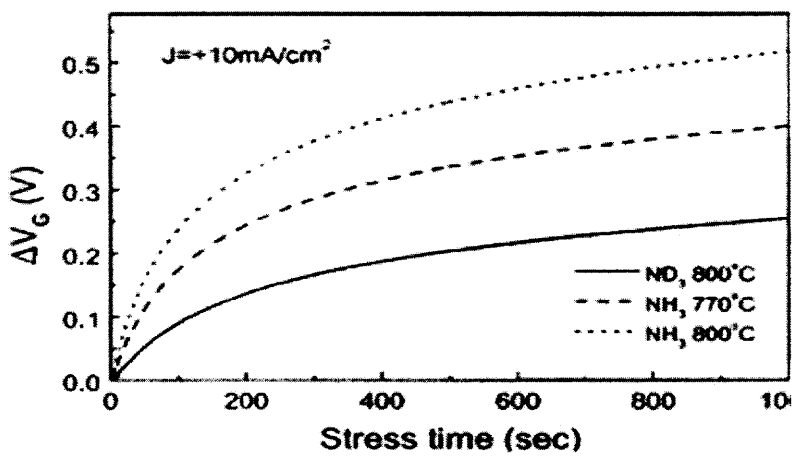

Figure 2.3 Gate Voltage shift under constant current (Jg= +10mA/cm^2) stress for both samples. The gate voltage shift under constant stress is due to trapping of electrons in the oxide. Compared to NH_3 annealing, the MOS capacitors with an oxide annealed in a ND_3 ambient exhibited less electron trapping.
Source: [45]

2.5 Deuterium Pyrogenic Oxidation and Deuterated Poly-Si Deposition

The effect of deuterium incorporation by deuterium pyrogenic oxidation and deuterated poly-Si deposition on stress-induced leakage current (SILC) under Fowler–Nordheim (F–N) electron injection was reported [46]. Deuterium seems to be introduced during the growth of the gate oxide. A deuterated Poly-Si film deposited by deuterated monosilane (SiD_4) gas was also utilized as a gate electrode. It was observed that the stress induced leakage current is significantly reduced by deuterium pyrogenic oxidation and deuterated Poly-Si deposition compared to deuterium annealing (Figure. 2.4).

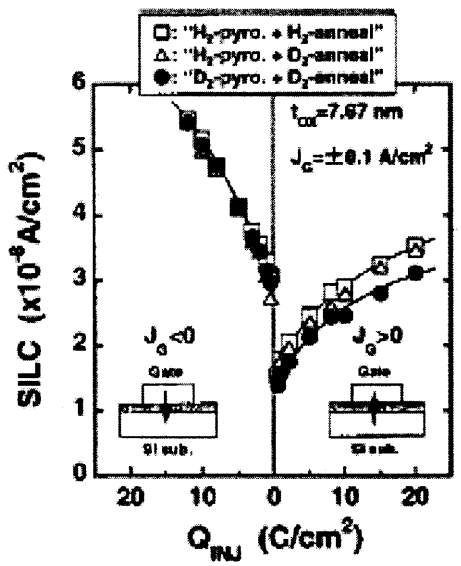

Figure 2.4 Stress-induced leakage current (SILC) of F-N stress as a function of electron fluence (Q_{inj}). Suppressed SILC is shown by deuterium pyrogenic oxidation under F-N electron injection, although SILC is not improved by the deuterium annealing.
Source: [46]

2.6 Surface Treatment

In order to incorporate deuterium ions at the interface a process involving deuterium prebake and deuterium post oxidation anneal was used. Using this technique, the deuterium ions were found to be distributed at the Si-SiO_2 interface and also in the bulk oxide. The isotope effects on constant voltage stress and D_{it} were observed for the deuterium treated MOS device. Figure 2.5 shows the gate current versus stress time for both hydrogen and deuterium treated devices. The variation in leakage current before and after stress for both hydrogen and deuterium treated devices is shown in the inset, which shows a suppressed SILC for the deuterium case [47].

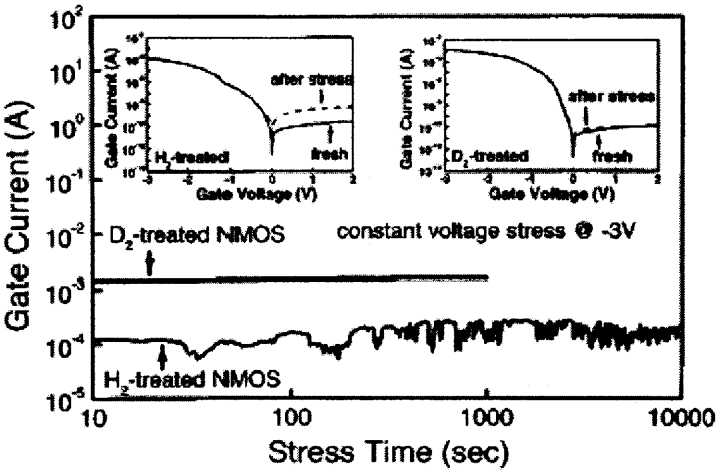

Figure 2.5 Gate current versus stress time plot of H_2 and D_2 treated NMOS diodes under constant voltage stress with -3V. The insets are the I-V characteristics of the devices before and after stress.
Source: [47]

2.7 Hydrogen Implantation

The slow diffusion of hydrogen in SiO_2 and the also the retardation of the diffusion through polysilicon has been demonstrated in the study of TFT [48]. In order to overcome this, a technique involving incorporation of the hydrogen atoms at the interface using ion implantation after the gate oxide was grown has been presented. Implantation carried out at two different energies 70keV and 128keV at a dose of $3.0e14cm^{-2}$ were performed after gate oxide growth and forming gas anneal performed after first level metal interconnect. An incomplete removal of the interface states was observed with the hydrogen annealing alone, which, yielded an improvement with the implantation.

CHAPTER 3

DEVICE FABRICATION AND EXPERIMENTAL PROCEDURE

3.1 Device Fabrication

Device fabrication has been carried out in the clean room at the NJIT Microfabrication Center, which is a 1200-sq.-ft, and class 10-clean room. It is equipped with the following tools for processing our devices on 5 inch diameter wafers. The equipment includes: Wafer Inspection - microscope, Dektak profile meter, Nanometrics optical line width, Wet chemical station Ultratek mask/wafer scrub, Semitool spin/rinse dryers, Nanometrics FTM, Inspection microscope, MTI Coat and develop system, Drytek reactive ion etching system, Varian sputtering system, BTU diffusion furnace, BTU LPCVD furnace, MDA toxic gas monitors, Tubewash station, MG Industries gas cabinets.

3.2 Process Flow for MOS Capacitor Fabrication

A detailed description of the individual process steps is presented below in Section 3.2.1 through 3.2.8. Figure 3.1 (a) through 3.1(h) describes the various steps. The following describe the outline for the fabrication of capacitors.

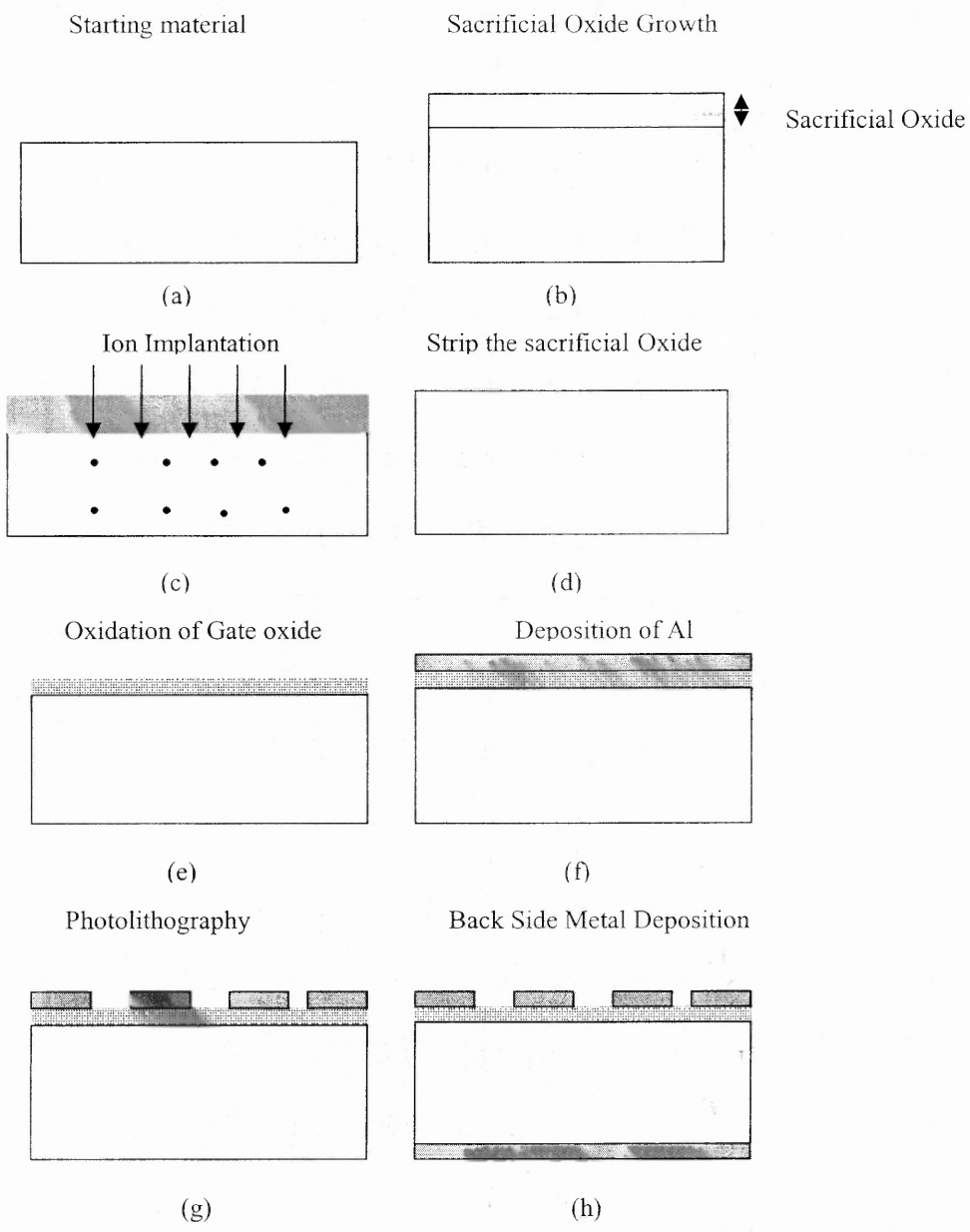

Figure 3.1 Fabrication of MOS capacitor (a) Starting- Silicon wafer (b) Deposition of denuding oxide and cleaning (c) Ion implantation according to conditions in Table (1) at Core systems (d) Stripping of sacrificial oxide (e) Deposition of gate oxide (65 Å) and annealing (f) Deposition of Aluminum (g) Photolithography to pattern Al (h) Stripping of photo resist and back side Al deposition.

3.2.1 Starting Materials

The starting material for the process was p-type (boron doped), <100> oriented CMOS grade silicon wafers, with a resistivity of 0.8-1.20 Ω-cm as shown in (Figure 3.1(a)).

3.2.2 Cleaning

Impurities can degrade the performance of circuits or even cause failure. Hence for high yield and device reliability, it becomes imperative to eliminate all possible sources of contamination. Surface cleaning is especially important prior to high temperature processes because impurities react and diffuse at much higher rates at elevated temperatures. The most commonly used wet chemical cleaning technology is based on hot alkaline or acidic peroxide (H_2O_2) solutions. These are used to remove chemically bonded films from the wafer surface prior to critical steps. P-clean, H_2SO_4 (75%) and H_2O_2 (25%), an aqueous alkaline solution that removes organic films, while m-pyrol (methyl pyrolidine) is an acidic mixture used to remove metallic contaminants. The processing temperature is maintained at 80 °C.

3.2.3 Sacrificial Oxide Growth

Wet oxide of thickness 200Å was grown at 850^0C with a flow rate of 3.5SLM oxygen and 530SCCM H_2O flow (bubbler) (Figure 3.1(b)).

3.2.4 Ion Implantation

Ion Implantation was carried out at room temperature with an inclination angle of 7^0 at CORE SYSTEMS. This was done to avoid the channeling effect on the wafers. Table (1) shows the implantation conditions. To optimize the implantation conditions for interface passivation of various MOS capacitors, implanted energies starting from 15keV to 35keV

with different implantation doses were used to implant deuterium into 5-inch *p*-type Si wafers. Hydrogen was also implanted at 20keV and 25keV. Table 3.1 summarizes the implantation conditions and the group names. The implantation was carried out after sacrificial oxide growth to prevent the direct exposure wafer surface to minimize damage. The wafer without any implantation was used as a control wafer (Figure 3.1(c)).

Table 3.1 Ion Implantation Conditions

IMPLANTATION ENERGY & DOSE	**15keV**	**20keV**		**25keV**		**30keV**	**35keV**
	Deuterium (D)	Deuterium (D)	Hydrogen (H)	Deuterium (D)	Hydrogen (H)	Deuterium (D)	Deuterium (D)
Dose A $1 \times 10^{13}/cm^2$	-	D20A	-	D25A	-	-	-
Dose B $1 \times 10^{14}/cm^2$	D15B	D20B	H20B	D25B	H25B	D30B	D35B
Dose C $1 \times 10^{15}/cm^2$	D15C	D20C	H20C	D20C	H25C	D30C	D35C

3.2.5 Gate Oxide Growth

The actual thin gate oxide was grown by dry oxidation technique. The thickness tried to obtain was 6.5nm. The temperature and time for the oxidation was 800^0C for 30 min. (Figure 3.1(e)). The conditions maintained for the gate oxidation were as shown in Table 3.2.

Table 3.2 Gate Oxide Growth Conditions

Type	Dry Oxidation
Oxygen	7.5 SLM
Temperature	800 °C
Time	30min

Flow Chart Showing the Oxide Deposition

P-clean, 5:1 H_2SO_4: $H_2O_2$110^OC, 10minutes→ Rinse Hot DI Water, 10 minutes→ Rinse Cold DI Water 5 minutes → Spin Dry → Furnace Pre-clean 100:1 H_2O: HF 1 minute → Rinse Cold DI Water 10 minutes→ Spin Dry → Thermal Oxidation.

3.2.6 Annealing

The wafers were annealed in N_2 atmosphere at 600^{0}C, 700^{0}C for 20 min.

3.2.7 Metal Deposition

After having undergone the various conditions of annealing the wafers were deposited with metal (Al) using sputtering technique (Figure 3.1(f)).

3.2.8 Photolithography

Photolithography was conducted to produce devices with diameters 50um 100um, 200um, 250um, 300um, 400um, and 500um.

3.3 Electrical Characterization

Passivation of dangling bonds at the Si/SiO_2 interface by implanted deuterium can be evaluated by estimating interface state density, D_{it}. The Low frequency or the quasistatic capacitance-voltage (C-V) technique is the common interface trapped charge measurement method. The Low frequency method at 20 Hz was used. The method of obtaining was the Low frequency-High frequency method (LF-HF) method. HF measurements were carried out at 1Mz.

3.3.1 High Frequency and Low Frequency C-V Measurements

The high frequency (HF) and low frequency (LF) measurements were carried out using HP 4284. C-V measurements were carried out by measuring at least 10 devices per device type. The HF measurements were carried out at 1Mz and the LF at 20Hz.The devices were probed using cascade microtech probe station. From the low frequency curve and the high frequency curve information of the interface state density can be obtained. Using (C-V) techniques interface states or "fast states" can be detected as a stretch out of the high frequency C-V curve of a MOS capacitor or a distortion in the LF C-V curve [49]. Oxide charge on the other hand causes a rigid shift along the voltage axis of the high frequency CV curve, and is detected as a change in the flat band voltage of the device [50]. A shift in the HF curve towards the ideal flat band voltage indicates annealing effect due to reduction of oxide charges, which includes the interface charge, oxide trapped charge, fixed oxide charge and mobile ionic charge.

3.3.1.1 Computation of Interface State Density. The Interface state density D_{it} was computed by [50].

$$D_{it} = \frac{1}{q}\left(\frac{C_{ox}C_{LF}}{C_{ox}-C_{LF}} - \frac{C_{ox}C_{HF}}{C_{ox}-C_{HF}}\right) ev^{-1}cm^{-2} \tag{3.1}$$

Where C_{ox} is the accumulation gate capacitance, C_{LF} is the low frequency capacitance measured at 20Hz and C_{HF} is the high frequency capacitance measured at 1 MHz. Interface trap level density is obtained as a function of the gate bias where the silicon band gap is scanned by varying the surface potential ϕ_s, which is modified by changing the gate bias. The relationship between gate voltage and the surface potential is given by

$$\phi_s = \int_{V_{G1}}^{V_{G2}} \left[1 - \frac{C_{LF}}{C_{OX}}\right] dV_G + \Delta \tag{3.2}$$

The integrand is obtained by integrating the measured C_{LF}/C_{ox} versus V_G curve with V_{G1} and V_{G2} arbitrarily chosen since integration constant is unknown. However integrating from $V_G = V_{FB}$ makes $\Delta=0$ which gives

$$\phi_s(V_G) - \phi_s(V_{FB}) = \int_{V_{FB}}^{V_G} \left[1 - \frac{C_{LF}}{C_{OX}}\right] dV \tag{3.3}$$

The energy level in the silicon band gap where the interface trap is located is given by

$$\frac{E_T - E_V}{q} = \frac{E_g}{2q} + \phi_S - \phi_B \tag{3.4}$$

Where E_T is the energy level of the interface trap, E_V is the valence band energy, Eg is the band gap, ϕ_s is the surface potential and ϕ_B is the bulk potential.

3.3.2 Stress Measurement

Ultra thin gate oxides in MOS devices when subjected to high filed stress during device operation are known to degrade the oxide quality and eventually lead to oxide breakdown. Charge trapping in the oxide has been used to monitor the degradation of the oxide [51]. In order to study the isotope effect H_2 and D_2 implanted devices were studied under a constant voltage stress (CVS). HP4156 was used to give a CVS.

The initial characteristics of the device-leakage current and the high frequency (HF) and low frequency (LF) C-V measurements were conducted. Following this the devices were stressed for a constant period of time (before the oxide breakdown) and then again the leakage current and HF and LF C-V measurements were conducted to study the effect of the stress at the interface of Si-SiO_2 and the bulk of the oxide to compare the effect of the stress given for the control case (no implantation), hydrogen implanted case and the deuterium implanted case. The stress level was fixed at –5V and –6V.

Gate injection was chosen as it induces more damage at the Si/SiO_2 interface compared to the substrate injection [52]. The level was decided based on the initial IV measurements, which indicated a breakdown voltage around –6V. The production of the traps with the application of the stress was being monitored measuring the leakage current after the stress was applied which is referred to as stress induced leakage current (SILC). The interface state generation was computed using the HF-LF method and the conductance method.

The investigation of the trap induced damage mechanism within the SiO_2 of the hydrogen/deuterium implanted MOS capacitors was conducted by subjecting to a lower

stress level at a constant voltage stress (gate negative) with a field of 9.2 MV/cm for 500 seconds.

3.3.3 TDDB (Time Dependent Dielectric Breakdown)

Dielectric breakdown in silicon oxide is described in terms of Time Dependent Dielectric Breakdown. The breakdown is measured using either constant current or constant voltage stress. A breakdown is detected when a permanent low resistance path is formed between the cathode and the anode [53]. CVS was given in this case and the I-t characteristics were monitored to obtain the time to breakdown.

The charge to breakdown (Q_{BD}) was computed using (5). Q_{BD} is defined as the charge flowing through the oxide to break it down.

$$Q_{BD} = \int_0^{t_{BD}} I_G dt \tag{3.5}$$

Where t_{BD} is the time to break down and the Ig is the gate current. Q_{BD} was used to as a comparison for the various implanted cases. The measurements were carried out for 15 devices in each case to obtain the oxide breakdown statistics.

3.3.4 Conductance Measurements

The conductance measurements were carried out at various frequencies using HP4184. The frequencies were 1 KHz, 100 KHz, 1 MHz. This was used to measure the interface state density which was computed using equation (6) and (7) [54].

$$\frac{G_P}{W} = \frac{W G_m C_{ox}^2}{G_m^2 + W^2 (C_{ox} - C_m)^2} \tag{3.6}$$

$$D_{it} = \frac{2.5}{q}\left(\frac{G_P}{W}\right)_{max} \quad (3.7)$$

Where G_m is the conductance measured, C_{ox} is the accumulation capacitance, w is the frequency, C_m is the capacitance at the particular frequency and gate voltage.

3.3.5 Leakage Current

The measurement of the leakage current of the MOS devices was carried out using semiconductor parameter analyzer HP4156.

CHAPTER 4

SIMULATION AND PHYSICAL CHARACTERIZATION

The energy and the dose that were used for implantation were computed using the initial simulation results of SRIM (Stopping Range of Ions In Matter) [65]. The energy of the implanted ions was selected depending upon the projected range that was obtained from the simulation results and also based on the earlier studies [37]. The energy of the implantation chosen was 15keV, 20keV, 25keV, 30keV, and 35keV.

The dose of the ions was selected depending upon the concentration of dangling bonds present at the surface. For standard oxidation temperatures (800-950^{0}C), the naturally incorporated density of defect sites (P_b) at the interface is found to be ~ $5x10^{12}$ cm^{-2} [46]. For incorporation of the Deuterium / Hydrogen ions at the interface the implantation doses were $1x10^{13}cm^{-2}$ (Dose-A), $1x10^{14}cm^{-2}$ (Dose-B), $5x10^{15}cm^{-2}$ (Dose-C). The upper limit of the dose was decided based on the extent of damage obtained from the simulation results. Table 3.1 shows the implantation conditions. For 20keV, 25keV all the doses were chosen while for 15keV, 30keV, 35keV only two doses were chosen for implantation - $1x10^{14}cm^{-2}$, $5x10^{15}cm^{-2}$. This is based on the earlier studies [37], which yielded the best result for the 25keV case, and also minimum deuterium ions had been found in the case of 15keV and 35keV - thus only the higher doses were used to see the effect at the interface.

4.1 Simulation of Implanted Range

The simulations were carried out for both hydrogen implantation and deuterium implantation. The data extracted from the simulations results were the implantation-projected range and the implantation damage. The number of ions selected for the simulation was 99999 for all cases. The projected range for various conditions for hydrogen and deuterium is demonstrated in Figure 4.1 and Figure 4.2 respectively. Since the implantation was carried out through the sacrificial oxide as discussed in Chapter-3 the SiO_2 film thickness is clearly identified in the respective figures. The X-axis shows the target depth (um) and the Y-axis has units of (atoms/cm^3 /atoms/cm^2) which when multiplied by the dose of the implanted ions yields the net concentration. The projected range and straggle were calculated and provided in the respective figures. The hydrogen implantation for 15, 20, 25, 30, 35keV are shown in Figure 4.1(a) through 4.1(e) respectively.

The deuterium implantation results for 15, 20, 25, 30,35keV are shown in Figure 4.2(a) through 4.2(e), respectively.

Table 4.1 and Figure 4.3 summarize the projected range for the implanted ions for all the cases for deuterium implantation. It is clearly observed that with the increase in the energy of implantation the implantation depth and projected straggle increases [59]. Figure 4.4 summarizes the dose effect for energy of implantation 25keV, which shows that the implantation-projected range remains same with the change in the dose of the implantation, only the peak concentration of the ion changes. With the increase in the dose of implantation, the peak concentration increases.

Figure 4.5 shows the comparison of the projected range in hydrogen and deuterium case is plotted as a function of implantation energy. It is observed that the projected range of the deuterium ions are more compared to the hydrogen ions – this happens due to the quantum mechanical nature of the electronic stopping power [47] and also hydrogen ion being 1.2 times lighter, it diffuses at faster in silicon.

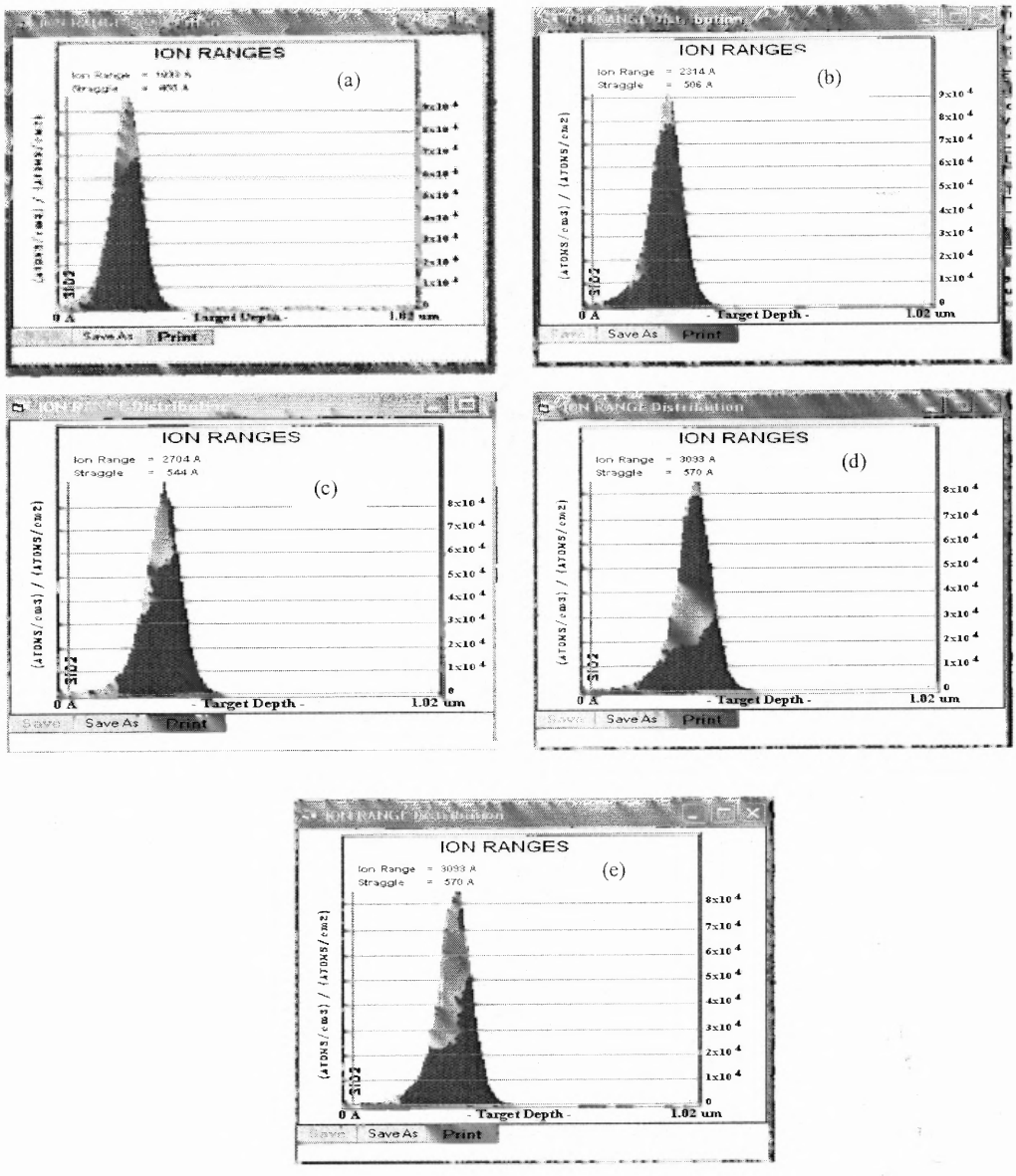

Figure 4.1 Hydrogen Implantation at various Energies (a) 15keV (b) 20keV (c) 25keV (d) 30keV (e) 35keV.

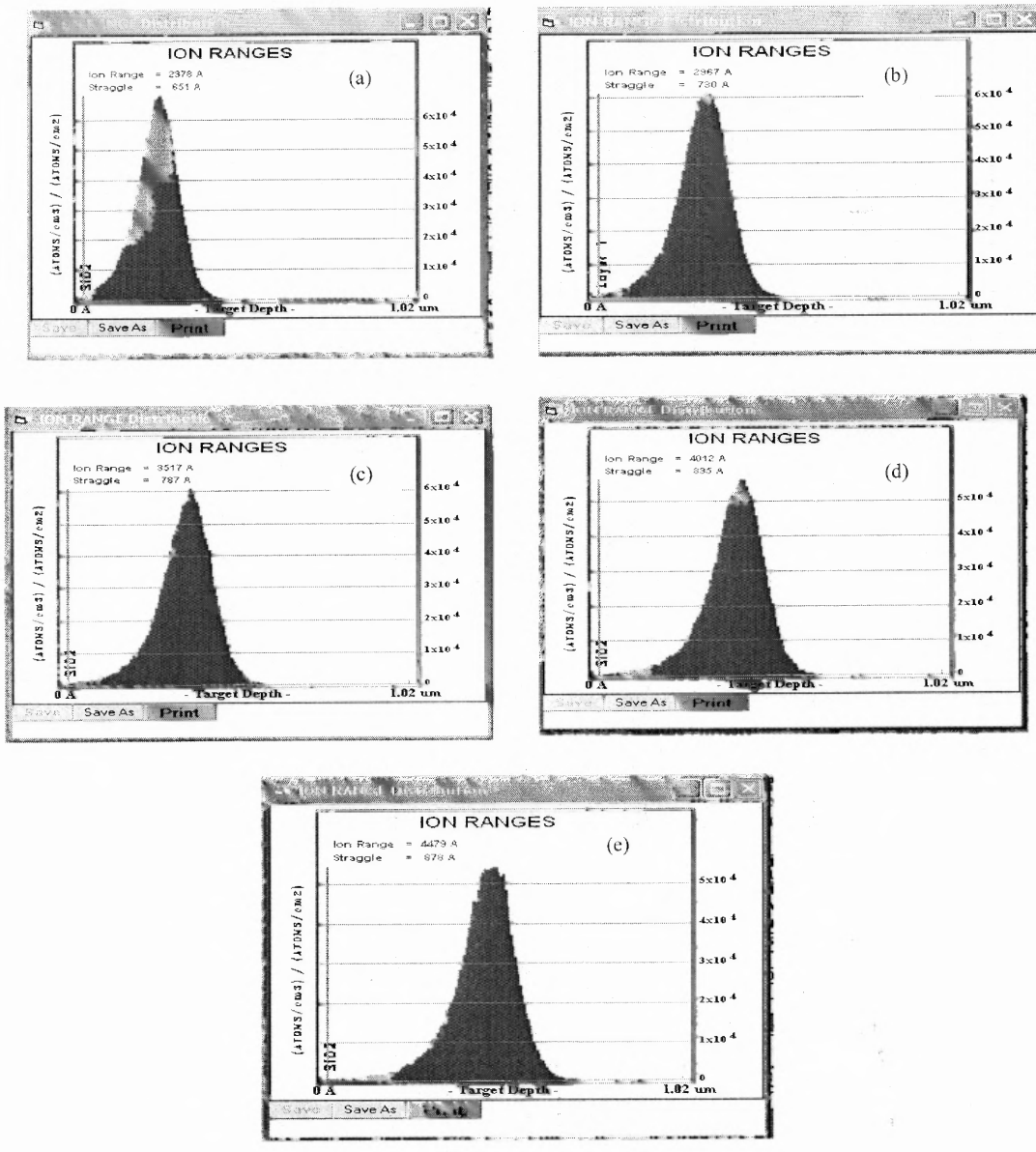

Figure 4.2 Deuterium Implantation at various Energies (a) 15keV (b) 20keV (c) 25keV (d) 30keV (e) 35keV.

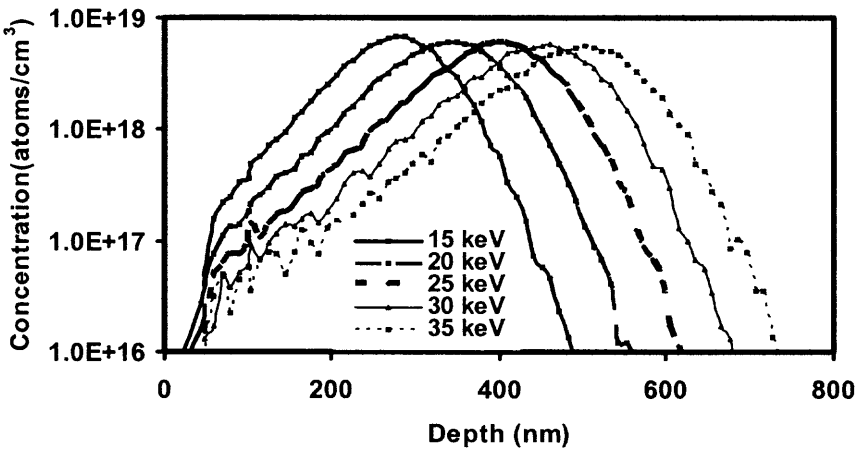

Figure 4.3 Comparison of implanted profile for energies of implantation 15keV, 20keV, 25keV, 30keV, 35keV simulated using SRIM for Deuterium. Shows increase in the projected range and straggle with increase in energy.

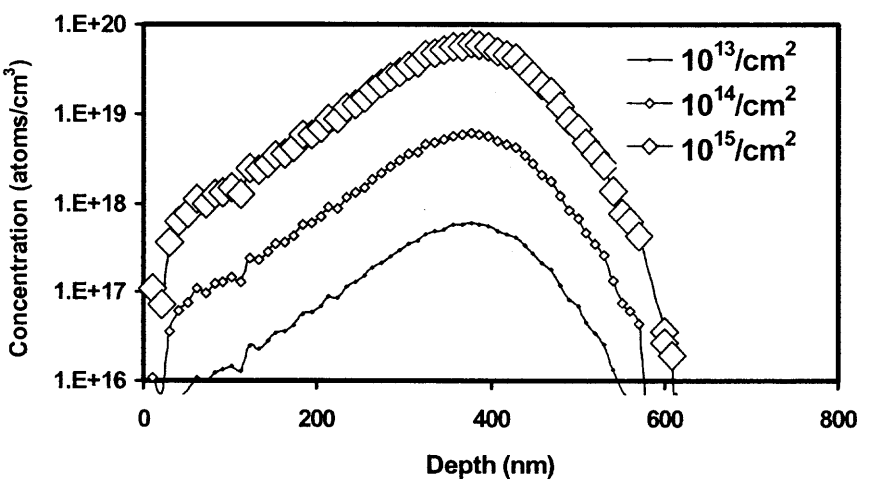

Figure 4.4 SRIM deuterium implantation depth profiles for energies of implantation 25keV for doses of implantation $1x10^{13}/cm^2$, $1x10^{14}/cm^2$, and $1x10^{15}/cm^2$. Shows increase of peak concentration with increase in dose of implantation.

Table 4.1 Depth shown for various cases of Hydrogen and Deuterium Implantation

	15 keV	20 keV	25 keV	30 keV	35 keV
Hydrogen	0.1893μm	0.2314μm	0.2704μm	0.3093μm	0.3483μm
Deuterium	.2400μm	0.2967μm	0.3517μm	0.4012μm	0.4479μm

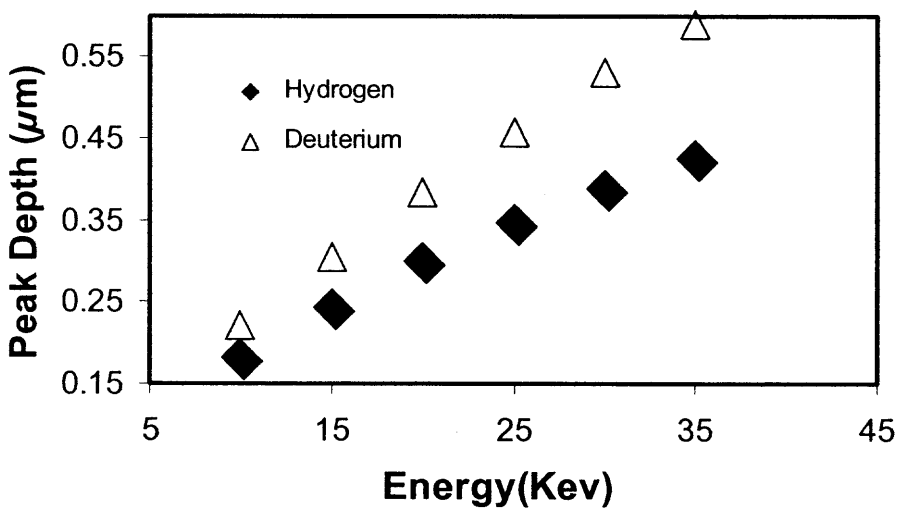

Figure 4.5 Peak Depth as a function of energy for implantation of Hydrogen and Deuterium implanted cases.

4.1.1 Peak Ion Concentration of Implanted Ions

The peak concentration of the implanted ions implanted in to the substrate has been evaluated.

The Peak concentration, N has been calculated using [59]

$N = 0.4 * \Phi / \Delta Rp$ atoms cm^{-3}

Δ Rp – is the projected straggle which is obtained from the simulation results, Φ - Dose which is in atoms cm^{-2}

Table 4.2(a) Hydrogen Peak Concentration

	Dose – A ($1 \times 10^{13}/cm^2$)	Dose – B ($1 \times 10^{14}/cm^2$)	Dose – C ($1 \times 10^{15}/cm^2$)
Energy	Peak Concentration/cm^3	Peak Concentration/cm^3	Peak Concentration/cm^3
15Kev	6.25E+17	6.25E+18	6.25E+19
20Kev	5.48E+17	5.48E+18	5.48E+19
25Kev	4.75E+17	4.75E+18	4.75E+19
30Kev	4.25E+17	4.25E+18	4.25E+19
35Kev	4E+17	4E+18	4E+19

Table 4.2(b) Deuterium Peak Concentration

	Dose – A ($1 \times 10^{13}/cm^2$)	Dose – B ($1 \times 10^{14}/cm^2$)	Dose – C ($1 \times 10^{15}/cm^2$)
Energy	Peak Concentration/cm^3	Peak Concentration/cm^3	Peak Concentration/cm^3
15Kev	4.6E+17	4.6E+18	4.6E+19
20Kev	4.2E+17	4.2E+18	4.2E+19
25Kev	3.6E+17	3.6E+18	3.6E+19
30Kev	3.5E+17	3.5E+18	3.5E+19
35Kev	3.2E+17	3.2E+18	3.2E+19

4.2 Damage Simulation

Implantation damage if not annealed completely, can degrade device reliability. The implantation damage induced to the Si substrate has also been simulated. Figure 4.6(a) through 4.6(e) shows the results of the hydrogen implantation for 15, 20, 25, 30, 35keV cases respectively. The projection view is in the X-Y direction, X-axis being the depth (um). From the results, it was observed that the damage volume in the substrate increases with the increase in the energy of the implantation. From the damage profile, information about the number of Frenkel pairs, (Vacancy-Interstitial) which are produced is obtained. Figure 4.6(a) through 4.6(e) shows the results of the deuterium implantation for 15, 20, 25, 30, 35keV cases, respectively. The trend remained the same for deuterium except the depth and volume.

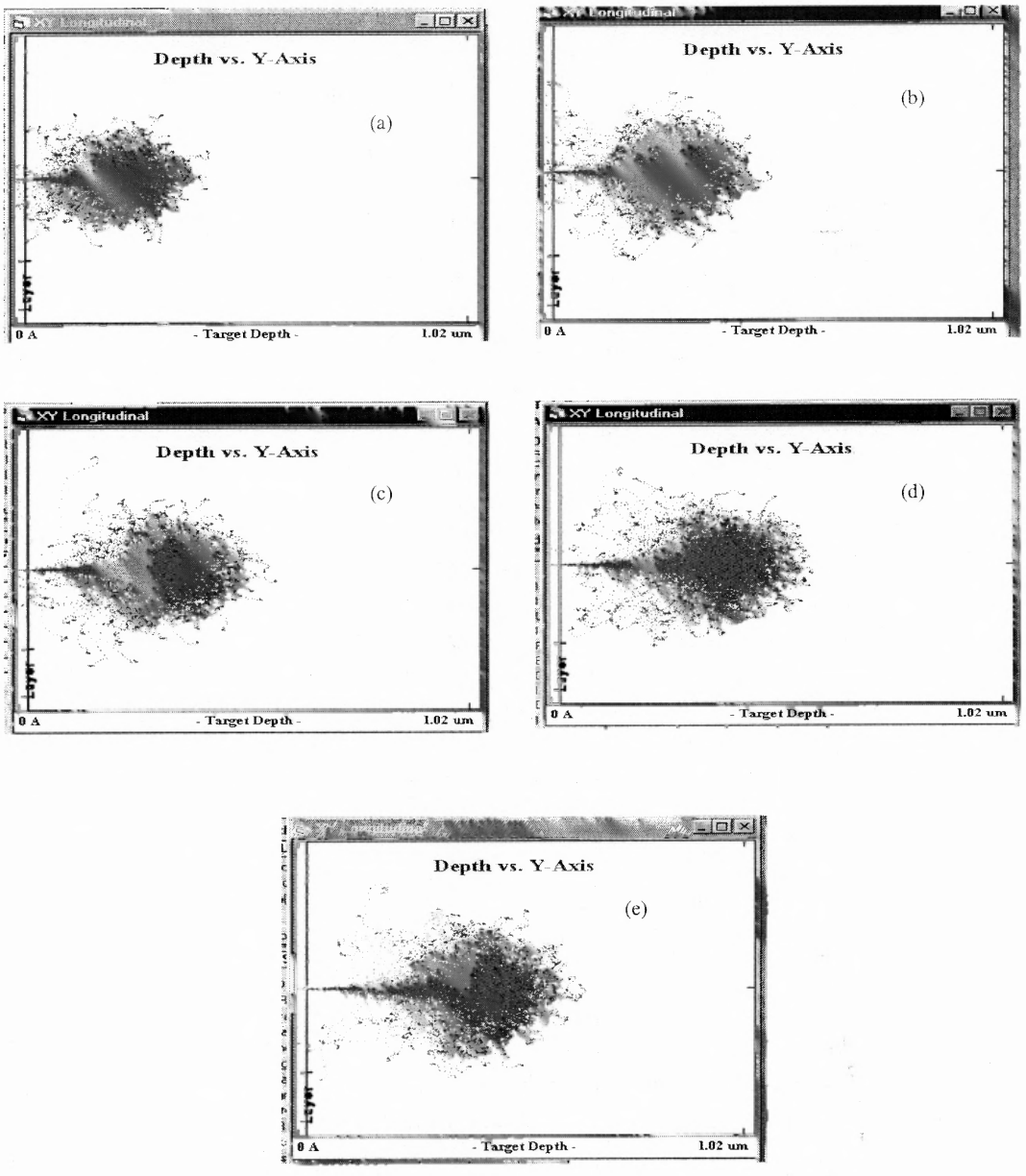

Figure 4.6 Hydrogen Ion Implantation at various Energies –Damage creation (a) 15keV (b) 20keV (c) 25keV (d) 30keV (e) 35keV.

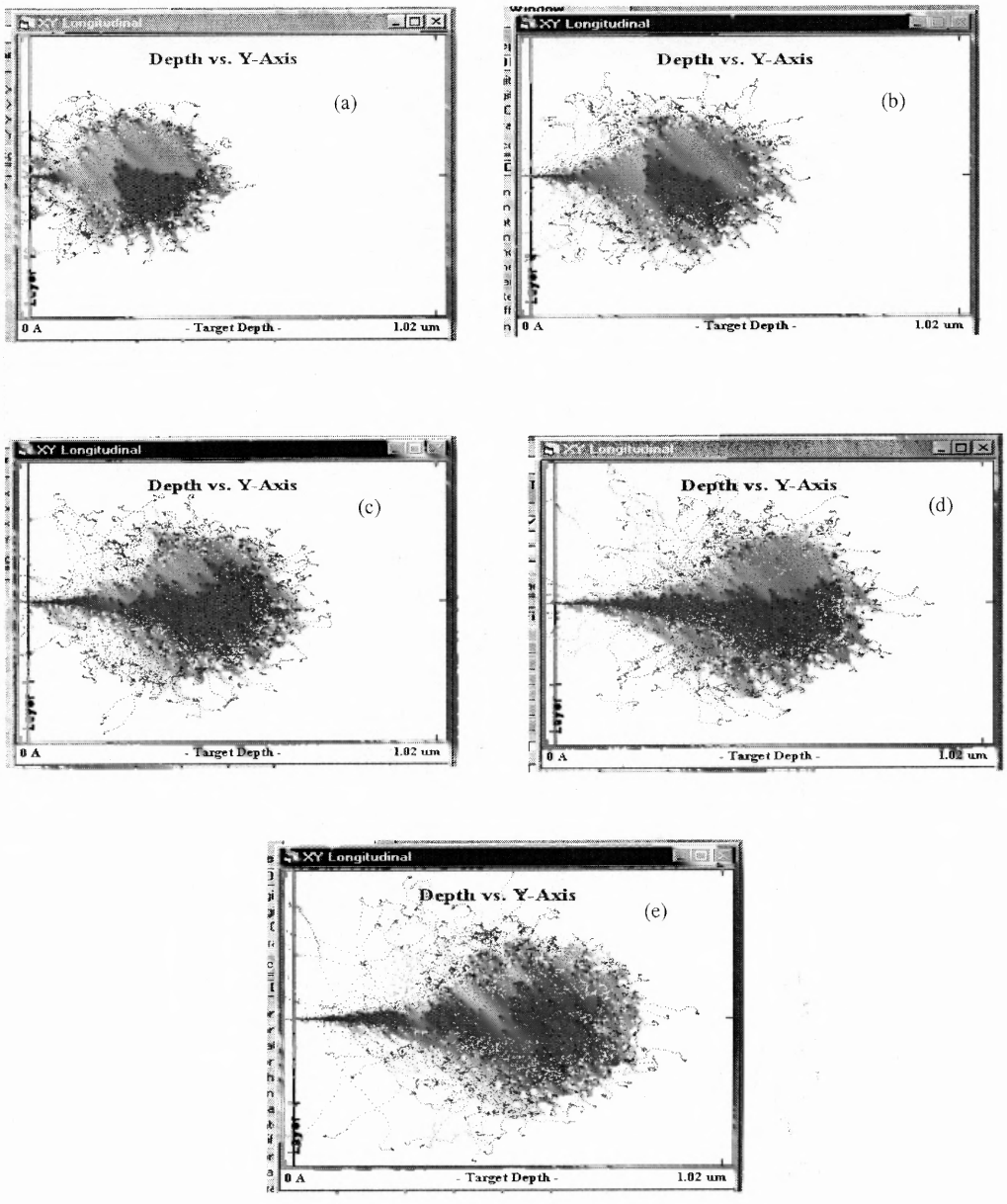

Figure 4.7 Deuterium Ion Implantation at various Energies –Damage creation (a) 15keV (b) 20keV (c) 25keV (d) 30keV (e) 35keV.

Figure 4.8 shows the summary of the damage induced in the substrate as a function of various implantation energies for deuterium case is shown. The thickness of the sacrificial oxide, 20nm is also shown in the figure. From the figure it is observed that the point defects are created along the entire ion path, starting from the surface and extending deep in to the bulk, with a yield, increasing with depth. The defect induced in the substrate increases with energy of implantation. On the other hand near the interface, the surface damage is found to decrease with the increase in the energy of implantation, being more for 15keV case and less for 35keV. Figure 4.9 shows the damage induced to the substrate with the variation in the dose of implantation for Dose-B and Dose-C cases. The damage to the substrate and the interface increases with the increase in the dose of implantation, being more for Dose-C compared to Dose-B.

The summary of the damage results plotted as a function of dose for various energies of implantation is shown in Figure 4.10 and Figure 4.11 for hydrogen and deuterium implanted cases, respectively. As a function of dose, the damage induced in to the substrate is found to increase with the increase in the dose. Dose-C is shown to produce the maximum damage in the substrate compared to Dose-A and Dose-B.

Comparison of the hydrogen and deuterium damage creation in the substrate has been plotted in Figure 4.12. As shown, the damage produced immediately after the implantation and before any annealing is almost identical for hydrogen and deuterium implantation in case of Dose-B ($1x10^{14}cm^{-2}$) for both 20 and 25keV implantation energies but significant difference in defect density due to implantation was observed for Dose-C ($1x10^{15}cm^{-2}$), which was higher in case of deuterium compared to Hydrogen due to the mass of deuterium being higher.

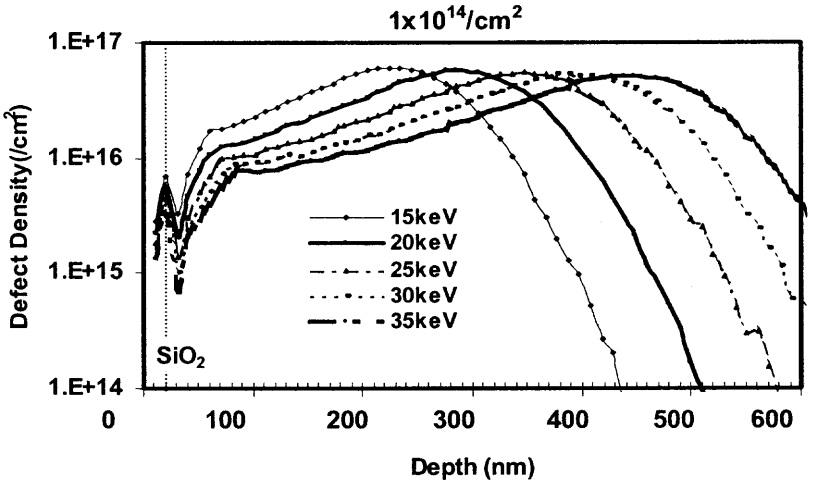

Figure 4.8 Defect densities for deuterium as a function of implantation energy for 15keV, 20keV, 25keV, 30keV, 35keV for implantation dose of $1x10^{14}/cm^2$. Shown defect density increases rapidly with increase in the energy and dose of implantation.

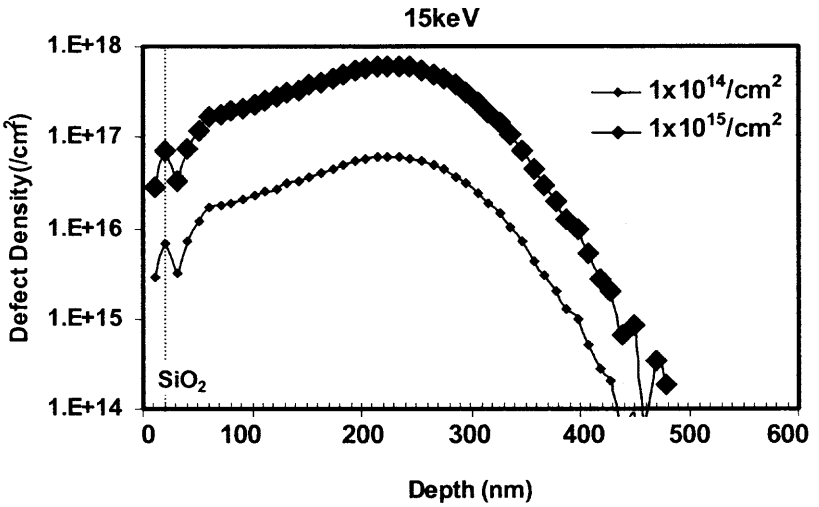

Figure 4.9 Defect density for deuterium as a function of implantation dose, for Dose-B ($1x10^{14}/cm^2$) and Dose-C ($1x10^{15}/cm^2$) for 15keV energy of implantation. Shown defect density increases rapidly with increase in the dose of implantation.

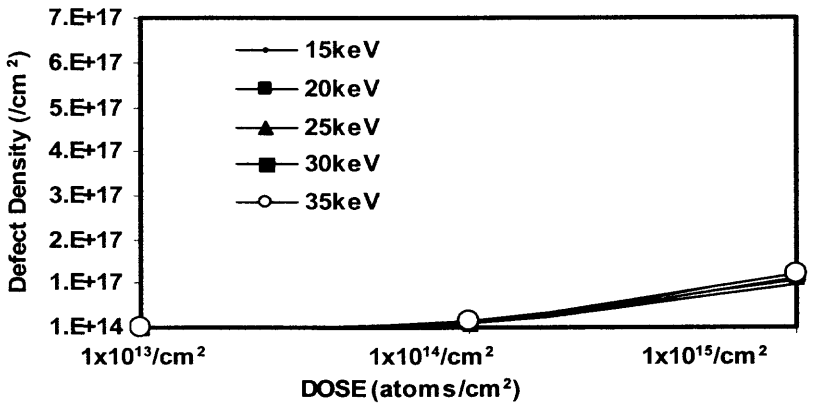

Figure 4.10 Defect density as a function of implanted dose for Hydrogen implantation at different energies. Shows vacancy concentration increases rapidly from Dose-B ($1x10^{14}cm^{-2}$) to Dose-C ($1x10^{15}cm^{-2}$) compared to Dose-A ($1x10^{13}cm^{-2}$) to Dose-B ($1x10^{14}cm^{-2}$).

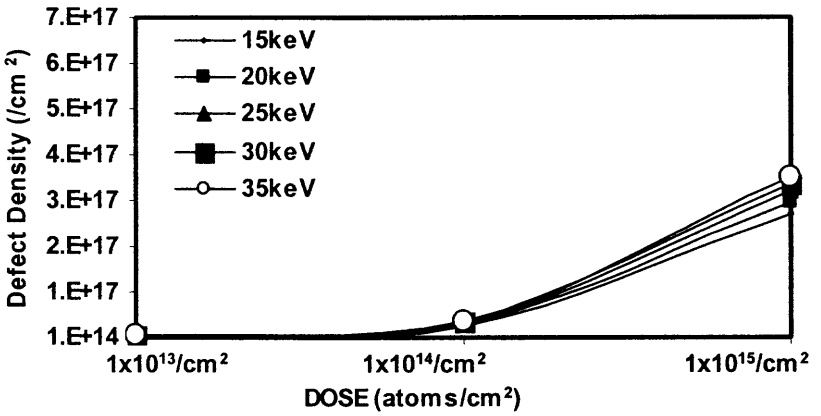

Figure 4.11 Defect density as a function of implanted dose for Deuterium implantation at different energies. Shows vacancy concentration increases rapidly from Dose-B ($1x10^{14}cm^{-2}$) to Dose-C ($1x10^{15}cm^{-2}$) compared to Dose-A ($1x10^{13}cm^{-2}$) to Dose-B ($1x10^{14}cm^{-2}$).

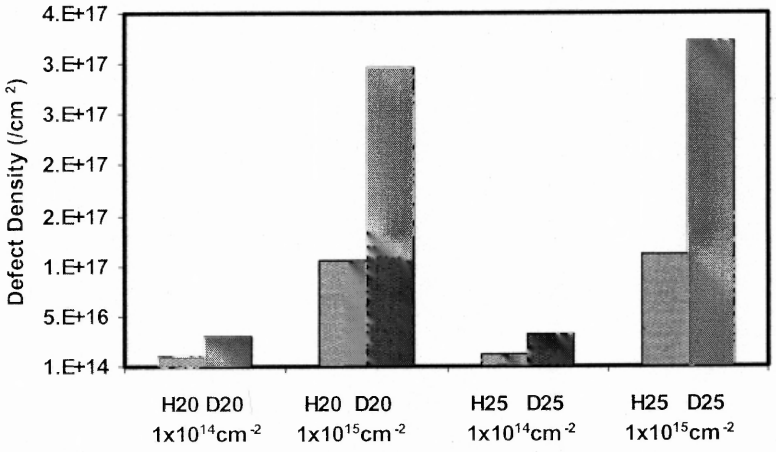

Figure 4.12 SRIM simulation shows the damage creation immediately after the implantation and before any annealing, which is almost identical for hydrogen and deuterium implantation in case of Dose-B ($1x10^{14}cm^{-2}$) for both 20 and 25 keV implantation energies but significant difference in defect density due to implantation was observed for Dose-C ($1x10^{15}cm^{-2}$).

4.3 Physical Characterization

Physical characterization was conducted using the technique of secondary ion mass spectroscopy (SIMS) [62]. The deuterium depth profiles immediately after implantation (as-implanted case) and also after the wafers underwent gate oxidation. SIMS measurement was done at the Advanced Materials Processing and Analysis center – University of Central Florida [63]. Dynamic SIMS sputter-depth-profiling analyses were carried out on a PHI Adept 1010 Dynamic SIMS System using Cs^+ (3kV) as the primary ion beam Cesium ion (Cs^+) bombardment with a current of 75nA.

SIMS profiling to study the depth distribution of the as-implanted samples were conducted for the implantation cases D20B and D25B. Figure.4.13 Show the obtained depth profiles. The depth profiles using SIMS were 325nm and 390nm for D20B and D25B respectively. A peak concentration of $6.16x10^{18}/cm^3$ and $5.96x10^{18}/cm^3$ has been obtained for 20keV and 25keV case respectively. Comparing the obtained results with SRIM simulation results, Figure 4.14 it is observed that the similar peak concentration is obtained. The peak implantation depth obtained from SRIM is 297nm and 352nm for D20B and D25B, respectively. The difference in the shift of the peak obtained is on account of the effect of channeling, which is not taken in to consideration in SRIM models to evaluate concentration profiles [64].

The characterization for the hydrogen-implanted case was not conducted, as the detection limit of the PHI Adept 1010 Dynamic SIMS System was $2\text{-}3x10^{18}/cm^3$ for hydrogen, which was comparable to the expected peak concentration. The incorporation and detection of deuterium after oxidation was carried out for samples D20B, D20C,

D25B, and D35C. The selection of the samples was carried out based on the initial D_{it} results as discussed in Section 5.1, which yielded the best interface passivation for D20B. D20C was chosen to study and compare the dose effect whereas D25B and D35C were chosen to study the effect of energy in the incorporation process and diffusion of deuterium ions from the silicon substrate towards the Si-SiO_2 interface.

Figure 4.15 shows the measured SIMS profiles in SiO_2 films obtained by SIMS after the wafers underwent gate oxidation up to depth of 9nm. The concentration profiles have been shown for implantation conditions- 20keV- $1x10^{14}/cm^2$; 25keV, $1x10^{14}/cm^2$; 25keV, $1x10^{15}/cm^2$; 35keV, $1x10^{15}/cm^2$. It is observed that the deuterium incorporation after diffusion is obtained not only at the Si/SiO_2 interface but also in the entire SiO_2 film with a peak concentration being obtained within the SiO_2 near to the interface of Si/SiO_2.

It is observed that, for all the samples after having undergone the gate oxidation the concentration in the silicon substrate reduces to the background level and the concentration profile itself shows a large shift (about 300nm) with a peak obtained within the oxide near the Si/SiO_2 interface at a depth of 5nm. Comparing the peak concentration for the 20keVand 25keV case with the as implanted case in Figure 4.12 it is observed that, concentration reduces from $6x10^{18}/cm^3$ to $1.71x10^{18}/cm^3$ and $5.79x10^{18}/cm^3$ to $1.71x10^{18}/cm^3$ for 20keV and 25keV cases of implantation, respectively. During oxidation deuterium diffuses either to the bulk or to the surface. The shift in the concentration profile obtained after oxidation indicates the driving force of the implanted ions diffusing towards the surface owing to the chemical potential difference between SiO_2 and Si [37], which being lower in SiO_2 compared to Si drives the diffusion of the implanted deuterium from the silicon substrate to the silicon oxide. The pile up of

deuterium atoms towards the oxide and silicon interface during oxidation results from the low activation energy for diffusion in SiO_2 compared to silicon [65]. The activation energy for the diffusion of deuterium is found to be 1.53eV and 1.9eV in silicon and silicon dioxide respectively [66]. In addition, the grain boundaries and dislocations are also to know to act as trapping sites for the diffusion of deuterium ions [67]. Note that, the interface concentration of deuterium is much higher than the ground level observed in the silicon substrate.

In case of deuterium-annealed oxide, the deuterium atoms exist mainly at the Si/SiO_2 interface, whereas using the technique of ion implantation the deuterium atoms are contained in the entire SiO_2 film as shown in Figure 4.16. From the obtained result, it is also evident that the diffused deuterium atoms are not only incorporated at the Si/SiO_2 interface reacting with the interface dangling bonds to form Si-D bonds, but also form Si-D bonds in the bulk SiO_2, which has also been observed in deuterium pyrogenic oxide growth [68].

Comparing the diffusion profiles of the ions it is observed that, at the interface of $Si\text{-}SiO_2$ the incorporation of ions for D20B, D20C, D25B and D35C are $7.8X10^{17}$, $6.5X10^{17}$, $5.8X10^{17}$ and $5.563X10^{17}$ and the peak concentration obtained within the oxide are $1.7X10^{18}$, $1.73X10^{18}$, $1.72X10^{18}$ and $1.9X10^{18}$, respectively. An increase in the oxide concentration in D35C was observed compared to other case reflects the contribution from the higher dose of implantation. For the implantations conditions at 20keV and 25keV, the depth being shallower than for higher energy (35keV) have governed the out diffusion of some ions leading to a reduced concentration within the oxide.

It is therefore, inferred from the obtained profile that most of the deuterium atoms implanted in to the silicon substrate diffuse towards the SiO_2 and takes part in the formation of Si-OD bonds during oxidation and passivation of the dangling bonds at the interface.

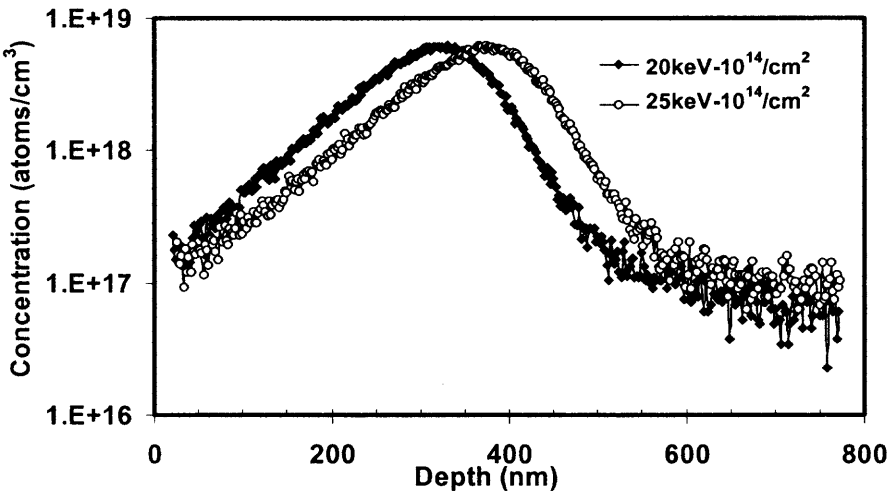

Figure 4.13 Deuterium depth profiles generated by secondary ion mass spectroscopy (SIMS) of the as implanted wafers for energies of implantation 20keV and 25keV for Dose-B ($1x10^{14}/cm^2$).

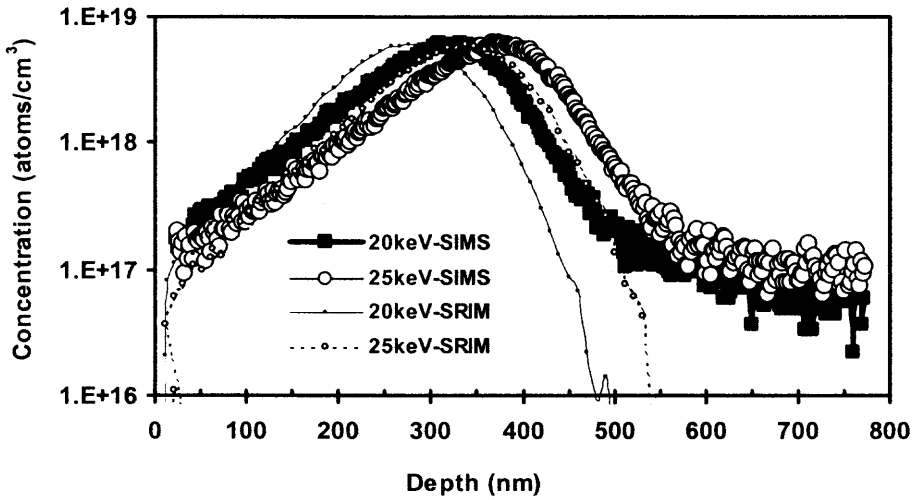

Figure 4.14 Comparison of Deuterium depth profiles from secondary ion mass spectroscopy (SIMS) and Stopping range of ions in matter (SRIM) of the as implanted wafers for energies of implantation 20keV and 25keV.

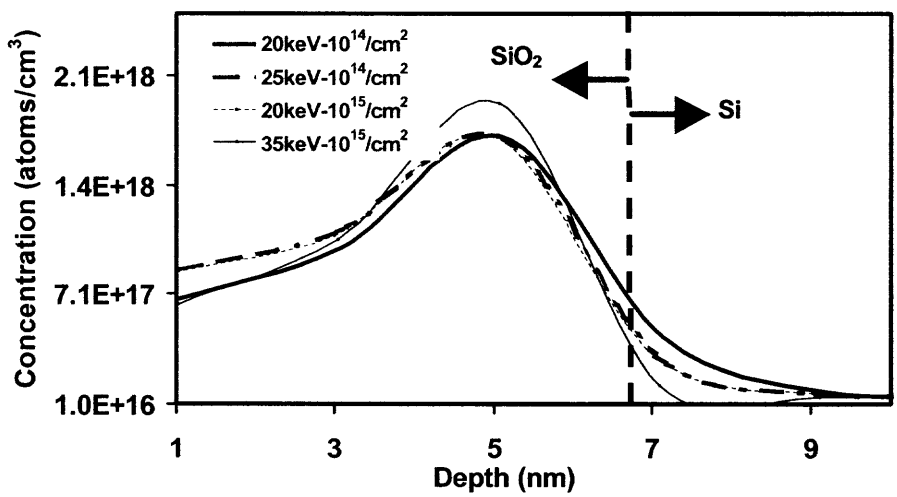

Figure 4.15 SIMS profiles after gate oxidation for cases of implantation 20keV-$1x10^{14}/cm^2$; 25keV- $1x10^{14}/cm^2$; 20keV- $1x10^{15}/cm^2$; 35keV- $1x10^{15}/cm^2$.

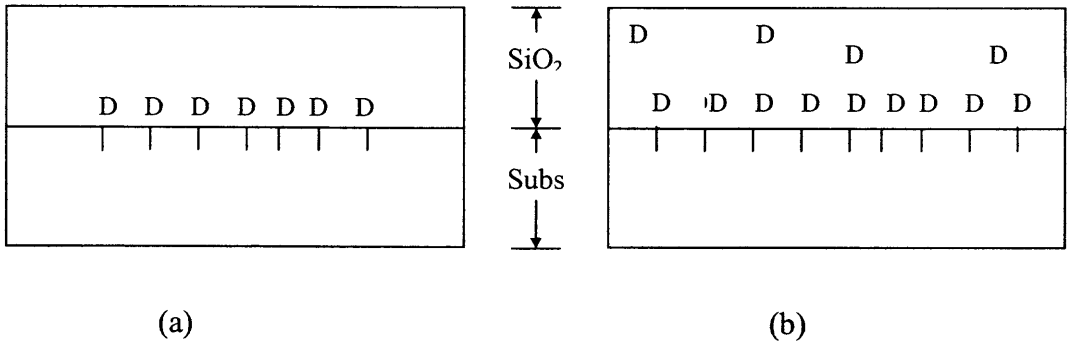

Figure 4.16 Schematic diagram of deuterium incorporation in (a) Deuterium annealed gate oxide where the incorporation of deuterium ions only at the interface of Si-SiO_2 (b) Deuterium implanted gate oxide, deuterium ions exist both at the Si-SiO_2 interface and bulk SiO_2.

4.4 Summary

This chapter involves the discussion of the obtained simulations results using Stopping Range of Ions in Matter (SRIM) and the physical characterization results measured using Secondary Ion Mass Spectroscopy (SIMS). The simulation has been carried out to obtain the peak implantation depth, concentration and damage of the implanted ions in the silicon substrate.

SIMS profile was carried out for the as implanted (immediately after implantation) and also for the samples after they underwent gate oxidation. As–implanted profiles yielded similar results to that obtained from the simulation. The profiles obtained after gate oxidation showed deuterium retention and incorporation both at the interface and the bulk oxide with a peak obtained in SiO_2 near the Si/SiO_2 interface. Thus it is inferred that, using the technique of implantation the incorporation of the deuterium ions not only take place at the interface but also the bulk oxide.

CHAPTER 5

RESULTS AND DISCUSSIONS- INTERFACE PASSIVATION

This chapter discusses the electrical characterization to compute the interface state density of the as fabricated devices in Section 3.2, to study the deuterium and hydrogen passivation effect at the interface. It is known that passivation of dangling bonds at the interface can be evaluated by estimating the interface charge density (D_{it}). Therefore, in order to investigate the passivation effect of the implanted deuterium and hydrogen ions D_{it} has been computed. From Table 3.1 it is seen that the deuterium implantation was carried out at energies 15, 20, 25, 30, 35keV for Dose-B (1 x 10^{14}/ cm^2) and Dose-C (1 x 10^{15}/ cm^2) and Dose-A (1 x 10^{13}/ cm^2). Dose-A has been implemented only for 20, 25keV. The choice of the implantation condition has been discussed in Chapter 4. From the earlier results [38] it was observed that deuterium at 25keV yielded the best results. This lead to the implantation of hydrogen at two energies at 20, 25keV for Dose-B and Dose-C to investigate the isotope effect in depth at these conditions and compared with deuterium implantation. The samples were further subjected to higher annealing conditions and the D_{it} has been studied to understand the effect of the deuterium ions in the oxide-interface and the substrate and also investigate the implantation induced damage effect.

5.1 Interface State Density Computation

D_{it}, has been computed using the low frequency and high frequency C-V technique, as discussed in Section 3.3.1. The following sections discuss the passivation study for various cases of deuterium implantation, hydrogen implantation, and a comparison of deuterium and hydrogen cases.

5.1.1 Deuterium Implantation

The high frequency, low frequency C-V curves and the derived D_{it} for the various implantation energies (15, 20, 25, 30, 35Kev) are shown in Figure 5.1 through Figure 5.5 respectively. Table 3.1 shows the implantation conditions. Figure 5.1(a) and (b) shows the HF-LF C-V characteristics and the D_{it} distribution in the silicon band gap respectively for the implantation condition D15B (deuterium 15 keV, 1x10 ^{14}/ cm^2) and D15C (deuterium 15 keV, 1x10 ^{15}/ cm^2) along with the control device. The HF C-V curves sows a shift in the flat band voltage closer to the ideal flat band for D15B compared to the control device, indicating a reduction of net oxide charge, which includes the trapped oxide charge, fixed oxide charge and interface charge. The net oxide charge is computed from the shift in the flat band voltage. The net oxide charge obtained for the control case is 9.47x10^{-8} C/cm^2, 4.74x10^{-8} C/cm^2 and 6.55x10^{-8} C/cm^2 for D15B and D15C cases respectively. The significant reduction in the oxide trap charges in case of D15B indicates an improvement in the oxide quality, which is observed due to the deuterium ions passivating the defects in the bulk oxide [50]. From the D_{it} distribution graph (Figure 5.1 (b)) it is observed that Dose-C leads to similar passivation characteristics as the control case, however a decrease in D_{it} is obtained for Dose-B.

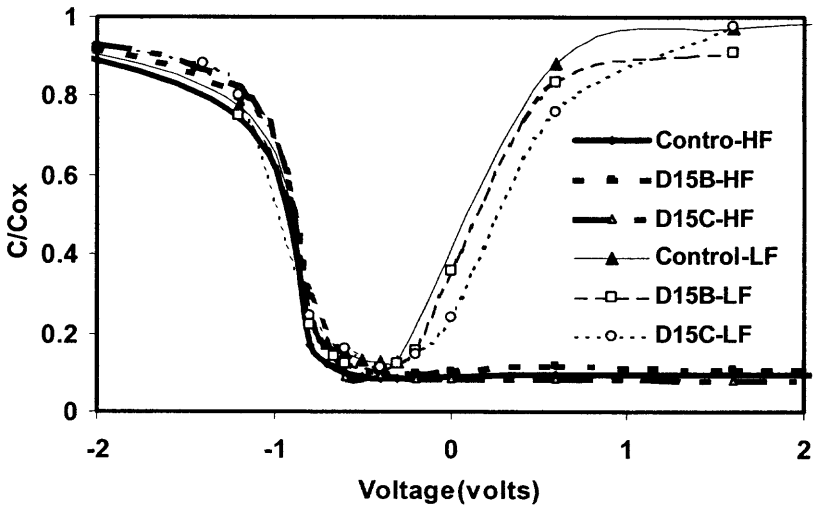

(a)

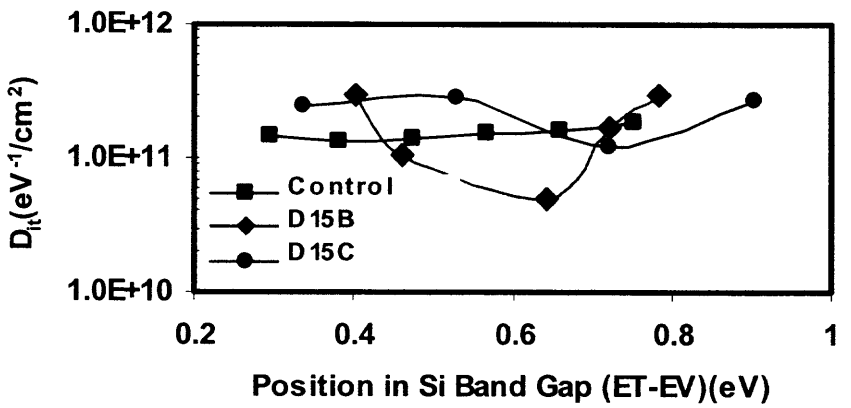

(b)

Figure 5.1 15keV Deuterium Implanted case for Dose-B (1x10 ^{14}/ cm^2) and Dose-C (1x10 ^{15}/ cm^2) (a) LF-HF C-V curves (b) Energy levels of the interface states (D_{it}) at the SiO_2 interface in the silicon band gap for devices with implantation energy 15keV for deuterium implanted devices. The control device plotted for comparison.

The depth at which concentration peak occurs was obtained form initial Stopping and Range of Ions in Matter (SRIM) simulation results as shown in Table 4.1(a). Devices implanted at 15keV, the implantation depth were shallow and the out diffusion of the ions during oxidation has lead to the reduced interface passivation. The increase in the value of interface states for D15C compared to D15B is due to the implantation induced damage effect which is higher in Dose-C (Figure 4.9), the effect of which is also noticed with an increase in the net oxide charge in D15C case of implantation.

The HF-LF C-V measurements and the D_{it} distribution in the silicon bandgap for the implantation condition D20A (deuterium 20keV, $1x10^{13}/cm^2$), D20B (deuterium 20keV, $1x10^{14}/cm^2$) and D20C (deuterium 20keV, $1x10^{15}/cm^2$) along with the control device are shown in Figure 5.2(a) and Figure 5.2 (b) respectively. The bulk oxide trapped charge for is $9.47x10^{-8}$ C/cm^2, $5.20x10^{-8}$ C/cm^2, $5.04x10^{-8}$ C/cm^2 and $5.86x10^{-8}$ C/cm^2 for the control, D20A D20B and D20C cases respectively. This suggests a marked improvement in the bulk oxide charges and interface state density for D20B. From the LF plots a reduced distortion is observed for the implanted cases compared to the control case indicating a reduction of the interface traps, which is clearly reflected in the D_{it} distribution graph in Figure 5.2 (b). An enhanced passivtaion is obtained for D20B and D20C compared to D20A with a minimum value of D_{it} obtained for D20B.

Minimum D_{it} and oxide charge obtained in case of D20B indicates effective diffusion and Si-D bond formation, suggesting presence of more deuterium ions during oxidation. The incorporation of deuterium ions after oxidation as shown in Figure 4.15 show considerably more number of deuterium ions present at the interface, which contributes the improvement in passivation in D20B. In case of D20A the ions have out diffused, the

diffused, the peak concentration being less compared to Dose-B and Dose-C, for D20C the implantation damage was more evident as shown in Figure 4.11, suggesting a degraded interface and oxide.

Similar results are observed for the 25keV case shown in Figure 5.3 indicating the effect of the deuterium ions at the interface and the oxide. D20B and D25B (deuterium 25keV, 1x10 ^{14}/ cm^2) yielded lower D_{it} compared to the D20C and D25C (deuterium 25keV, 1x10 ^{15}/ cm^2). The value of Dit obtained is $1.2x10^{10}$ eV^{-1} cm^{-2} and $1.28x10^{10}$ eV^{-1} cm^{-2} for the D20B and D25B. D20C shows an improvement in the D_{it} compared to D25C, which are $2.59x10^{10}$ eV^{-1} cm^{-2} and $4.32x10^{10}$ eV^{-1} cm^{-2} respectively in samples with deuterium-implantation at 20 keV with a dose of $1x10^{15}$/cm^2 (Dose-C).

It was observed that from the distribution of D_{it} in silicon band gap (Figure.5.2 (b), 5.3(b)) for D20B, D25A, D25B, P_b centers below the midgap are passivated. It known that in (100) Si/SiO_2 interface, contribution of P_{b0} centers to D_{it} is through the significant +/0 and 0/- levels at approximately E_v + 0.2 eV and E_v + 0.85 eV and the P_{b1} centers to D_{it} is through the significant +/0 and 0/- levels at approximately E_v + 0.45 eV and E_v + 0.8 eV [69]. In addition to passivation of the dangling bonds, incorporation and bonding of deuterium to other defects in the structural transition region (including strain, sub oxide states) near the interface are known and is discussed in detail in Section 5.3.1.

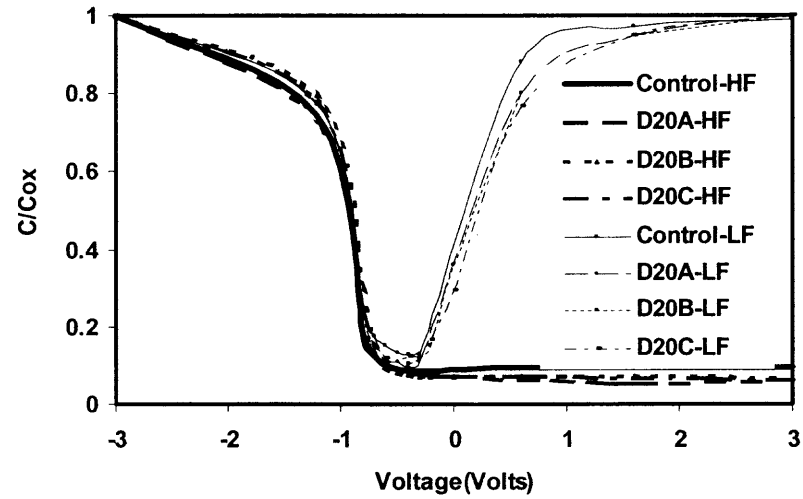

(a)

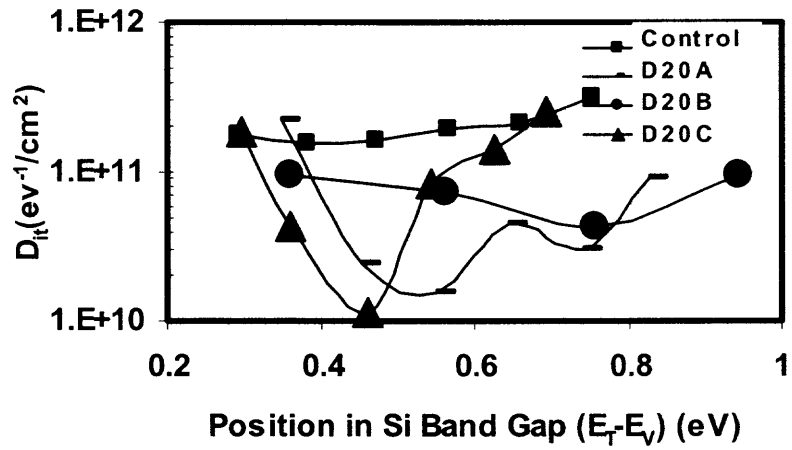

(b)

Figure 5.2 20keV Deuterium Implanted case for Dose-A (1x10 ^{13}/ cm^2), Dose-B (1x10 ^{14}/ cm^2) and Dose-C (1x10 ^{15}/ cm^2) (a) LF-HF C-V curves (b) Energy levels of the interface states (D_{it}) at the SiO_2 interface in the silicon band gap . The control device plotted for comparison.

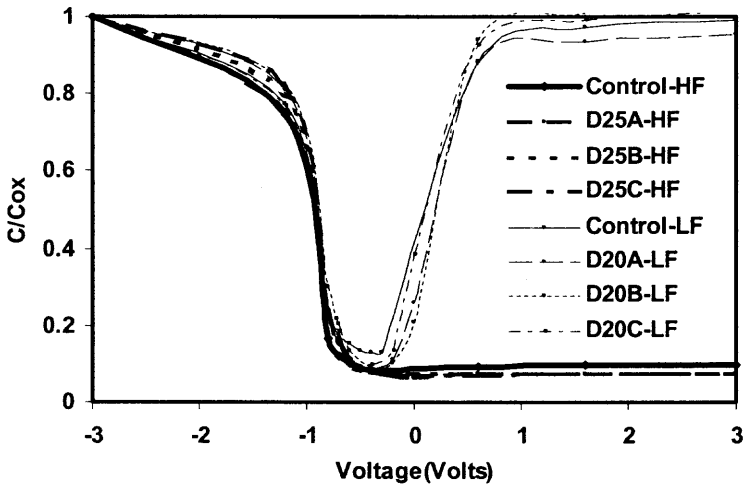

(a)

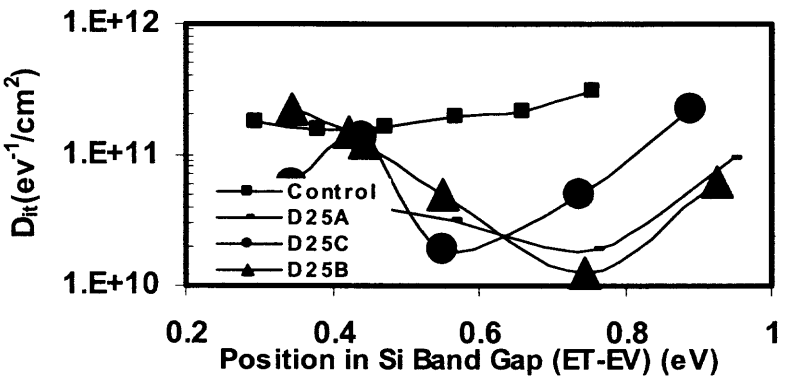

(b)

Figure 5.3 25keV Deuterium Implanted case for Dose-A (1x10 ^{13}/ cm^2), Dose-B (1x10 ^{14}/ cm^2) and Dose-C (1x10 ^{15}/ cm^2) (a) LF-HF C-V Curves (b) Energy levels of the interface states (D_{it}) at the SiO_2 interface in the silicon band gap . The control device plotted for comparison.

Figure 5.4 and Figure 5.5 shows the HF-LF and the D_{it} distribution curves for the implantation condition D30B (deuterium 30keV, 1x10 ^{14}/ cm^2), D30C (deuterium 30keV, 1x10 ^{15}/ cm^2) and D35B (deuterium 35keV, 1x10 ^{14}/ cm^2), D35C (deuterium 35keV, 1x10 ^{15}/ cm^2) cases respectively. The HF curves do not show any flatband voltage shift indicating improvement in the oxide and the interface. This is reflected in the D_{it} distribution graph, which shows not much improvement, compared to the control case for both 30keV and 35keV. This effect can be attributed to the higher implanted range and higher implantation damage for the above cases, as shown in Table 4.2. The increased damage is also indicated in Figure 4.6. With the increase in the damage, the defect centers act as a sink for the impurities; this inhibits the ions movement to the interface during the oxide growth [51]. This is also reflected from the SIMS profile (Figure 4.15) wherein a reduced concentration is obtained at the interface for D35C compared to D20B, which leads to a reduced passivation of the interface states in higher energies of implantation.

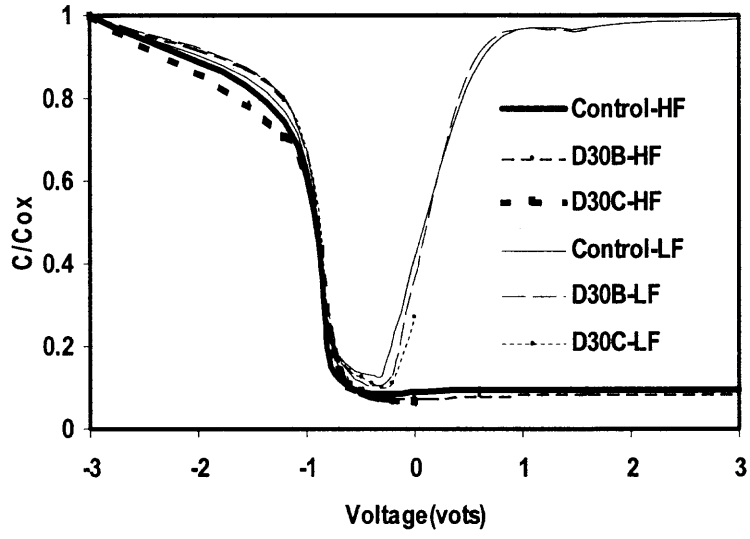

(a)

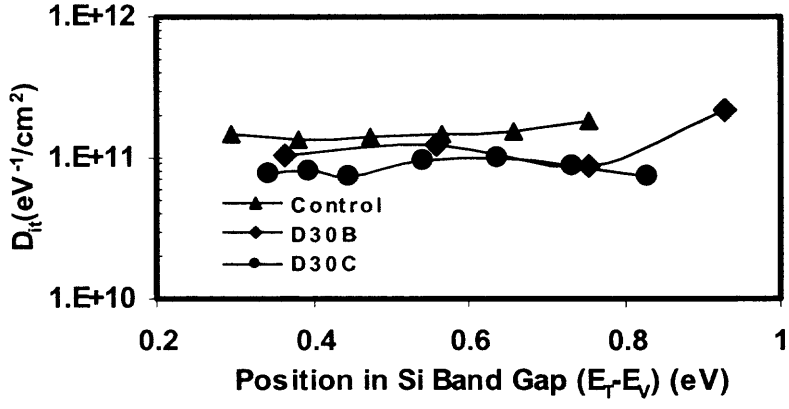

(b)

Figure 5.4 30keV Deuterium Implanted case for Dose-B (1x10 ^{14}/ cm^2) and Dose-C (1x10 ^{15}/ cm^2) (a) LF-HF C-V curves (b) Energy levels of the interface states (D_{it}) at the SiO_2 interface in the silicon band gap. The control device plotted for comparison.

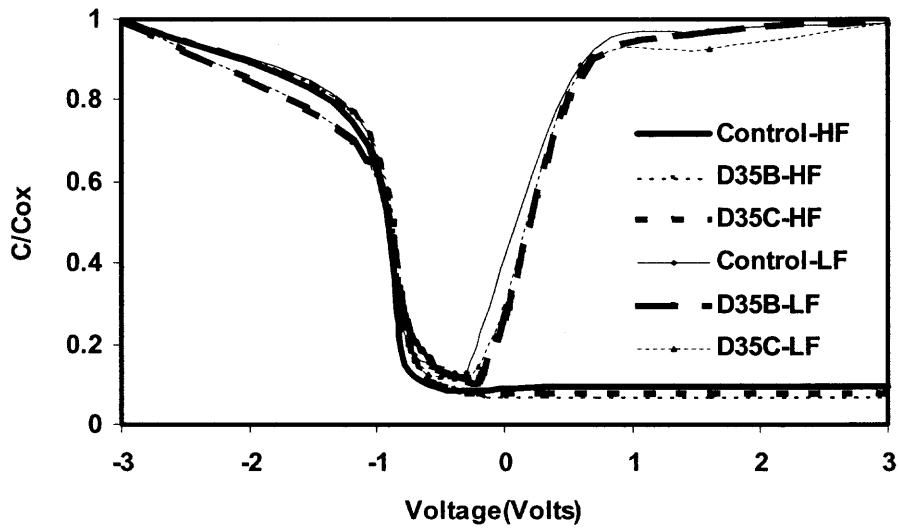

(a)

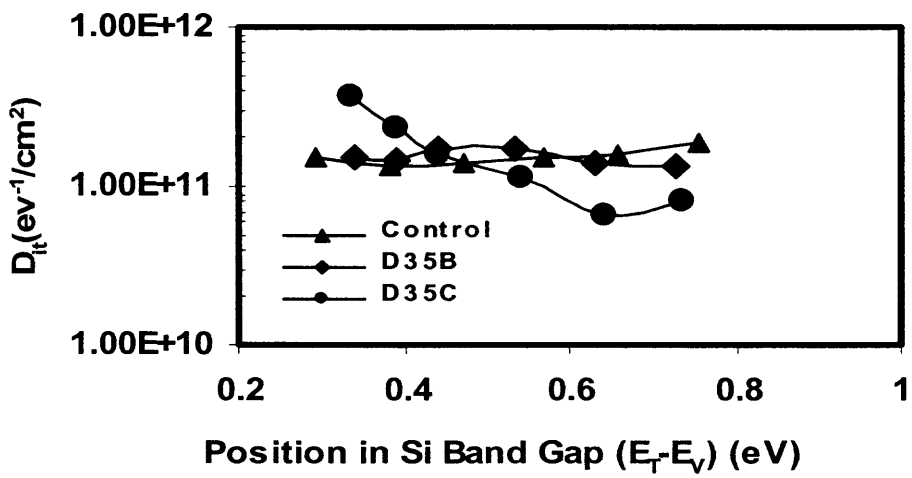

(b)

Figure 5.5 35keV Deuterium Implanted case for Dose-B (1x10 ^{14}/ cm^2) and Dose-C (1x10 ^{15}/ cm^2) (a) LF-HF C-V curves (b) Energy levels of the interface states (D_{it}) at the SiO_2 interface in the silicon band gap. The control device plotted for comparison.

5.1.2 Comparison of Various Energies for Deuterium

Figure 5.6 shows the lowest value of midgap D_{it} for various cases of deuterium implantation From the D_{it} distribution it is clearly evident that for control case interface states is high with a value $1.4x10^{11}eV^{-1}cm^{-2}$. It is observed that D_{it} decreases initially with increase in the implantation energy (15-25keV) but increases again once the implantation energy is increased further (25-35keV) for implantation doses, Dose-B and Dose-C. The line shown in Figure 5.6 serves as a visual guide. A significant improvement in the obtained value of D_{it} is observed for Dose-B for the implantation energies 20 and 25 keV. For 20 KeV, Dose-B the obtained value of D_{it} is $1.1x\ 10^{10}\ eV^{-1}cm^{-2}$ and a higher value for Dose-C, which is $7.4x\ 10^{10}\ ev^{-1}\ cm^{-2}$; For 25keV, Dose-B the obtained value of D_{it} is $1.2x\ 10^{10}\ eV^{-1}cm^{-2}$ and for Dose-C is $1.9x\ 10^{10}\ ev^{-1}\ cm^{-2}$. For devices with implantation energies 30 and 35 keV, on the other hand, the interface states were lower for Dose-C compared to Dose-B even though the overall D_{it} is much higher compared to 20 and 25 keV.

Dose-A ($1x10^{13}/cm^2$) was only used for 20 and 25 keV implantation energies where the devices show comparable results to that of Dose-B. The explanation to the above can be given based on the implantation range, damage peak produced, the interactions of the ions with the defects during the oxide growth, interstitials and dislocations induced in the substrate during oxidation and the diffusion of the ions during oxidation giving rise to the passivation of the dangling bonds.

For devices implanted at 15keV the implantation depth being shallow (Table 4.2), have lead to the out diffusion of the ions after implantation and during oxide growth showing similar passivation as the control case. The observed degradation in passivation

of Dose-C compared to Dose-B could be accounted due to the dose governed damage peak effect. Figure 4.11 shows the damage profile obtained. It is observed that with increase in the dose the damage induced in the silicon substrate increases at a much higher rate. The peak implantation damage being shallower in 15keV, and the defect density being more in Dose-C compared to Dose-B induces more damage in the growing oxide, which is reflected as an increase in the oxide charges and degraded interface passivation.

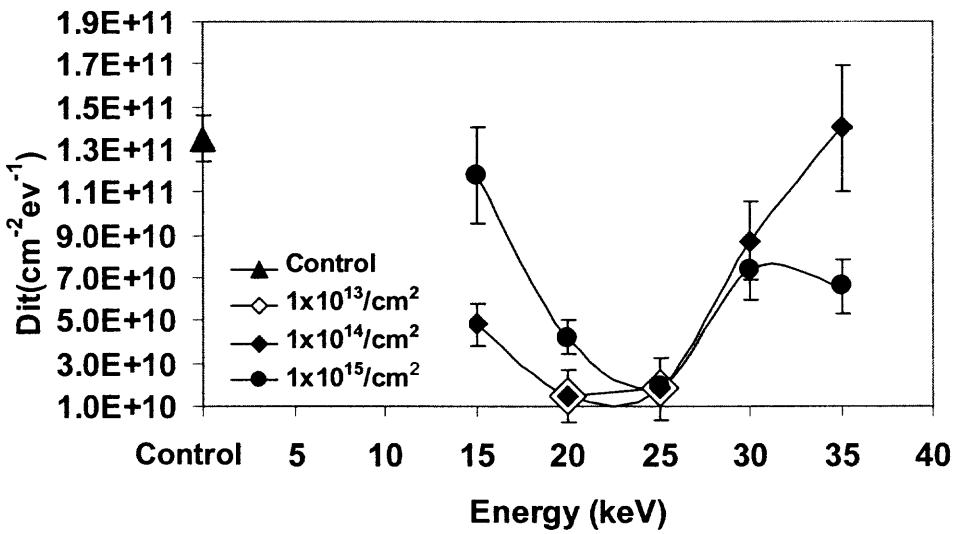

Figure 5.6 Interface state density D_{it} as a function of deuterium implantation energy at different doses indicates that an optimal interface passivation is possible in the range of 20-25keV implantation energies with a dose of $1x10^{14}/cm^2$ (Dose-B).

Similar arguments are valid for 20 and 25keV deuterium-implanted devices where Dose-B has shown better D_{it} values compared to Dose-C. However, the thermal budget during oxide growth is such that optimal interface passivation was observed for devices with deuterium implanted at 20keV with Dose-B. Observed from SRIM simulation results (Figure 4.9) the vacancy created during implantation increase rapidly with

increase in dose, which has resulted in a degraded interface passivation in case of Dose-C ($1x10^{15}/cm^2$) compared to Dose-B ($1x10^{14}/cm^2$).

In case of 30keV and 35keV implantation cases even though the implantation damage is relatively higher deuterium has to travel a longer distance to reach at the interface. Figure 4.3 and Table 4.1 show the comparison of the implantation-projected range for all cases of deuterium implantation. Since simultaneous annealing of defects during oxide growth is expected the peak deuterium concentration immediately after implantation will make a difference. It is believed the higher peak concentration of deuterium and higher implantation straggle, as computed from SRIM simulation, shown in Table 4.2, for devices implanted 35keV with Dose-C ($1x10^{15}/cm^2$) has resulted in better D_{it} values.

5.1.3 Hydrogen Implantation

Figure 5.7 and Figure 5.8 show the HF-LF and Dit distribution in the band gap for hydrogen implantation case for 20keV and 25keV respectively. The LF plots for control case show a comparatively high value of the capacitance and distortions compared to both the hydrogen-implanted conditions indicating high interface states. Similar results are observed for the 25keV case indicating the presence and passivation of hydrogen atoms at the interface and in the oxide.

The D_{it} distribution graph clearly indicates Dose-B has lower value midgap D_{it} compared to the Dose-C. This behavior can be attributed to defect creation during implantation, which increases with dose, as also observed in case of deuterium implantation.

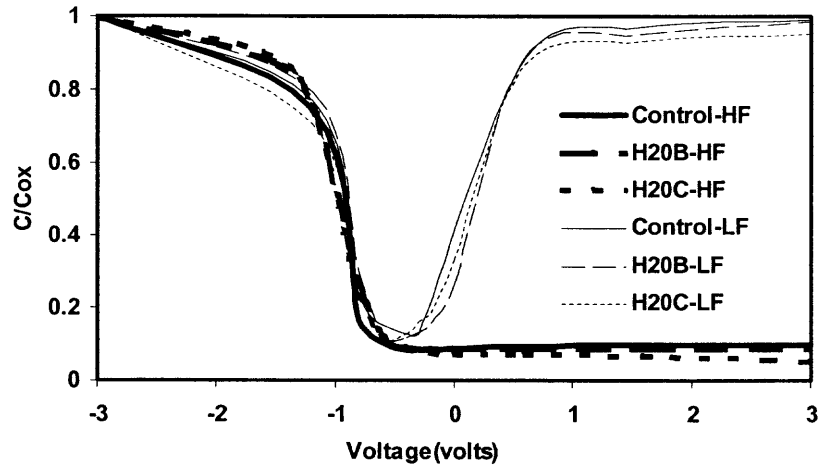

(a)

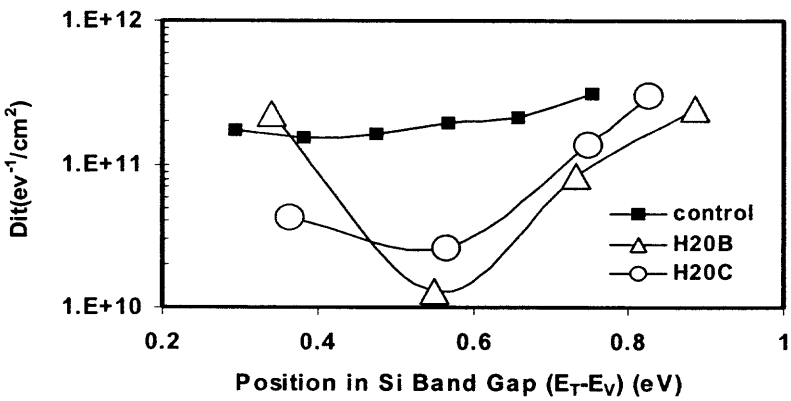

(b)

Figure 5.7 20keV hydrogen implanted case for Dose-B (1x10 ^{14}/ cm^2) and Dose-C (1x10 ^{15}/ cm^2) (a) LF –HF C-V curves (b) Energy levels of the interface states (D_{it}) at the SiO_2 interface in the silicon band gap. The control device plotted for comparison.

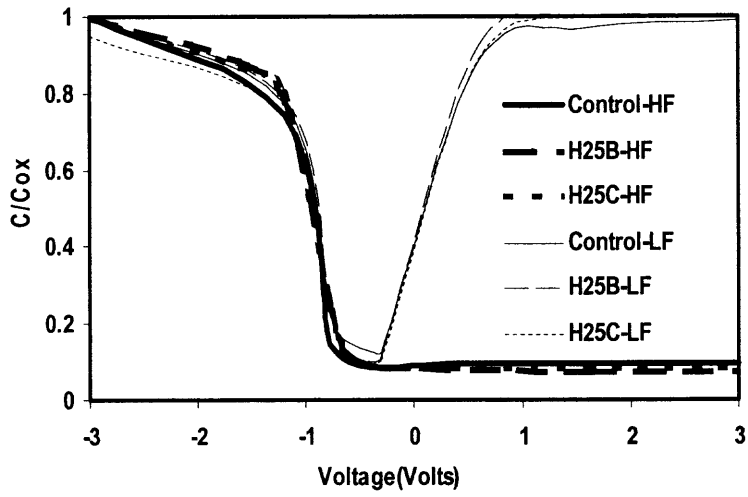

(a)

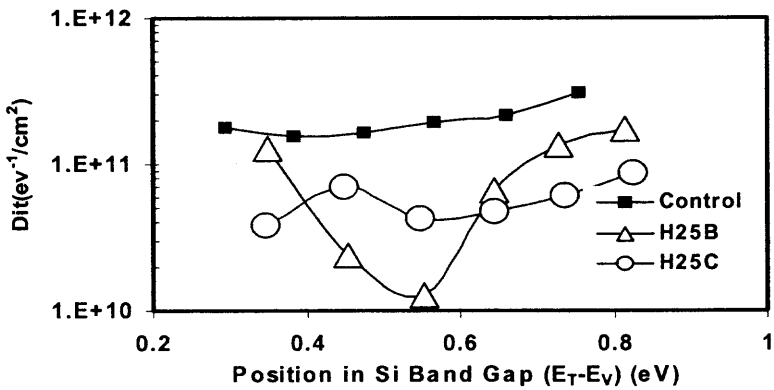

(b)

Figure 5.8 25keV Hydrogen Implanted case for Dose-B (1 x 10 ^{14}/cm^2) and Dose-C (1 x 10 ^{15}/cm^2) (a) LF-HF C-V curves (b) Energy levels of the interface states (D_{it}) at the SiO_2 interface in the silicon band gap. The control device plotted for comparison.

5.1.4 Hydrogen Versus Deuterium Implantation

The details of the passivation of the dangling bonds at the interface was evaluated for both deuterium and hydrogen implantation for investigating for possible isotope effects. The hydrogen implantation was carried out at energies of implantation 20keV and 25keV. This was based on the initial simulation results as discussed in Chapter 4. All experiments were performed with Dose-B ($1x10^{14}/cm^2$) and Dose-C ($1x10^{15}/cm^2$) for both the implantation energies for hydrogen and deuterium. The low frequency and high-frequency C-V measurements for both hydrogen and deuterium implanted devices along with D_{it} distributions are given in Figure 5.9 and Figure 5.10 for 20keV and 25keV respectively. The C-V characteristic of the control sample has also plotted for reference.

From the LF curves obtained for the hydrogen and deuterium implanted cases, Figure 5.9(a), (b) and Figure 5.10(a), (b) it is observed that the distortions obtained in the curves is less and the capacitance obtained is found to be lower in the depletion region compared to the control case, which suggests an improvement (Section 3.3.1) in the interface for the implanted devices. The C-V characteristics suggest an identical passivation behavior in both hydrogen and deuterium implanted cases. The improved passivation for the implanted devices is seen in Figure 5.9(c), (d) and 5.10(c), (d). The high frequency C-V characteristics show a shift closer to the ideal flat band for deuterium and hydrogen implanted devices compared to control sample indicating the incorporation of hydrogen and deuterium ions at the interface and in the bulk oxide. The retention and incorporation of deuterium at the interface and the bulk SiO_2 ions after gate oxidation can be clearly observed from Figure 4.13.

Out of all cases Dose-B is the most optimized implantation dose for both deuterium and hydrogen that passivates the interface states.

By carefully comparing the interface state density D_{it} distribution in silicon bandgap for both hydrogen and deuterium (Figure 5.9) and (Figure 5.10) it is noticed that there is no significant difference in interface states for Dose-B but there is a difference observed in Dose-C. But in both the cases the interface states are significantly lower compared to control devices. But in case of Dose-C the D_{it} values for deuterium-implanted device is higher than that of hydrogen-implanted device for 20keV but lower for 25keV.

For 20keV, Dose-B, hydrogen-implanted devices the value of D_{it} is1.2x 10^{10} $eV^{-1}cm^{-2}$ and for deuterium implanted devices it is 1.1x 10^{10} $eV^{-1}cm^{-2}$ and for Dose-C case hydrogen-implanted devices the value of D_{it} is 2.5x 10^{10} $eV^{-1}cm^{-2}$ and for deuterium-implanted devices it is 7.4x 10^{10} ev^{-1} cm^{-2}. This behavior can be attributed to defect creation during implantation, implantation depth and straggle and implanted ion concentration. For 25keV, Dose-B, hydrogen-implanted devices the value of D_{it} is 1.28x 10^{10} $eV^{-1}cm^{-2}$ and for deuterium implanted devices it is 1.2x 10^{10} $eV^{-1}cm^{-2}$ and for Dose-C case hydrogen-implanted devices the value of D_{it} is 4.23x 10^{10} $eV^{-1}cm^{-2}$ and for deuterium-implanted devices it is 1.9x 10^{10} ev^{-1} cm^{-2}.

As shown in Figure 4.8 the vacancy creation based on SRIM simulation immediately after the implantation and before any annealing is almost identical for hydrogen and deuterium implantation in case of Dose-B for both 20keV and 25keV implantation energies. In case of Dose-C, significant difference in vacancy creation due to implantation was observed for both the implantation energies. Because of the depth

difference D20C devices showed worse D_{it} values (Figure 5.9(b)) compared to H20C (hydrogen 20keV, 1x10 ^{15}/ cm^2) whereas D25C (deuterium 25keV, 1x10^{15}/ cm^2) devices showed better D_{it} values compared to H25C devices. For Dose-C and 20keV implantation energy it is possible that the deuterium diffuses to the vacancies instead of the interface and the implantation damage is not sufficiently annealed, but for hydrogen case the damage produced is less and also the diffusing species can reach faster to the interface. Figure 5.11 shows the comparison of the D_{it} for the hydrogen and deuterium implanted cases.

From the D_{it} distribution it is clearly evident that in deuterium-implanted at 20keV and 25keV with a dose of 1x10^{14}/cm^2 (Dose-B) and devices at 20keV with a dose of 1x10^{15}/cm^2 (Dose-C) P_b centers above the midgap are passivated. The high concentration of the D/H near the interface may be caused (in addition to the dangling bond passivation) by deuterium bonding to other defects in the structural transition region (including strain, sub oxide states) near the interface. It is known that silicon-dangling bonds are not only the primary source for deuterium accumulation at the interface [70]. Other than the silicon dangling bonds, deuterium accumulation also, arises from the breaking of strained Si-Si and/or Si-O bonds at the interface to form unstrained Si-D and Si-OD bonds. Also an alternate possibility of deuterium being incorporated in the strain filed at the interface [71]. The trap sites due to O-Vacancy and Si-Si weak bonds at the interface produce trap states at the energy range higher than the midgap, whereas Si-O weak bonds at the interface produce trap states at the energy lower than the midgap [72]. The energy levels of these trap states vary with changing bonding parameters such as bond lengths and bond angle. Therefore, the shift in the D_{it} level in the energy band gap

for deuterium implantation case indicates the interaction of deuterium with the others defects other than the dangling bonds such as Si-Si weak bonds and Si-O weak bonds which are possible origins of the obtained interface states distribution in silicon bandgap.

Hydrogen and deuterium are electronically equivalent as static electronic structure of S-H and S—D bonds are identical [31]. The difference in behavior can be attributed to dynamics of these bonds. As discussed earlier, implanted deuterium and hydrogen ions initially tend to diffuse to the defect sites that were formed during implantation damage. If these ions initially passivate the bulk dangling bonds the mechanism of these ions diffusing to interface during oxidation (annealing) will be entirely different because of the isotope effect.

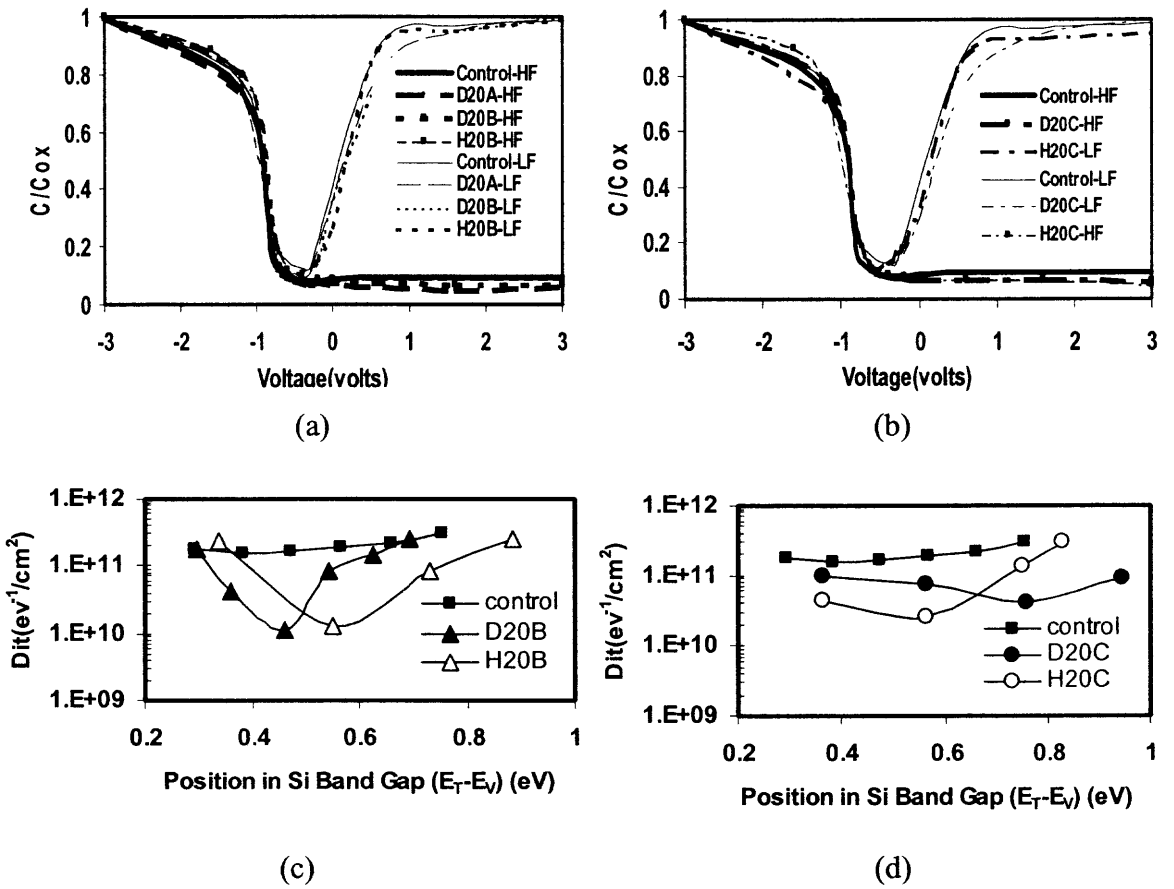

Figure 5.9 Comparison of deuterium versus hydrogen implantation for 20keV (a) LF-HF C-V curves for all Dose-A and Dose-B (1 x $10^{14}/cm^2$) (b) HF-LF C-V Curves for all Dose-C (1 x $10^{15}/cm^2$) (c) Energy levels of the interface states (D_{it}) at the SiO_2 interface in the silicon band gap for devices with implantation energy 20keV For Hydrogen and Deuterium for Dose-B (d) Energy levels of the interface states (D_{it}) at the SiO_2 interface in the silicon band gap for devices with implantation energy 20keV For Hydrogen and Deuterium for Dose-C. The control device plotted for comparison.

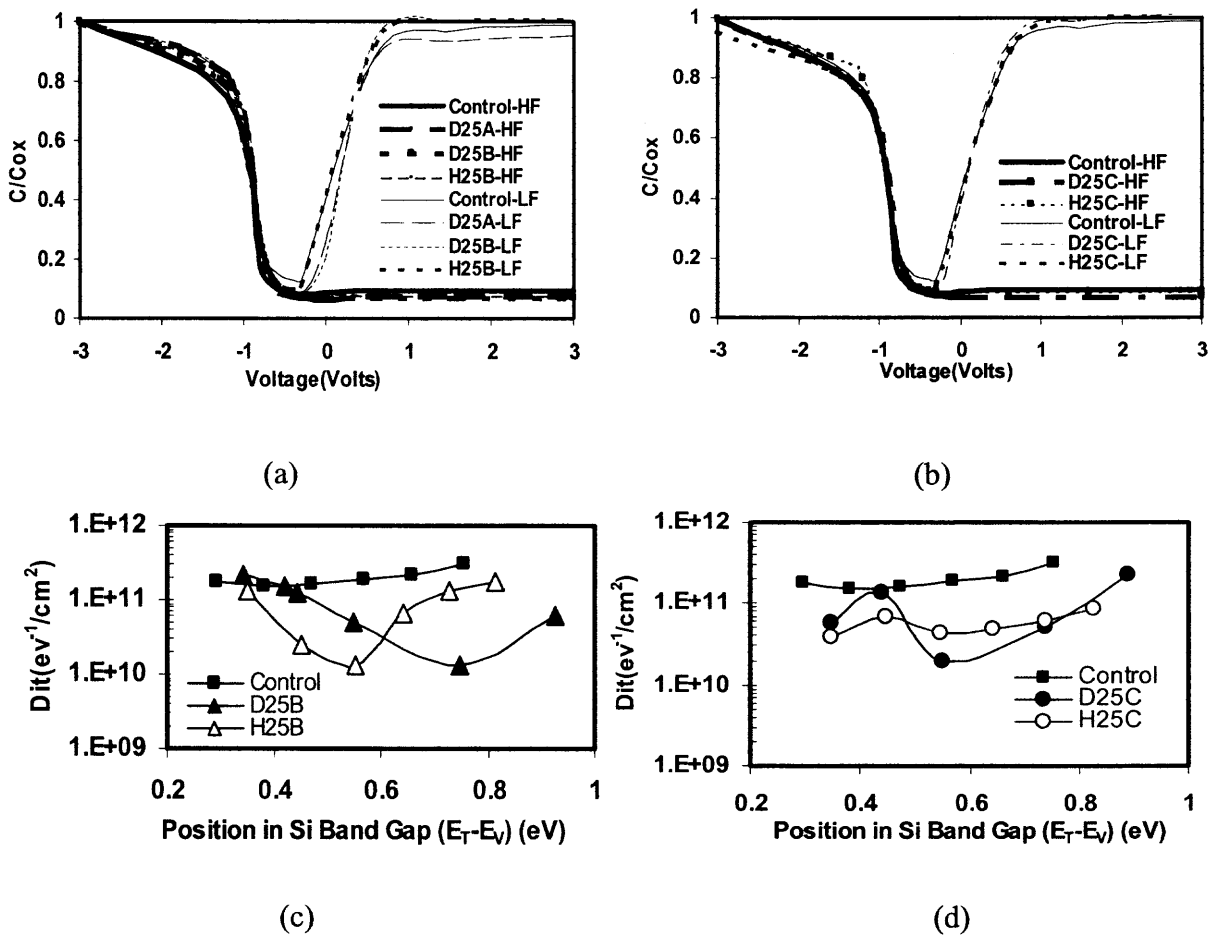

Figure 5.10 Comparison of deuterium versus hydrogen implantation for 25keV (a) LF-HF C-V curves for all Dose-A and Dose-B (1 x $10^{14}/cm^2$) (b) HF-LF C-V Curves for all Dose-C (1 x $10^{15}/cm^2$) (c) Energy levels of the interface states (D_{it}) at the SiO_2 interface in the silicon band gap for devices with implantation energy 25keV for Hydrogen and Deuterium for Dose-B (d) Energy levels of the interface states (D_{it}) at the SiO_2 interface in the silicon band gap for devices with implantation energy 25keV For Hydrogen and Deuterium for Dose-C . The control device plotted for comparison.

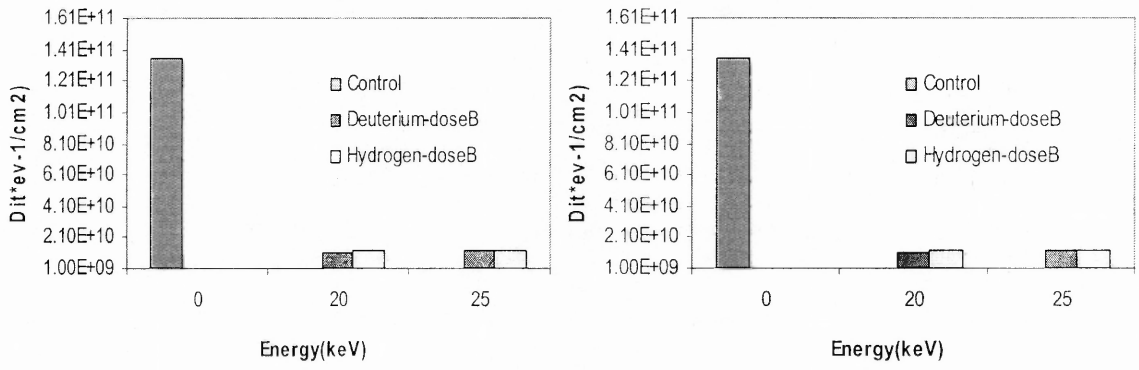

Figure 5.11 Comparison of interface states between hydrogen and deuterium implanted devices at different implantation energies and doses where (a) Dose-B and (b) Dose-C.

5.2 Diffusivity Estimation

In this section the diffusivity of deuterium during oxidation step has been estimated. The diffusion coefficient is computed separately for each case of the implantation condition. The diffusion coefficient is computed using the equation [59]

$$x_j = 2\sqrt{Dt}\left(\ln\frac{C_s}{C_{sub}}\right)^{1/2}$$

C_S = Peak Concentration of the implanted ions, C_{sub} = the concentration of the deuterium ions at the interface, t = the time the ions undergo diffusion, D = Diffusivity, X_j = Projected range of the implanted ions

C_{sub} was estimated by computing the concentration of deuterium ions at the interface for each case, which was obtained by comparing D_{it} in each case with that of the D_{it} of the control case. The Pb density was computed from the D_{it} using the relationship $2*Pb = 1.1*D_{it}$ [28]. The units of Pb are cm^{-2}. The volume concentration was obtained by dividing in to very small intervals Δx – in which the concentration is assumed to be

constant and also the interface between Si and SiO_2 is of thickness 1nm. The interval value was assumed to be 1nm to compute the volume concentration. The computed values for diffusivity for various conditions of deuterium implantation are shown in Table 5.1 (a), (b) and (c) for Dose-A, Dose-B and Dose-C respectively. Figure 5.12 shows the diffusivity plot for where the diffusivity for Dose-C obtained is lower compared to Dose-B. The diffusivity of deuterium in silicon was obtained to be $4.0x10^{-15}/cm^2$ [73] at 350^0C. The diffusivity of deuterium in silicon is expected to be higher than $4.0x10^{-15}cm^{-1}sec^{-1}$ in single crystal silicon at 350 °C since the temperature is higher in our case. Besides, the diffusivity of the ions is also governed by the implantation damage [74], wherein the disordered regions both at the surface and subsurface, directly inhibit the movement of deuterium. Since the damage induced to the substrate increases with dose, Figure 4.8, the reduced diffusivity obtained in case of Dose-C compared to Dose-B of implantation is due to the effect of the damage-inhibited diffusion. The disordered regions act as a sinks, gettering centers [74, 75] for diffusing deuterium and accumulation of the ions (deuterium) in these regions accounts for the low diffusivity obtained for a higher dose of implantation during oxidation. It is also known that the diffusivity of H in a-Si is known to slower than in C-Si [77].

Simultaneous oxide growth and diffusion also adds a contributing factor to the obtained diffusivity. During oxidation the injection of interstitials and dislocations [60] will lead to oxidation retarded diffusion in the present case, as the diffusion of hydrogen is governed by {H-V} mechanism [78].

With the increase in energy for a particular dose of implantation, the diffusivity increases though the magnitude being significantly lower compared to the dose effect

(Dose-C leading to a lower diffusivity compared to Dose-B). The increase in the diffusivity with the increase in the energy can be attributed to the effect of the surface damage. Figure 4.8 shows that the surface damage (near interface) decreases with the increase in energy. Simultaneous oxidation, diffusion, low peak implanted projected range and greater surface damage induced in case of low energy of implantation leads to increased damage inhibited diffusion which contributes to low diffusivity compared to higher energies of implantation.

The diffusivity has also been estimated from the SIMS concentration profile. The final concentration obtained at the interface, C_{sub} was obtained from the concentration profile of SIMS. Table 5.2 shows the obtained interface and peak concentration from SIMS profile and the computed diffusivity. The diffusivity obtained from this case also has been plotted for cases of implantation D20B, D20C and D25B as shown in Figure.5.12, which shows a close relationship to the derived diffusivity from the Dit.

Table 5.1 Range, Peak Concentration, Diffusivity and concentration of ions at the interface for various conditions of deuterium implantation (a) Dose-A ($1x10^{13}/cm^2$) (b) Dose-B($1x10^{14}/cm^2$) (c) Dose-C($1x10^{15}/cm^2$).

DOSE A ($1 \times 10^{13}/cm^2$): (a)

Energy	Range (um)	Peak Concentration Cs (cm^{-3})	Diffusivity (cm^{-2} sec^{-1})	Concentration at the interface C_{sub} (cm^{-3})
15Kev				
20Kev	0.2970	4.1841E+17	2.18852E-13	1.81062E+17
25Kev	0.3520	3.5587E+17	3.01595E-13	1.46683E+17
30Kev				
35Kev				

DOSE B ($1 \times 10^{14}/cm^2$): (b)

Energy	Range (um)	Peak Concentration Cs (cm^{-3})	Diffusivity (cm^{-2} sec^{-1})	Concentration at the interface C_{sub} (cm^{-3})
15Kev	0.2400	4.5997E+18	3.4776E-14	1.65915E+17
20Kev	0.2970	4.1841E+18	5.90563E-14	1.87724E+17
25Kev	0.3520	3.5587E+18	8.51588E-14	1.54206E+17
30Kev	0.4012	3.4572E+18	8.53582E-14	5.19787E+16
35Kev	0 .4479	3.2076E+18	9.28012E-14	2.40469E+16

DOSE C ($1 \times 10^{15}/cm^2$): (c)

Energy	Range (um)	Peak Concentration Cs (cm^{-3})	Diffusivity (cm^{-2} sec^{-1})	Concentration at the interface C_{sub} (cm^{-3})
15Kev	0.2400	4.5997E+19	1.59182E-14	3.24202E+16
20Kev	0.2970	4.1841E+19	3.21925E-14	1.40793E+17
25Kev	0.3520	3.5587E+19	4.8676E-14	1.46683E+17
30Kev	0.4012	3.4572E+19	5.72307E-14	6.60563E+16
35Kev	0 .4479	3.2076E+19	7.34719E-14	6.63694E+16

Table 5.2 Range, Peak Concentration and concentration of ions at the interface for various conditions of deuterium implantation obtained from SIMS profile and the computed diffusivity.

Implantation Condition	Range (um)	Peak Concentration Cs (cm^{-3})	Diffusivity (cm^{-2} sec^{-1})	Concentration at the interface C_{sub} (cm^{-3})
20keV-DoseB	0.325	$6.1x10^{18}$	6.24028E-14	$7.8x10^{17}$
25keV-DoseB	0.390	$5.9x10^{18}$	8.51769E-14	$5.8x10^{17}$
20keV-DoseC	0.325	$6.1x10^{19}$	2.76704E-14	$6.5x10^{17}$

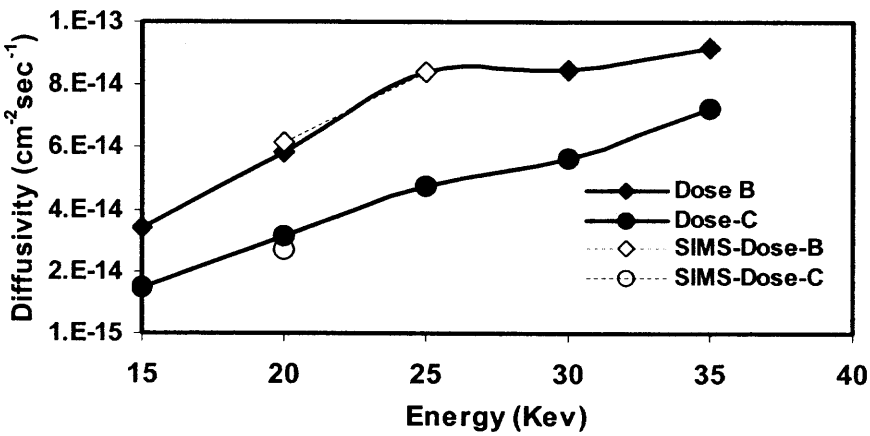

Figure 5.12 Diffusivity estimated for the implanted deuterium ions during gate oxidation. Indicates higher diffusivity for Dose-B ($1x10^{14}/cm^2$) compared to Dose-C ($1x10^{15}/cm^2$). The diffusivity obtained from SIMS is also shown.

5.3 Annealing Results

The samples fabricated under the same conditions underwent the annealing at various conditions as has been discussed in Chapter 3. The annealing was carried out at three different conditions- 600°C and 700°C for 20 min in nitrogen atmosphere which will be referred to as annealing condition A1, A2 respectively. This was carried out to study the movement and understand the effect of the implanted ions in the substrate and at the interface and further investigate the effect of the damage induced degradation. The following section describes the discussion of the variation of D_{it} obtained under various annealing conditions for both deuteriun and hydrgen cases of implantation.

5.3.1 Deuterium Implantation

Figure 5.13 (a) and (b) shows the value of D_{it} computed for Dose-B and Dose-C case respectively for all the cases of implantation with the variation in annealing condition. The control case has also been plotted for reference. The interface states of the control-annealed wafer is found to improve after subjected to annealing A1, which indicates that initial post oxidation annealing eliminates some interface defects [17]. On further annealing at a higher temperature at condition A2, the interface state density shows no additional variation.

For the dose $1x10^{14}/cm^2$ for energies of implantation 20keV, 25keV, 35keV it is observed the interface degrades Figure 5.13(a), with the increase in the annealing temperature compared to the non-annealed case. Since this behavior is different from the control sample, which showed an improvement at the interface, this is clearly due to the deuterium ions, which is known to out diffuse from the oxide with increase in the temperature [2].

For the dose $1x10^{15}/cm^2$ for energies of implantation 15keV, 20keV, 25keV, 30keV, 35keV, the interface state density decreases after being subjected to annealing condition A1, which is due to the repair of the damage and incorporation of diffused deuterium ions from the damaged regions leading to the passivation of the interface states. On further annealing at condition A2 the interface degrades indicating an effect similar to Dose-B case of implantation indicating an out diffusion of the passivated ions.

5.3.2 Hydrogen Implantation

Figure 5.14 shows the effect of annealing for hydrogen implantation case. The degradation of the interface with the temperature clearly indicates the out diffusion of the ions with the increase in the temperature.

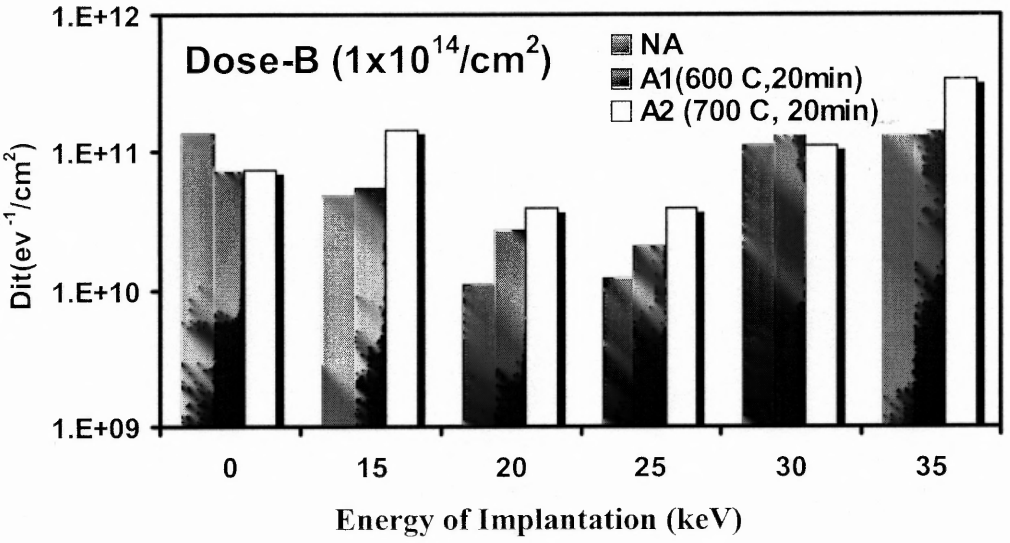

(a)

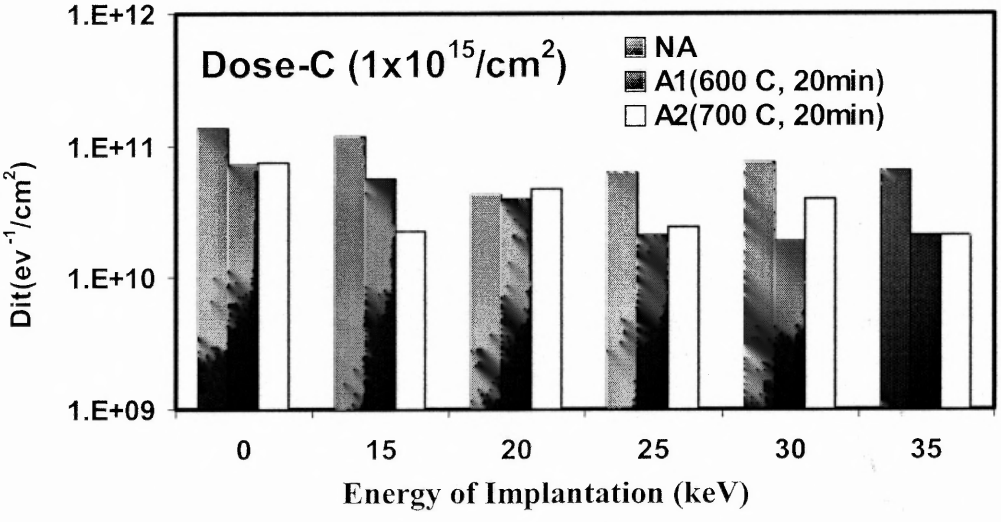

(b)

Figure 5.13 Comparison of D_{it} for Deuterium Implanted devices at various annealing temperatures –Non-annealed (NA), 600°C (A1) and700°C (A2) anneal. The control case has also been plotted (a) Dose-B at different annealing temperature (b) Dose-C at different annealing temperature

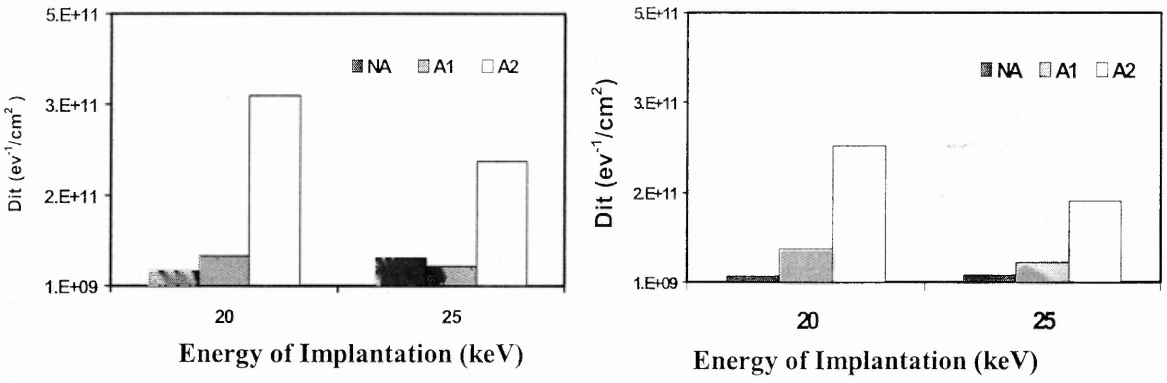

Figure 5.14 Comparison of D_{it} for Hydrogen Implanted devices at various annealing temperatures –Non-annealed (NA), 600^0C (A1), 700^0C (A2) anneal for 20keV and 25keV energy of implantation. The control case has also been plotted (a) Dose-B at different annealing temperature (b) Dose-C at different annealing temperature.

5.4 Summary

In this Chapter incorporation of deuterium ions at the oxide / Si-interface when gate oxide was grown on deuterium-implanted silicon substrate has been investigated. An optimization of the implantation condition has been studied in detail for maximum incorporation of deuterium ions at the interface and thereby effective passivation of the dangling bonds. This has been extended further to study the effect of annealing at various temperatures following ion implantation. Hydrogen implantation also has been carried out at certain conditions (conditions at which deuterium implanted devices yielded best results) to investigate the isotope effect.

Deuterium implanted at energies 15keV, 30keV, 35 keV did not yield significant improvement in interface states compared to the control case. On the other hand at 20keV and 25keV significant reduction in the value of D_{it} was observed. A study of the variation of the dose at these two energies yielded the best result with an implantation dose of

$1x10^{14}$atoms/cm^2. At higher doses more damage is being induced in the substrate, which acts as a sink for the implanted ions that inhibits the diffusion of the ions to the interface. Confirmation of this mechanism was obtained further when the devices with high energy and dose of implantation were subjected to annealing. An improvement in the D_{it} value was obtained for the devices implanted at 30Kev and 35Kev and at dose of $1x10^{15}$atoms/cm^2 when subjected to annealing at higher temperatures indicating the repair of the damage and thereby diffusion of the ions towards the interface.

Comparison of deuterium and hydrogen implanted devices under similar conditions showed lower values for D_{it} in deuterium-implanted devices. However for dose-$1x10^{15}$atoms/cm^2 (Dose-C) case the D_{it} value for deuterium-implanted device was higher than that of hydrogen-implanted device for 20keV. This can be attributed to lower diffusivity and higher damage in case of deuterium compared to hydrogen.

CHAPTER 6

RELIABILITY STUDY OF DEUTERIUM IMPLANTED DEVICES

This Chapter discusses reliability characteristics of the as fabricated devices in Section 3.2. The reliability study of the fabricated MOS capacitors was conducted using the time dependent dielectric breakdown measurements, which has been discussed in Section 3.3.3. The stress induced trap creation within the bulk of the oxide has been systematically studied by measuring the C-V, I-V and interface state density characteristics after subjecting to electrical stress to investigate the isotope effect. To further investigate the dose and energy induced damage effect on reliability; breakdown characteristics were also examined for the devices, subjected to high temperature anneal after oxide growth.

6.1 Breakdown Characteristics

Figure 6.1 shows the Weibull plot of charge to breakdown characteristics of devices for different cases of deuterium implantation. The X-axis of the plot show the charge to breakdown (Q_{BD}) and the Y-axis represents the failure rate, which has been computed from the cumulative % breakdown. It is observed that deuterium implanted samples-D20B and D25B exhibit a significant improvement in the charge to breakdown characteristics in comparison to the control device, the difference being three orders of magnitude greater (considering at the 63% failure level) in comparison to the control device. For devices implanted at D15B condition, the breakdown characteristics obtained are similar to the control case. For higher energies of implantation, in case of D30B and

D35B two orders of magnitude of improved reliability is obtained in comparison to control devices and an order of magnitude inferior reliability in comparison to D20B and D25B.

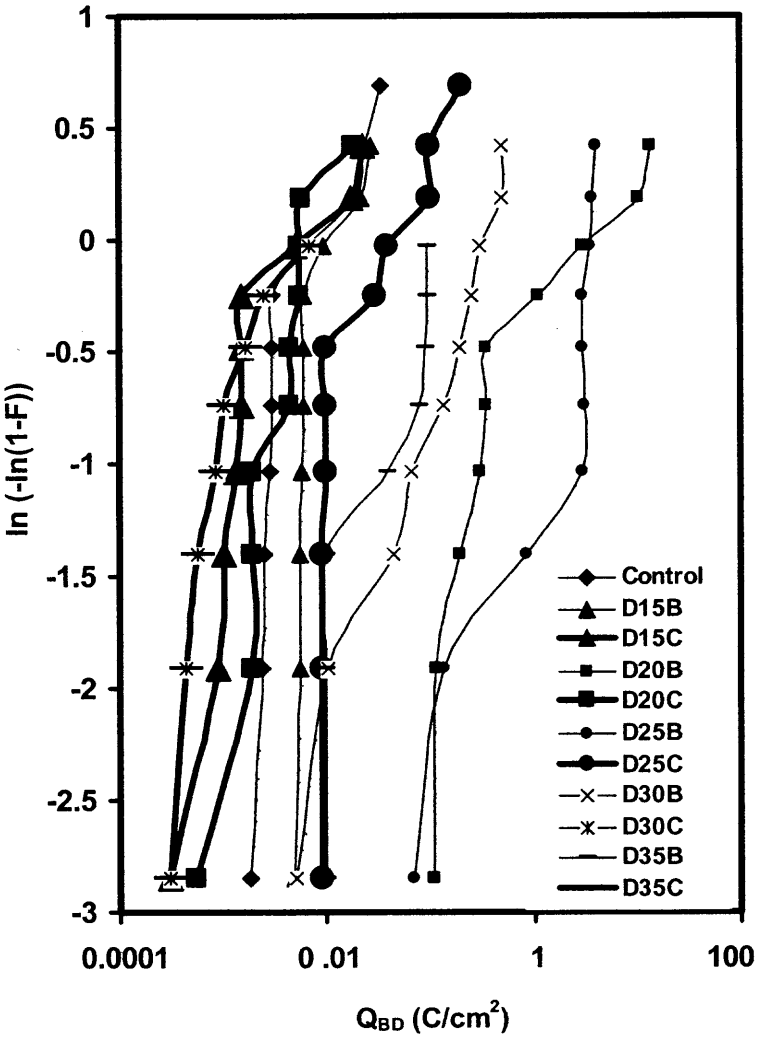

Figure 6.1 Weibull plot for Q_{BD} under constant voltage stress of –7V for different cases of deuterium implantation with variation in energy and dose of implantation.

For devices implanted at a higher dose, Dose-C it is observed that for D15C, D20C, D25C, D30C and D35C there is a degradation obtained in the breakdown characteristics compared to Dose-B case for implantation conditions- D15B, D20B, D25B, D30B and D35B cases respectively.

Devices implanted at low energy, for D15B and D15C no significant improvement in the interface passivation was obtained from the D_{it} results (Section 5.1.1). Out diffusion of the ions had resulted on account of shallow implantation induced peak depth. The out-diffusion of the deuterium ions has resulted in breakdown characteristics similar to the control case. On the other hand degradation in Q_{BD} for D15C is due to the implantation induced damage which increases with the dose of implantation as shown in Figure 4.9, which incorporates defects in the growing oxide leading to a of inferior quality oxide compared to the control device.

6.1.1. Devices with Lower Implantation Dose

The significant improvement in breakdown characteristics for D20B and D25B can be accounted for the effective passivation of the interface dangling bonds has been discussed in Section 5.1.1. During oxidation the chemical potential difference between SiO_2 and Si [11], drives the diffusion of implanted deuterium from the silicon substrate to the silicon oxide. Diffused deuterium atoms are not only incorporated at the Si/SiO_2 interface reacting with the interface dangling bonds to form Si-D bonds, but also form Si-D bonds in the bulk SiO_2 [66]. The distribution of deuterium is clearly seen from the SIMS results in Figure 4.15. The presence of deuterium at the interface and the bulk oxide, therefore, suppresses the hole-induced increase in the electron traps at the interface region during stress.

It has been reported that, the stability of Si-H bond increases when silicon atoms bond with large electronegative oxygen atoms [79]. It is known that, the strength of the Si-D bond that forms during oxidation is stronger than that of the Si-D bonds that passivates the interface dangling bonds by deuterium annealing. An observed 7% difference in the activation energy of desorption has been observed between deuterium pyrogenic oxide (deuterium incorporated during oxidation) compared to deuterium annealed oxides [68] in which case the deuterium atoms does not take part in the oxidation process, using thermal desorption spectroscopy. Therefore, it is believed that in the present case deuterium implantation brings about a more robust and a stable SiO_2 structure and a suppressed trap creation and enhanced reliability characteristics. Similar arguments are also valid for D30B and D35B, which shows an improvement in the reliability compared to the control case. The inferior reliability compared to D20B and D25B is governed by the implantation-induced damage, which increases with energy as shown in Figure 4.8.

6.1.2. Devices with Higher Implantation Dose

For a higher dose of implantation, Dose-C, incase of D20C, D25C, D30C and D35C it is observed that obtained Q_{BD} is lower compared to D20B, D25B, D30B and D35B cases respectively. Degradation of oxide reliability at higher implantation doses is contributed to the implantation induced substrate damages [80], which are not completely removed during the post-implantation annealing (gate oxide growth). It is known the greater implantation dose induces more damage to the silicon substrate (Figure 4.11), which affects the electrical properties of the device [80-83]. Degradation of the Si-substrate integrity for the case of higher implantation energy and dose is expected to affect the

quality of oxide growth by introducing defects in the oxide. Incorporation of implantation-induced defects from the substrate in to the oxide leads to more traps and trap generation in the oxide, which causes an increase in the leakage current. In addition, a defected Si substrate enhances the electron-hole recombination process leading to degradation of device performance and an increase of the D_{it} (discussed in Section 5.1.1).

6.2 Comparison with Hydrogen Implantation

The D_{it} measurements obtained for both hydrogen and deuterium-implanted devices showed identical passivation of the interface states for 20keV energy of implantation and a moderately improved passivation in case of deuterium implanted deices for 25keV case. Generation of interface states and the trap induced damage mechanism in the SiO_2 film has been studied by subjecting the hydrogen and deuterium implanted devices under F-N injection of electrons from the gate in order to further investigate and study the isotope effect. Only devices that provided the optimized results (D20B, D25B, H20B and H25B) along with control devices were subjected to a constant voltage stress. The experimental setup of which has been discussed in Section 3.3.2.

6.2.1 Stress Induced Leakage Current

The current vs. time plot for deuterium and hydrogen implanted devices during constant voltage stress was monitored and is shown in Figure 6.2. The deuterium and hydrogen samples do not breakdown even after 7000sec. There is no apparent fluctuation in the gate current during the stress for deuterium-implanted devices and the I-V characteristics (as shown in the inset-1 in the Figure 6.2) of the devices after 5000sec is almost identical to the fresh one.

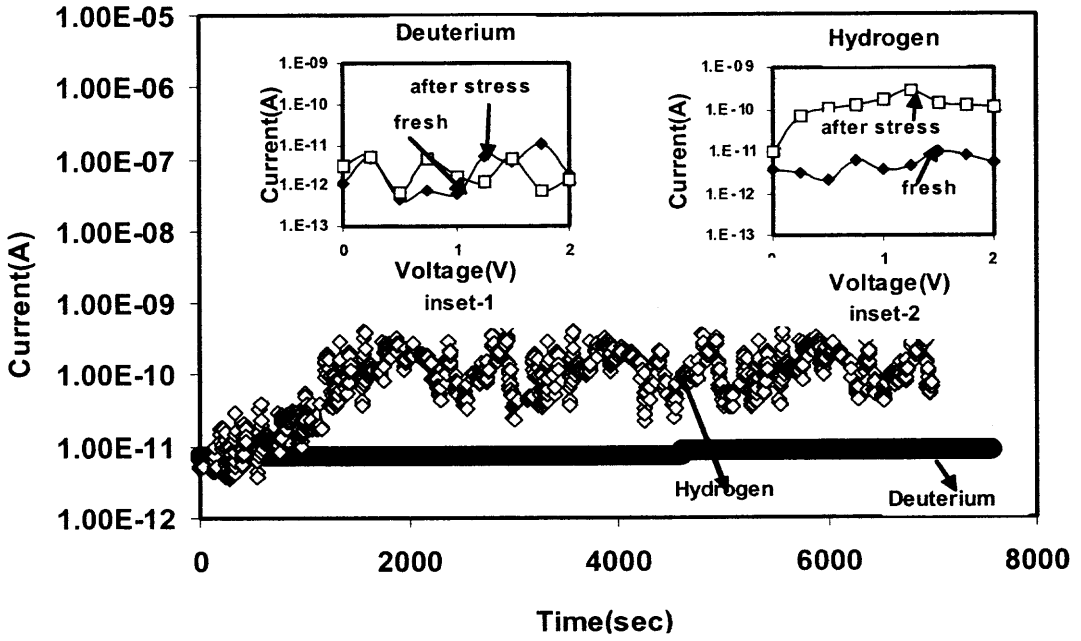

Figure 6.2 Gate current versus stress time plot of hydrogen and deuterium implanteddevices under a constant voltage stress with CVS -5V for 7500sec. The insets are the IV characteristics before and after stress. The insets are I-V characteristics before and after stress.

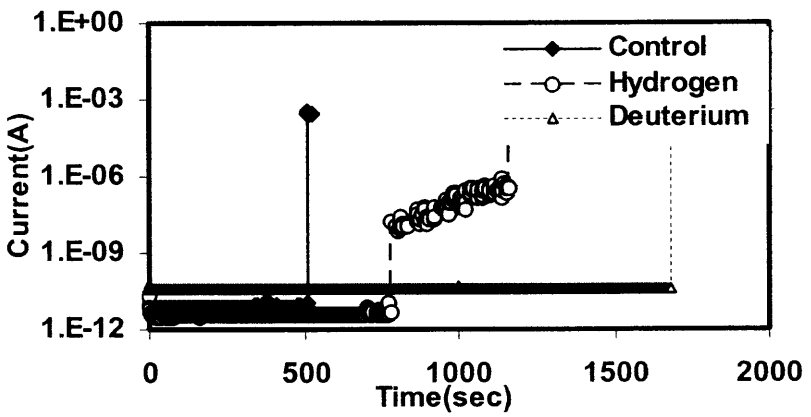

Figure 6.3 Gate current versus time plot for the control device, hydrogen and deuterium implanted device at –6V. Shows the comparison of the breakdown characteristics, indicating the longest time to breakdown for the deuterium-implanted device.

For hydrogen treated samples the fluctuation in the gate current under CVS implies that degradation in the oxide occurs [5] which is reflected in the increase in the stress-induced leakage current (SILC) after stress as shown in the inset-2 of Figure 6.2.

It is known that under constant voltage stress conditions, the injected electrons from the cathode gain kinetic energy from the oxide field and upon reaching the anode, breaks the Si-H, SiOH and strained Si-O bonds. The released hydrogen or holes, while traveling towards the cathode, create oxide traps [84]. Since SILC is attributed to generated bulk traps that contribute to trap assisted tunneling [85], the traps created during stress contribute to an increase in the post-tress leakage current in hydrogen-implanted devices. The suppressed SILC for the deuterium implantation case, on the other hand demonstrates an isotope effect, as it is harder to break the Si-D bonds compared to Si-H bonds at the interface.

For comparison, with the device without any implantations were also subjected to stress. Figure.6.3 shows the gate current as a function of time for the control, hydrogen and deuterium implanted cases at stress level of –6V. The times to breakdown are observed to be 500sec, 750sec, and 1730sec for the control, hydrogen and deuterium implanted devices respectively. Hydrogen-implanted shows a fluctuation in the gate current, indicating a soft breakdown behavior while the breakdown of deuterium-implanted devices extended beyond 1000 seconds without any such fluctuations. For control samples, oxide breakdown was observed at around 500 sec. The higher leakage current, observed for deuterium-implanted devices, is due to lower (10%) oxide thickness obtained during oxidation compared to the hydrogen-implanted case [15]. It should be noted that higher desorption rate for hydrogen, being 1.6 times that of deuterium, [86]

leads to lower oxide growth rate in deuterium-implanted case as the diffused hydrogen/deuterium takes part in the oxidation process. Lee et. al observed a similar effect during oxide growth conducted after deuterium prebake [15]. Deuterium implanted devices exhibit higher time to breakdown because the trap creation is higher in control sample and in hydrogen implanted devices because Si-H bonds break easily compared to S-D bonds.

6.2.2. Flat Band Voltage Shift

The flat band voltage shift, ΔV_{FB} before and after stress is observed in the capacitance-voltage measurement as shown in Figure 6.4. The shift in the post stressed CV curves towards the positive gate voltage direction is attributed to the creation of net negatively charged centers in the bulk oxide due to electron trapping [87]. However, a reduced ΔV_{FB} of 20 mV for deuterium-implanted samples indicate a suppressed electron trap creation in the oxide. The reduced electron trap concentration in the gate oxide further supports the lower SILC observed for the deuterium-implanted devices. The lower value of capacitance in the accumulation region for the hydrogen-implanted devices is attributed to higher oxide thickness compared to deuterium-implanted case.

6.2.3. Stress-Induced Interface States

The origin of the device degradation was investigated by measuring the stress-induced interface state density. D_{it} generation due to hydrogen release at the Si-SiO_2 interface was confirmed by measuring the after stress interface trap generation. Figure 6.5 shows the extracted interface state density (D_{it}) for both hydrogen and deuterium devices evaluated using the conductance technique [55] immediately after oxide growth. Almost

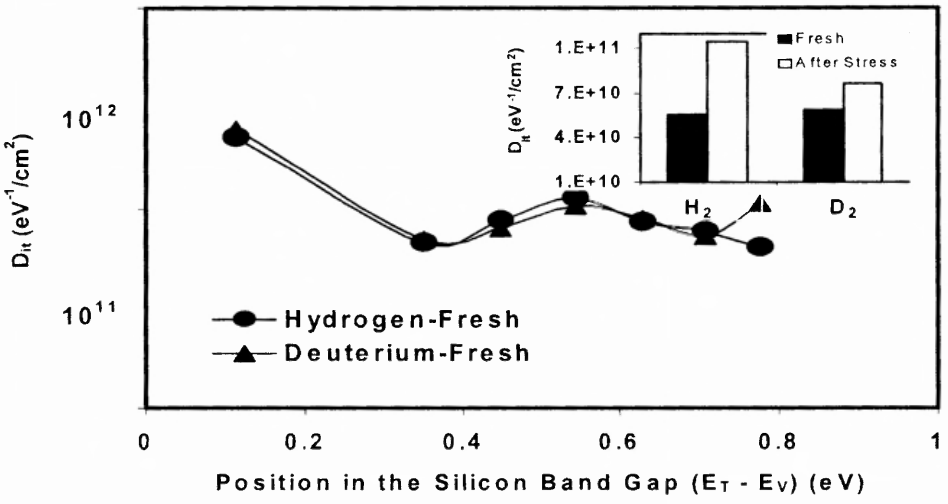

Figure 6.5 D_{it} distributions for deuterium and hydrogen implanted devices before stress shows an identical passivation of the interface. The inset shows a five fold increase in the value of D_{it} for hydrogen case compared to the deuterium case after a -6V constant voltage stress for 100sec.

6.2.3 TDDB Measurements

Furthermore, TDDB measurements were carried out to study the breakdown characteristics, for the both hydrogen and deuterium-implanted cases and were compared to control devices. The measurements were conducted at a stress level of –7V. Figure 6.6 shows the Weibull plot for the Q_{BD} characteristics for implantation conditions D20B, D25B, H20B, H25B and the control case. A significant improvement in charge to breakdown was observed for oxides implanted with deuterium in comparison to the hydrogen-implanted device, the difference being three orders of magnitude greater (considering at the 63% failure level). The larger charge to breakdown of deuterium-implanted wafers is due to less charge trap creation within the oxide and at the interface due to presence of deuterium at the interface [88].

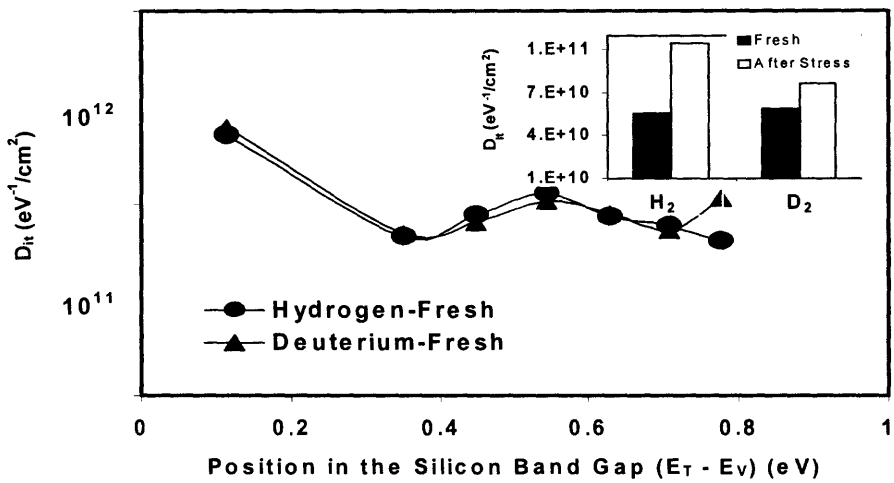

Figure 6.5 D_{it} distributions for deuterium and hydrogen implanted devices before stress shows an identical passivation of the interface. The inset shows a five fold increase in the value of D_{it} for hydrogen case compared to the deuterium case after a -6V constant voltage stress for 100sec.

6.2.3 TDDB Measurements

Furthermore, TDDB measurements were carried out to study the breakdown characteristics, for the both hydrogen and deuterium-implanted cases and were compared to control devices. The measurements were conducted at a stress level of –7V. Figure 6.6 shows the Weibull plot for the Q_{BD} characteristics for implantation conditions D20B, D25B, H20B, H25B and the control case. A significant improvement in charge to breakdown was observed for oxides implanted with deuterium in comparison to the hydrogen-implanted device, the difference being three orders of magnitude greater (considering at the 63% failure level). The larger charge to breakdown of deuterium-implanted wafers is due to less charge trap creation within the oxide and at the interface due to presence of deuterium at the interface [88].

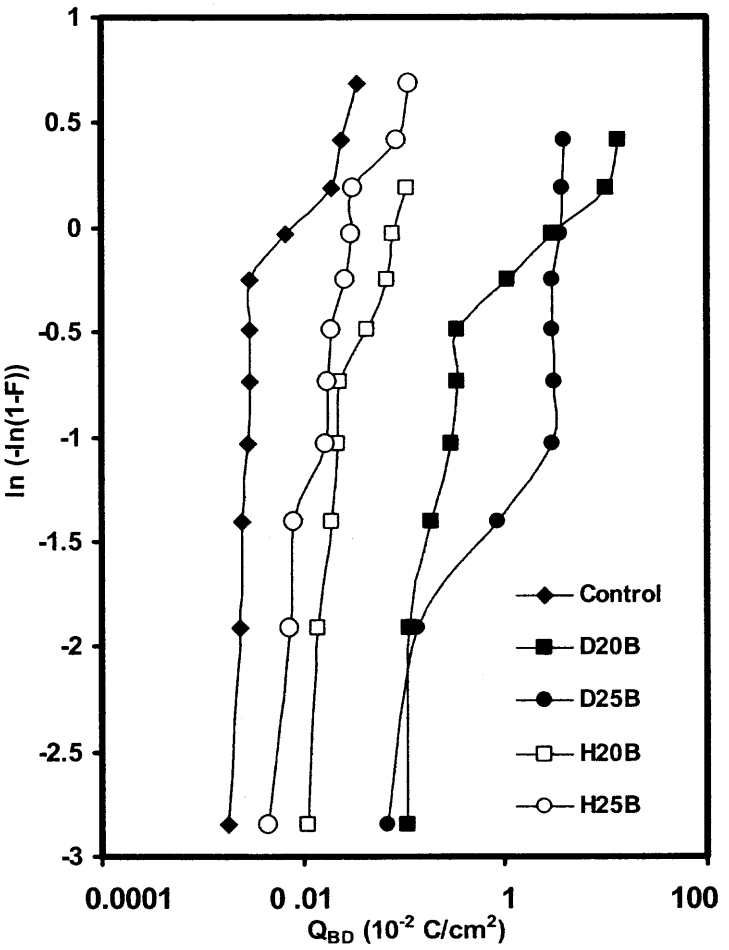

Figure 6.6 Weibull plot for Q_{BD} under constant voltage stress of –7V. Compared to the control case charge to breakdown characteristics of hydrogen and deuterium case have improved with the highest Q_{BD} obtained for the deuterium-implanted device.

6.3 Reliability Study of Annealed Devices

To investigate the effect of the deuterium ions wafers were further annealed in N_2 atmosphere at 600°C (A1) and 700°C (A2) for 20min. The leakage current and breakdown characteristics of the devices were studied and compared. Figure 6.7(a) shows the variation of leakage current density for the control sample whereas Figure 6.7 and Figure 6.8 shows the leakage current density for all cases of deuterium implantation with variation in annealing conditions (A1 and A2) including the non-annealed samples (NA) for Dose-B ($1x10^{14}/cm^2$) and Dose-C ($1x10^{15}/cm^2$) respectively. The comparison and summarization of the current density results obtained at 1V for has been plotted in Figure. 6.9 Dose-B and Dose-C cases. The results of control samples have also been plotted for reference.

6.3.1. Leakage Current

Comparing the variation in the current density for the control sample, it is observed that when subjected to annealing condition A1, a reduction in the current density is obtained compared to the no anneal (NA) case (Figure 6.7(a)). This is attributed to the annealing behavior of the traps, at the interface and in the bulk of the oxide [54]. Post Oxidation annealing is known to reduce the fixed oxide charges in the oxide [10]. A reduction in the interface state density as described earlier (Figure 5.13) also confirms this behavior. The breakdown characteristics, which will be presented later (Figure 6.10), an improvement in oxide quality further confirms the 600°C annealing effect.

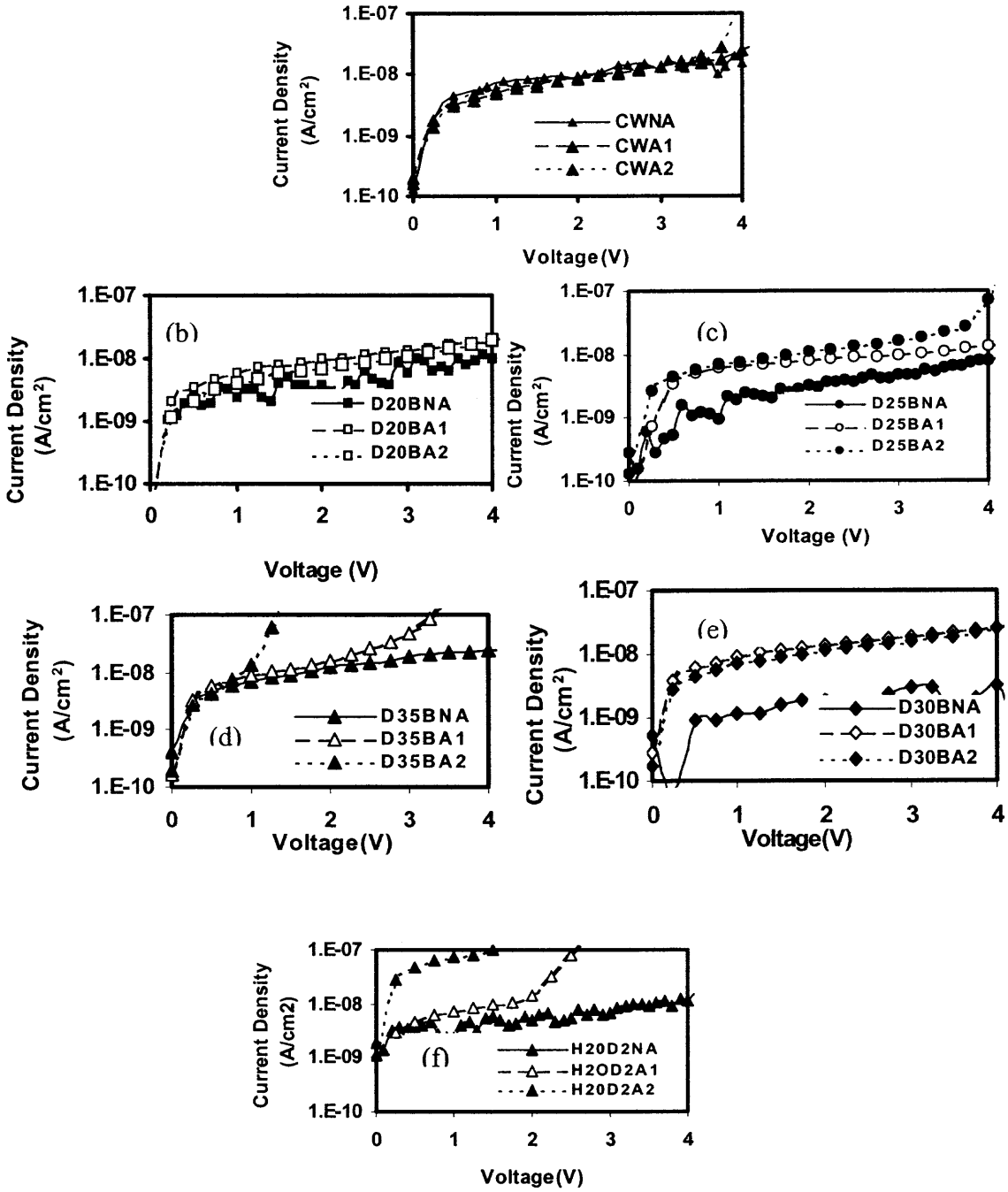

Figure 6.7 Leakage current density variation with different annealing conditions, NA (non-annealed), A1 (600°C), A2 (700°C) for the control device and Dose-B ($1x10^{14}/cm^2$) case of deuterium and hydrogen implantation (a) Control case (b) D20B (c) D25B (d) D30B (e) D35B (f) H20B.

An increase in current density is obtained for deuterium implanted cases, 20keV, 25keV, 30keV and 35keV for implantation dose of $1x10^{14}/cm^2$ under annealing condition A1 (Figure 6.7(b)(c)(d)(e)) compared to the NA case. A similar effect has also been observed earlier from the obtained D_{it} results, Figure 5.13 (a). Since this behavior is different from that of the control sample, which showed an improvement, clearly suggest that the reduction of deuterium ions, which is known to out diffuse from the oxide with increase in the temperature [37]. The passivation of defects by deuterium ions at the interface and the oxide has been discussed in Section 4.1 and Section 4.3, respectively. With the increase in the annealing temperature, the possible depassivation of deuterium ions from the interface and bulk traps accounts for an increase in the interface state density and leakage current. Trap assisted tunneling [54], therefore, contributes to higher leakage current. Figure 6.7(f) shows the leakage current variation for annealed hydrogen-implanted devices. Annealing seems to increase the leakage current significantly after both the annealing conditions.

The current density characteristics observed at annealing condition A2 is found to yield a further reduction of current compared to annealing condition A1, while the interface is found to degrade with D_{it} increasing, Figure 5.13 (a). An increase in the D_{it} has resulted from out diffusion of the deuterium ions from the interface and oxide, while the reduced current is attributed to the annealing behavior of the traps within the oxide after the out diffusion of deuterium from the SiO_2 network.

Figure 6.8 show the current density measurements for a higher dose of implantation, Dose-C, of D20C, D25C and D30C devices. In case of D20C a reduction in the current density (Figure 6.8(a)) is observed compared to the observed trend in non-

annealed (NA) case possibly due to complete annealing behavior of implantation damage. This trend is also reflected as an improvement in D_{it} value as shown earlier in Figure 5.13 (b). In other Dose-C cases similar trend is observed as in case of Dose-B.

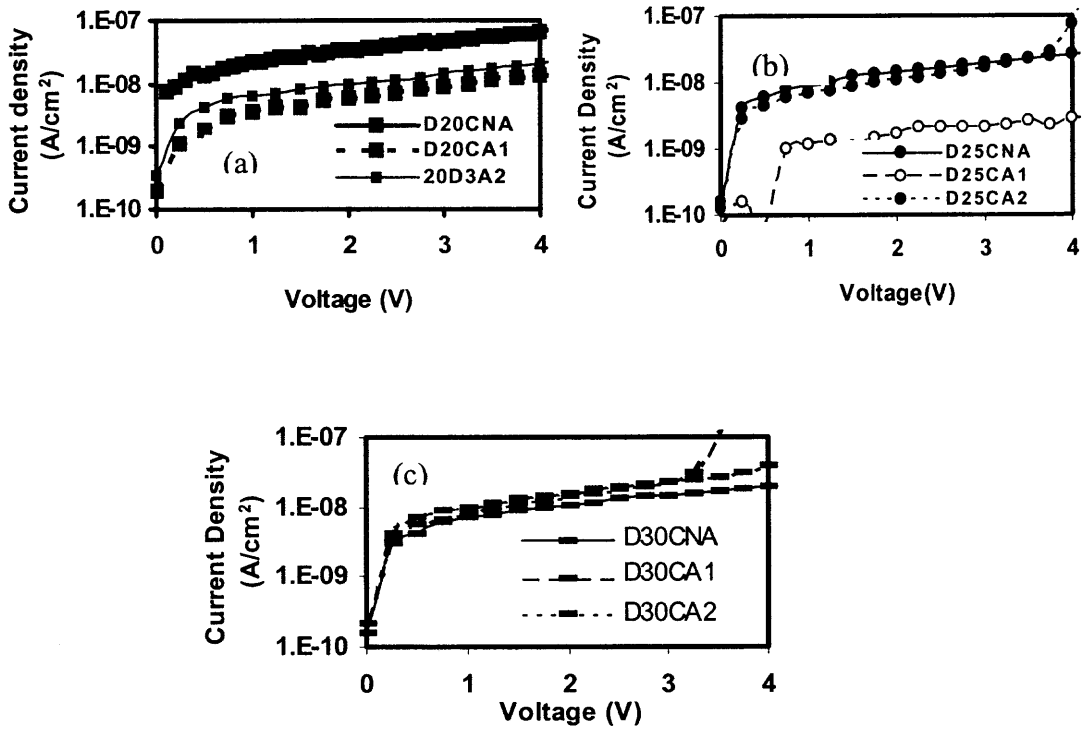

Figure 6.8 Leakage current density variations with different annealing conditions, NA (non-annealed), A1 (600°C), A2 (700°C) for the control device and Dose-C ($1x10^{15}/cm^2$) case of deuterium implantation (a) D20C (b) D25C (c) D30C.

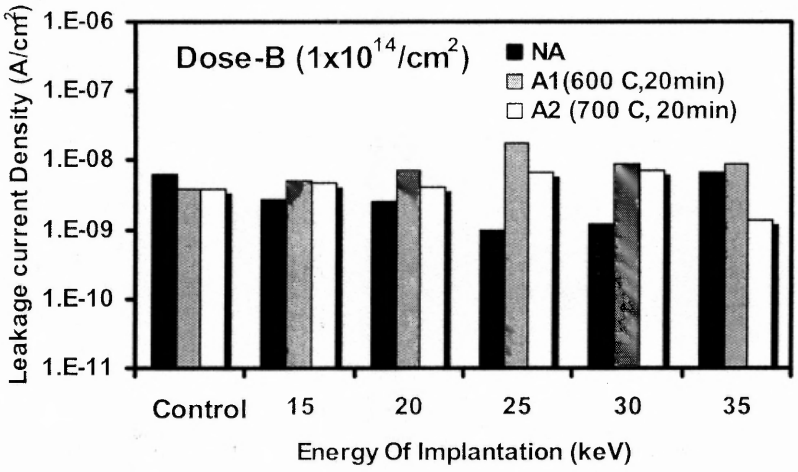

(a)

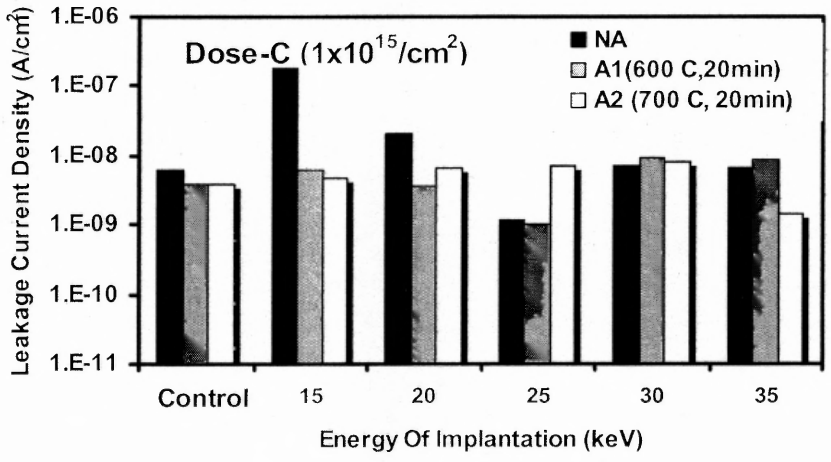

(b)

Figure 6.9 Comparison of Leakage current density for different cases of deuterium implantation with variation in annealing conditions, NA (non-annealed), A1 (600°C), A2 (700°C) for (a) Dose-B ($1x10^{14}/cm^2$) (b) Dose-C ($1x10^{15}/cm^2$) case of deuterium implantation. The control case has been plotted for reference.

Figure 6.9 compare the leakage current at 1 volt for all the samples for Dose-B ($1x10^{14}/cm^2$) (6.9(a)) and for Dose-C ($1x10^{15}/cm^2$) (6.9(b)). Notice that the explanations provided above clearly evident in the bar charts.

6.3.2. Breakdown Characteristics

The degradation in the breakdown characteristics, observed for all the annealed samples are provided in Figure.6.10 for control, 15keV, 20keV, 25keV and with Dose-B. The breakdown characteristics of the annealed hydrogen-implanted cases have also been added for comparison. A significant improvement in the breakdown characteristics is obtained for D20BNA and D25BNA, as discussed in Section 6.1. Comparing the characteristics obtained with variation in annealing, it is observed for the control sample an enhanced oxide charge to breakdown is obtained on annealing at 600°C (A1). This is due to the improved interface passivation, Section 5.13 and leakage current, Section 6.3.1 in the oxide due to improved oxide quality attributed to the annealing behavior of the traps. Also observed for D15B, the breakdown characteristics improve, though not significantly on being annealed at 600°C (A1). Since this behavior is similar to the control sample, this is attributed to the annealing behavior of preexisting traps.

For implantation conditions D20B, D25B oxide degradation is observed after annealing at 600°C (A1). This is in trend with the D_{it} and leakage current results as discussed in Section 5.13 and 6.3.1 respectively. The out diffusion of the deuterium incorporated ions and trap assisted tunneling lead to an increase in the leakage current and thereby a degradation in the breakdown characteristics. Further, annealing at 700°C (A2) did not yield any significant change in the breakdown characteristics compared to

600°C (A1). The behavior obtained for the hydrogen samples were similar to that as obtained for the deuterium devices as shown in the figure.

Figure 6.11 shows the breakdown characteristics for Dose-C ($1x10^{15}/cm^2$) of implantation for D20C, D25C and D30C. The breakdown characteristics showed improvement for devices D20C, D25C and D30C after being annealed at 600°C (A1) due to possible slow release of deuterium from the damage sites during annealing. As discussed in Section 6.1, for higher doses ($1x10^{15}/cm^2$) of implantation, greater implantation damage leads to the degradation in the electrical properties of the non annealed devices compared to the lower dose ($1x10^{14}/cm^2$) of implantation. And also as discussed in Section 5.2, the increase in damage, the disordered sites that act as a sink or gettering centers [74] for diffusing deuterium and accumulation of the ions (deuterium) in these regions accounts for the low diffusivity obtained for a higher dose of implantation during oxidation. However on being annealed at 600°C, the improvement in the breakdown characteristics is attributed to the partial recovery of the damage and simultaneous release of deuterium from these damage sites. This is further confirmed by the obtained breakdown characteristics of D25CA1, which shows similar magnitude of breakdown enhancement as compared to D20BNA (which yielded the best breakdown characteristics of the deuterium implanted devices after gate oxidation and before annealing, Section 6.2). The improved passivation of the interface states is further confirmed by the obtained D_{it} results as discussed in Section 5.3.1. At 700°C (A2) annealing a reduced leakage current is obtained for 15keV, 20keV, 30keV and 35keV. From the D_{it} distribution graph, Figure 5.13(b) it was also observed that the interface state density increases. The increased interface state density is attributed to the out diffusion

of the incorporated ions during condition A1. The reduced leakage current on the other hand is contributed to the annealing behavior of the traps in the SiO_2 network.

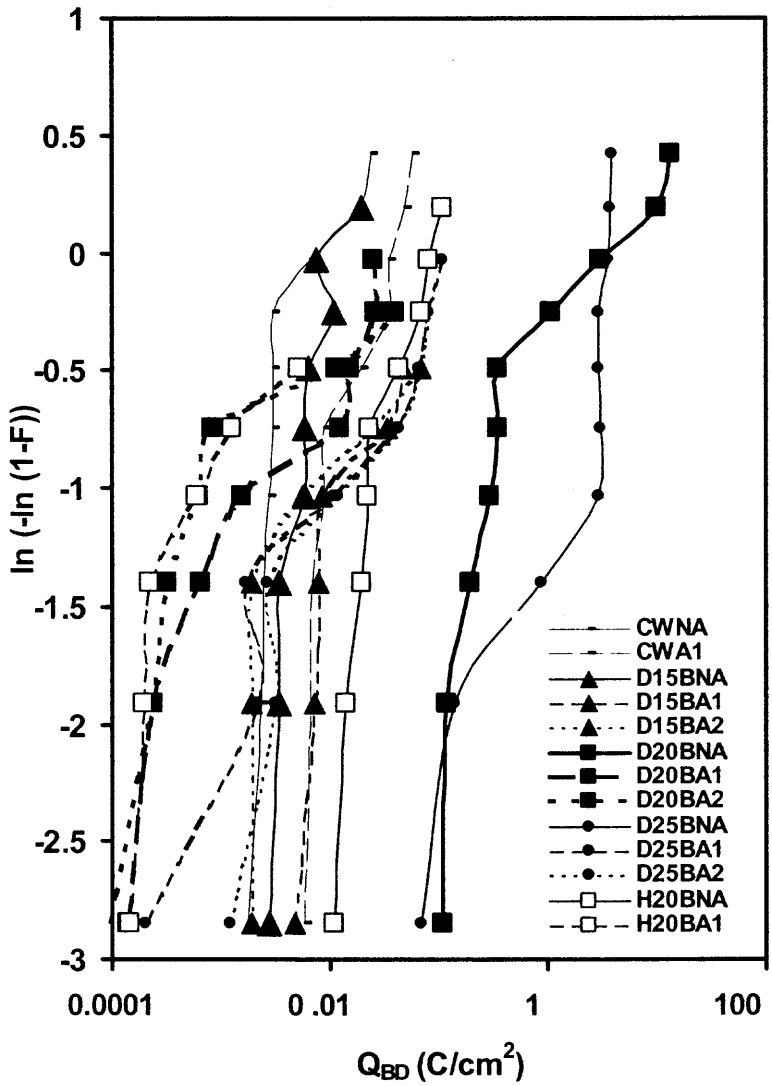

Figure 6.10 Q_{BD} characteristics for different cases of deuterium implantation with variation in annealing condition, NA (non-annealed), A1 (600°C) and A2 (700°C) for control, 15keV, 20keV and 25keV. Hydrogen devices have been plotted for comparison.

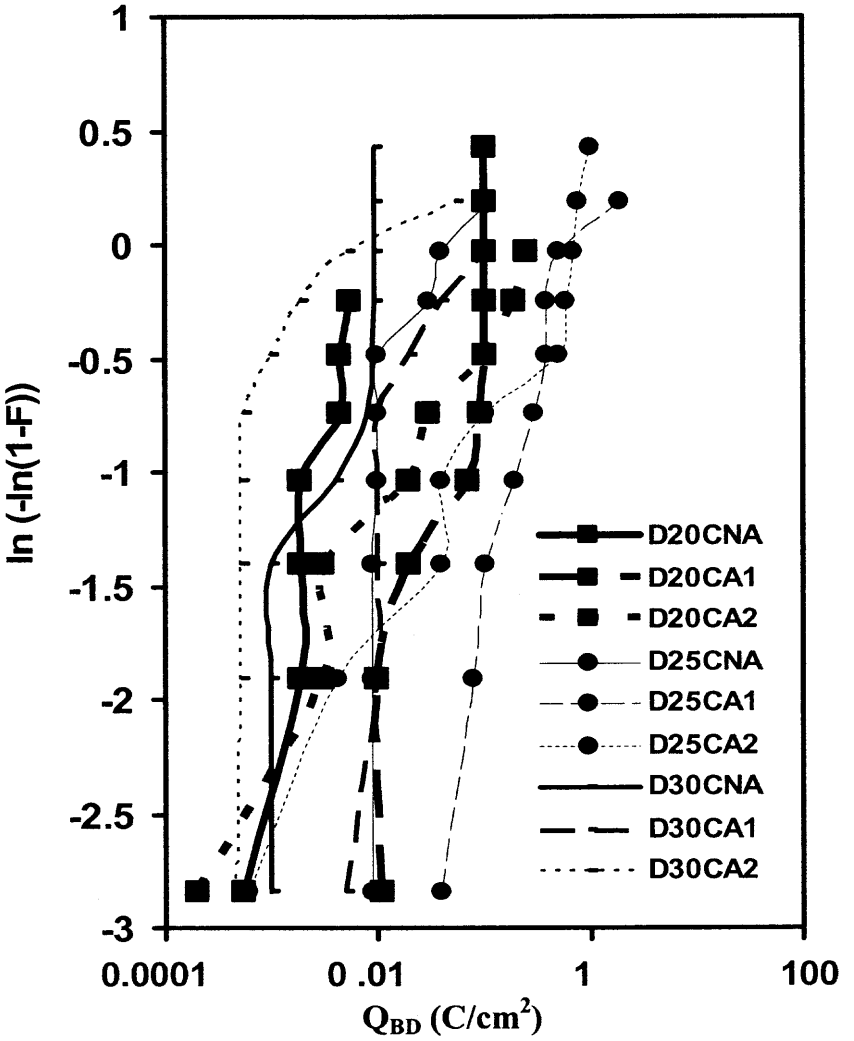

Figure 6.11 Q_{BD} characteristics for different cases of deuterium implantation with variation in annealing conditions, NA (non-annealed), A1 (600°C), A2 (700°C) for (a) 20keV, 25keV (b) 30keV.

6.4 Summary

The reliability of SiO_2 on deuterium and hydrogen implanted devices for various implantation conditions have been analyzed and discussed in this chapter. Lower implantation dose, $1x10^{14}/cm^2$, yielded enhanced reliability characteristics compared to higher doses of implantation, $1x10^{15}/cm^2$.

During oxidation, the implanted deuterium ions move towards the Si/SiO_2 interface owing to the chemical potential difference between Si and SiO_2. The diffusion of the deuterium ions from within the substrate during oxidation is governed by implantation-induced damage, which is dependent on the energy and dose of the implantation.

Figure 6.12 shows the schematic of the diffusion of the deuterium ions during oxidation through the damaged sites. The defects created in the silicon substrate during implantation include silicon self-interstitials (I), di-interstitials (I_2), vacancies and divacancies (V_2) and deuterium works as substitutional deuterium (D_S) or interstitial deuterium (D_I) (Figure 6.12).

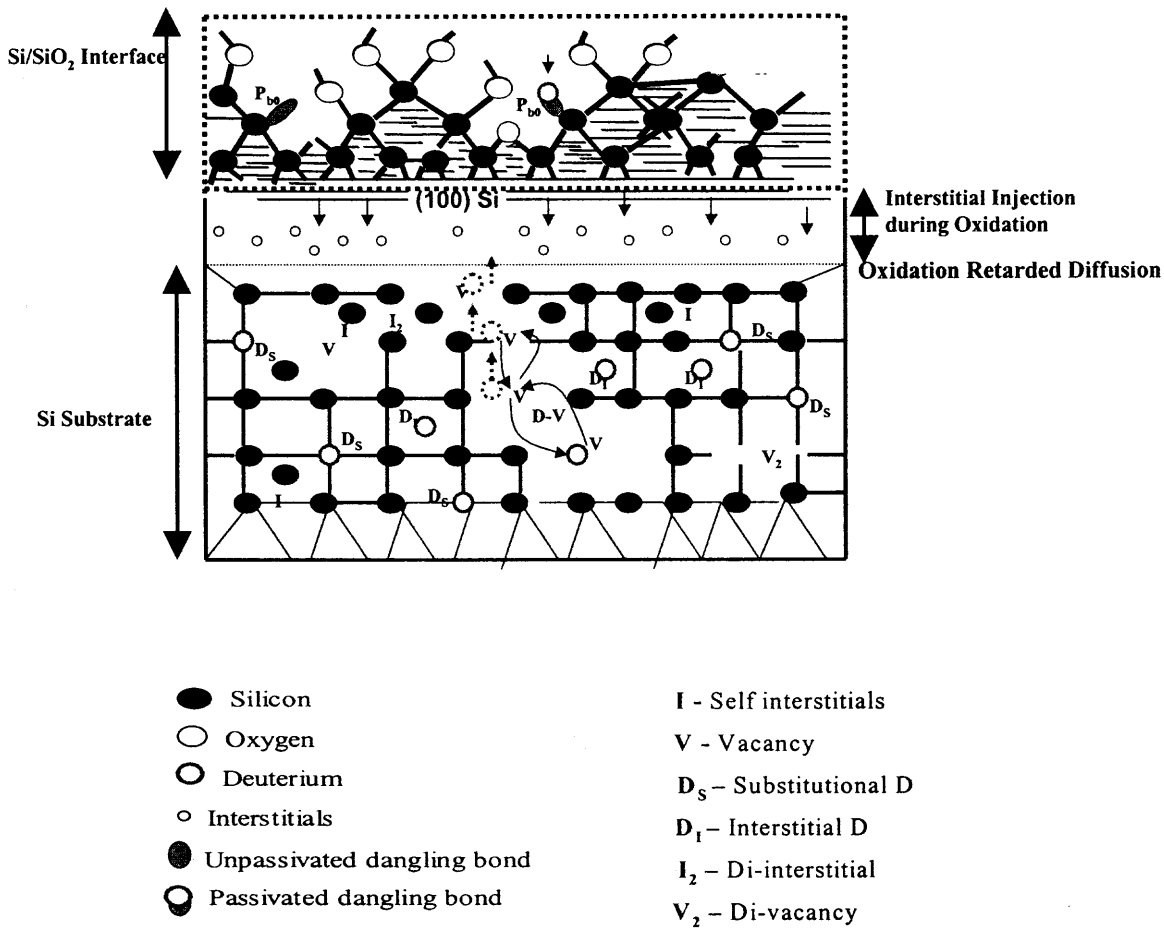

Figure 6.12 Damage created in the substrate during implantation and diffusion of the deuterium ions during oxidation.

Low energy and dose of implantation does not produce dense collision cascades [89]. With the increase in the dose, the peak concentration of the ions increases and brings about damage clusters forming larger clusters with deep traps. With increase in the dose of implantation, the trap density increases. These disordered and defective regions serve very effectively as sinks for the deuterium ions, which impede the diffusivity [90]. This explains the obtained reduced diffusivity for higher dose of implantation compared to lower dose. Furthermore, the diffusivity of the deuterium ions is retarded during oxidation due to the formation of oxidation induced stacking faults, which injects extra interstitials into the lattice as shown in Figure 6.12. During thermal treatment their density increases due to transfer of silicon interstitials from the smaller loops to form larger ones [91, 92]. The diffusivity is thus impeded by the implantation damage and also the interstitials injected during oxidation as the diffusion mechanism is controlled by vacancy and deuterium interaction {D-V}. For a lower dose of implantation, induced defects are quickly annealed and do not impact the interface or the oxide.

CHAPTER 7

CONCLUSIONS

We have investigated passivation of the dangling bonds that contributes to the interface states in the silicon band gap by deuterium ion implantation before the growth of a 6.5 nm thin oxide in MOS capacitors fabricated at the Microelectronics Fabrication Center at NJIT. Different implantation conditions were used to effectively passivate the silicon-dangling bonds with deuterium implantation energies of 15keV, 20keV, 25keV, 30keV and 35keV doses $1x10^{13}/cm^2$, $1x10^{14}/cm^2$ and $1x10^{15}/cm^2$. By computing the interface state density, D_{it}, gate leakage current and charge to breakdown characteristics we have found the optimum implantation conditions for the effective passivation process.

7.1 Implantation Condition Optimization

Extensive SRIM simulation provided an estimation of deuterium and hydrogen ion distribution in silicon and the intensity of implantation damage for various energies and doses. Deuterium-implanted devices showed an enhanced interface passivation due to incorporation of the diffused deuterium ions at the Si/SiO_2 interface reacting with the interface dangling bonds to form Si-D bonds. We have also observed significant improvement in oxide quality due to possible formation of Si-D bonds in the bulk SiO_2 [68]. The retention of deuterium at the interface and in the oxide was confirmed by the profiles obtained from the Secondary Ion Mass Spectroscopy (SIMS). The optimum condition for deuterium implantation was found to be at 20keV with dose of

$1x10^{14}$atoms/cm^2. Deuterium diffusivity was extracted from the measured SIMS profiles and the computed interface state density.

7.1.1 Reliability Enhancement

Stress-induced leakage current (SILC) and time dependent dielectric breakdown (TDDB) were investigated to examine the reliability of gate oxides grown on hydrogen and deuterium implanted silicon substrates. Significant reliability enhancement was observed which may be explained by the reduction of defects in the SiO_2 and Si/SiO_2 interface, such as Si dangling bonds, weak Si-Si and strained Si-O bonds. For low doses ($1x10^{14}$/cm^2) of implantation, the interface and oxide quality obtained was superior compared to that obtained for the higher dose of implantation, $1x10^{15}$/cm^2. The observed degradation in the reliability characteristics for the higher energy and dose of implantation was believed to be due to the implantation damage that was not completely removed during oxidation.

The results obtained with hydrogen implantation under similar conditions as deuterium suggests a strong isotope effect. An order of magnitude improvement in charge to breakdown was observed for deuterium implanted devices compared to hydrogen implantation. Deuterium implanted devices exhibited less charge trapping (reduced SILC and ΔV_{FB}), less generation of interface states, and a larger charge to breakdown under electrical stress, which confirmed the isotope effect based on hydrogen release model.

Devices subjected to annealing at 600°C and 700°C annealing demonstrated different distributions of deuterium in silicon/ silicon oxide systems. For low dose of implantation, $1x10^{14}$/cm^2, degradation of the interface and of the oxide quality was

observed due to the out diffusion of the deuterium when the annealing temperature was increased. On the other hand, for higher doses of implantation, $1x10^{15}/cm^2$, the increased interface passivation and breakdown characteristics at 600°C were governed by the partial recovery of the damage. Possible slow release of deuterium from the damage sites during annealing leads partial deuterium incorporation at the interface and in the oxide showing an improvement after 600°C annealing. At 700°C annealing almost all devices demonstrated interface and oxide degradation attributed to the possible out diffusion of some of the deuterium ions.

7.2 Suggested Future Work

The results of this study suggest that implantation may be incorporated in CMOS technology to meet the requirement of interface engineering. Below 1 nm, very large gate leakage currents degrade dielectric reliability and prevent use of the conventional SiO_2. Fabrication of nanoscale CMOS devices that will use strained silicon, SiGe channel and high-k gate materials could incorporate deuterium implantation for interface states passivation and reliability enhancement. High-k dielectrics, that require low temperature processing, can be deposited on deuterium implanted silicon substrate to effectively passivate the interface states and bulk oxide charges. A precise control on the incorporation of deuterium will be required.

REFERENCES

[1] A. Stesmans, Physical Review B, "Structural relaxation of P_b defects at the (111) Si/SiO_2 interface as a function of the oxidation temperature: the P_b generation stress relationship," vol. 48 (4), pp. 2418-435, (1993).

[2] C. R. Helms and E. H. Poindexter, Reports on Progress in Physics, "The silicon-silicon dioxide system: its microstructure and imperfections," vol. 57 (8), pp. 791-852, (1994).

[3] B. E. Deal, E. H. Poindexter and P. J. Caplan, J. Appl. Phys., "Interface states and electron spin resonance centers in thermally oxidized (111) and (100) silicon wafers," vol. 52 (8), pp. 879-884, (1981).

[4] K. L. Brower, Appl. Phys. Lett., "Si hyperfine structures of unpaired spin at the Si/SiO_2 interface," vol. 43, pp. 1111-1113, (1983).

[5] L. Biegelsen, D. K. Johnson, E. H. Poindexter and N. M. Stuzmann, Application of Surface Science, "Native defects at the Si/SiO_2 interface-amorphous silicon revisited," vol. 14, p. 211, (1983).

[6] E. H. Poindexter, P. J. Caplan, B. E. Deal and R. R. Razouk, J. Appl. Phys., "Interface states and oxide fixed charge in thermally oxidized silicon wafers," vol. 50 (9), pp. 5847-5854, (1979).

[7] E. H. Poindexter, G. J. Gerardi and M. E. Rueckel, J. Appl. Phys., "Electronic traps and P_b centers at the Si/SiO_2 interface: Band gap energy distribution", vol. 52, pp. 879-884, (1981).

[8] G. J. Gerardi and E. H. Poindexter, J. Appl. Phys., "Contribution of Pb_1 centers to midgap interface trap density in oxidized (100) silicon wafers," vol. 40, pp. 800-804, (1982).

[9] G. J. Gerardi, E. H. Poindexter and P. H. Caplan, Appl. Phys. Lett., "Interface traps and P_b centers in oxidized (100) silicon wafers," vol. 49 (6), pp. 348-350, (1986).

[10] P. N. Lenahan and P. V. Dressendorfer, Appl. Phys. Lett., "Paramagnetic trivalent silicon centers in gamma irradiated metal-oxide-silicon structures," vol. 44, pp. 96-98, (1984).

[11] A. Stesmans and K. Vanheusden, Physical Review B, "O environment of unpaired Si bonds (P_b defects) at the (111) Si/SiO_2 interface," vol. 44 (11), pp. 353-355, (1991).

[12] A. Stesmans, B. Nouwen and V. V. Afanas'ev, Physical Review B, "Pb1 interface defect in thermal (100) Si/SiO2", vol. 58, pp. 801-809, (1998).

[13] G. J. Gerardi and E. H. Poindexter, Appl. Phys. Lett., "Interface traps and Pb centers in oxidized (100) silicon wafers," vol. 49 (6), pp. 348-350, (1986).

[14] A. Stesmans and V. V. Afanas'ev, Physical Review B, "H-complexed oxygen vacancy in SiO_2: Energy level of negatively charged state," vol. 57, p. 10030, (1998).

[15] N. M. Johnson, D. K. Biegelsen and M. D. Moyer, J. Vac. Sci. Tech., "Characteristics electronic defects at the Si-SiO_2 interface," vol. 43 (6), pp. 563-565, (1983).

[16] K. Hess, I. C. Kizilyalli, and J. W. Lyding, IEEE Trans. Electron Devices, "Giant isotope effect in hot electron degradation of metal oxide silicon device," ED- 45, pp. 406-417, (1998).

[17] E. H. Nicollian, C. N. Berglund, P. F. Schmidt, and J. M. Andrews, J. Appl. Phys., "Electrochemical charging of thermal SiO_2 films by injected electron currents," vol. 42, 5654, (1971).

[18] E. H. Poindexter, Journal of Physical Sciences, "Physical chemistry of hydrogenous species in the Si/SiO_2 system," vol. 50a, pp. 653-665, (1995).

[19] D. J. Di Maria, E. Cartier and D. Arnold, Appl. Phys. Lett., "Degradation and breakdown of silicon dioxide on silicon," vol. 61 (19), pp. 2339-2331, (1992).

[20] A. Stesmans and K. Vanheusden, Physical Review B, "Observation of dipolar interactions between Pb_0 defects at the (111) Si/SiO_2 interface," vol. 42, pp. 3765-3768, (1990).

[21] P. H. Avouris, R. E. Walkup, A. R. Rossi, H. C. Akpati, P. Nordlander, T. C. Shen, G. C. Alben and J. W. Lyding, Surface Science, "Breaking individual chemical bonds via STM-induced excitations," vol. 33, pp. 368-377, (1996).

[22] K. Hess, I. C. Kizilyalli, and J. W. Lyding, IEEE Trans. Electron Devices, "Giant isotope effect in hot electron degradation of metal oxide silicon devices," ED-45, pp. 406-417, (1998).

[23] K. Chen, K. Hess and W. Lyding, J. Appl. Phys., "Kinetic study on replacement of hydrogen by deuterium at (100) Si/SiO_2 interfaces," vol. 90 (12), (2001).

[24] C. G Van de Walle and W. B. Jackson, Appl. Phys. Lett., "Comment on Reduction of hot electron degradation in metal oxide semiconductor transistors by deuterium processing," vol. 69 (16), pp. 2441-2443, (1996).

[25] J. W. Lyding, K. Hess and I. C. Kiziyalli, Appl. Phys. Lett., "Reduction of hot electron degradation in metal oxide semiconductor transistors by deuterium processing," vol. 68 (18), (1996).

[26] R. Biswas, Y. P. Li and B. C. Pan, Appl. Phys. Lett., "Enhanced stability of deuterium in silicon," vol. 72 (6), pp. 3500-3502, (1998).

[27] P. Guyot-Sionnest, P. H. Lin and E. M. Hiller, J. Chem. Phys., vol. 102 (10), (1995).

[28] J. W. Lyding, T. C Shen, J. S. Hubacek, J. R. Tucker and G. C. Abeln, Appl. Phys. Lett., "Nano scale patterning and oxidation of H passivated Si (100) 2x1 surfaces with ultra high vacuum scanning tunneling microscope," vol. 64 (15), (1994).

[29] P. H. Avouris and R. E. Walkup, Surface Science, "Breaking individual chemical bonds via STM-induced excitations," vol. 36, pp. 368-377, (1996).

[30] P. H. Avouris, R. E. Walkup, Chem. Phys. Lett., "STM induced H atom desorption from Si (100): isotope effects and site selectivity," vol. 254, pp. 148-154, (1996).

[31] H. C. Mogul, L. Cong, R. M. Wallace, P. J. Chen, T. A. Rost and K. Harvey, Appl. Phys. Lett., "Electrical and physical characterization of deuterium sinter on submicron devices," vol. 72 (14), p. 1721, (1998).

[32] R. A. B. Devine, J. L. Autran, W. L. Warren, K. L. Vanheusdan, and J. C. Rostaing, Appl. Phys. Lett., "Interfacial hardness enhancement in deuterium annealed 0.25μm channel metal oxide semiconductor transistors," vol. 70, p. 2999, (1997).

[33] I. J. R. Baumvol, E. P. Gusev, F. C. Stedile, F. L. Freire, M. L. Green and D. Brasen, Appl. Phys. Lett., "On the behavior of deuterium in ultrathin SiO_2 films upon thermal annealing," vol. 72 (4), p. 450, (1998).

[34] P. J. Chen and R. M. Wallace, J. Appl. Phys., "Deuterium transport through device structures," vol. 86 (4), (1999).

[35] J. Lee, Y. Epstein, A. C. Berti, J. Huber, K. Hess and J. W. Lyding, IEEE Trans. Electron Devices, "The effect of deuterium passivation at different steps of CMOS processing on lifetime improvements of CMOS transistors," vol. 46, pp. 1812-1815, (1999).

[36] I. C. Kizilyalli, G. Weber, Z. Chen, G. Abeln, M. Schonfield, B. Kotzias, F. Register, E. Harris, S. Sen, S. Chetlur, M. Patel, L. Stirling, R. Huang and A. Massengale, Electron Device Letters, "Improvement of hot carrier reliability with deuterium anneals for manufacturing multilevel metal/dielectric MOS systems," vol. 19 (11), pp. 444-446, (1998).

[37] H. Park and C. R. Helms, J. Electrochemical Society, "The effect of annealing treatment on the distribution of deuterium in Silicon and in Silicon/Silicon oxide systems", vol. 139 (7), (1992).

[38] D. Misra and S. Kishore, Electrochem. Solid-State Lett, "Gate oxides on Deuterium Implanted silicon substrate," vol. 2 (12), pp. 637-639, (1999).

[39] W. F. Clark, P. E. Cottrell, T. G. Ference, S.-H. Lo, J. G. Massey, S. W. Mittl, and J. H. Rankin, Tech. Dig. Int. Electron Devices Meet., "Improved hot electron reliability in high performance multilevel CMOS using deuterated barrier nitride processing," vol. 89, (1999).

[40] S. A. Abbas and R.C. Dockerty, Appl. Phys. Lett., "Hot carrier instability of IGFET's," vol. 27, pp. 147-148, (1975).

[41] Y. Lebleici and S. M. Kang, Appl. Phys. Lett., "Hot carrier Reliability of MOS VLSI circuits," vol. 28, (1993).

[42] Y. Lebleici and S.M. Kang, Appl. Phys. Lett., "Hot carrier Reliability of MOS VLSI circuits," vol. 28, (1993).

[43] Jinju Lee, Kangguo Cheng, Zhi Chen, Karl Hess, Joseph W. Lyding, Kwang Kim and Hyui-Seung Lee, IEEE Electron Device Letters, "On the mechanism for interface trap generation in MOS transistor due to channel hot carrier stressing," vol. 21 (5), May (2000).

[44] H. Kim and H. Hwang, Appl. Phys. Lett., "High-quality ultrathin gate oxide prepared by oxidation in D_2O," vol. 74, pp. 709-711, (1999).

[45] H. Kwon and H. Hwang, Appl. Phys. Lett., "Electrical characteristics of ultrathin gate oxide prepared by post oxidation annealing in ND_3," vol. 76 (6), pp. 772-773, (2000).

[46] Y. Mitani, H. Satake, H. Itoh, and A. Toriumi, Tech. Dig. Int. Electron Devices Meet. 2000, "Highly reliable gate oxide under fowler-nordheim electron injection by deuterium pyrogenic oxidation and deuterated Poly-Si deposition," IEDM 00-343, pp. 343-346, (2000).

[47] M. H. Lee, C. H. Lin and C. W. Liu, IEEE Electron Device Letters, "Novel methods to incorporate deuterium in MOS structures," vol. 22 (5), (2001).

[48] Avid Kamgar, D. P. Monroe and W. M. Mansfield, IEEE Electron Device Letters, "Passivation of interface states in large area Si devices using hydrogen implantation," vol. 24 (7), (2003).

[49] M. Khun, Solid state Electronics, "A quasistatic technique for MOS C-V and surface state measurements," vol. 13, pp. 873-885, (1970).

[50] Dieter K. Schroder, *Semiconductor material and Device Characterization,* John Wiley and Sons, (1998).

[51] Pushkar P. Apte and Krishna C. Saraswat, IEEE Trans. on Electron Devices, "Correlation of trap generation of charge to breakdown (QBD): A Physical model for dielectric breakdown," vol. 41 (9), (1994).

[52] D. J. Maria and E. Cartier, J. Appl. Phys., "Annode hole injection and trapping in silicon dioxide," vol. 78 (6), (1995).

[53] J. W. McPherson, H. C. Mogul, IEEE, "Distributed binding states in silicon dioxide thin films and their impact on time dependent dielectric breakdown," 36th Annual Inter. Reliability Symposium, pp. 47-56, (1998).

[54] E. H. Nicollian and J. R. Brews, *MOS (Metal Oxide Semiconductor) Physics and Technology,* p. 207, Wiley New York, (1982).

[55] E. H. Nicollian and J. R. Brews, *MOS (Metal Oxide Semiconductor) Physics and Technology*, p. 210, Wiley New York (1982).

[56] J. F. Ziegler, J. P. Biersack and U. Littmark, *The Stopping and Range of Ions in Solids*, Pergamon Press, New York, (1985).

[57] J. F. Ziegler, J. P. Biersack and U. Littmark, *The Stopping and Range of Ions in Solids*, Pergamon Press, New York, (2003).

[58] A. Stesman, and V. V Afanas'ev, Appl. Phys. Lett., "Si dangling bond type defects at the interface of (100) Si/SiO_2," vol. 82, (2003).

[59] Wolf and Tauber, Silicon Processing Technology for the VLSI era, Lattice Press.

[60] James D. Plummer, Michael D. Deal and Peter B. Griffin, *Silicon VLSI Technology, Fundamentals, Practice and Modeling,* Prentice Hall, 2000.

[61] J. Tatarkiewicz, Physica B, "Hydrogen implantation in semiconductors", vol. 170, pp. 188-196, (1991).

[62] Wilson Robert, *Secondary ion mass spectrometry: a practical handbook for depth profiling and bulk impurity analysis,* New York, Wiley, (1989).

[63] Advanced Materials Processing and Analysis center – University of Central Florida.

[64] Y. Li, J. Shyue and J. Hunter, Ion implantation Technology, "SIMS depth profiling and SRIM simulation to lower energy antimony implantation in to silicon," Proceedings of the 14th international conference on semiconductors, IEEE, (2002).

[65] C. G. Van de Walle and B. R. Tuttle, IEEE Trans. on Electron Devices, "Microscopic theory of hydrogen in silicon device," vol. 47 (10), pp. 1779-1786, (2000).

[66] S. M. Meyers, J. Appl. Phys., "Interaction of deuterium gas with dry SiO_2 on Si: An ion beam study," vol. 61, p. 5428, (1987).

[67] N. H. Nickel, N. M. Johnson and W. B. Jackson, J. Appl. Phys., " Hydrogen passivation of grain boundary in polycrystalline silicon thin films," vol. 62 (25), (1993).

[68] H. Y. Mitani, H. Satake, H. Itoh, and A. Toriumi, Tech. Dig. Int. Electron Devices Meeting, "Suppression of stress induced leakage current after Fowler-Nordheim stressing by deuterium pyrogenic oxidation and deuterated Poly-Si deposition," vol. 49, p. 1192, (2002).

[69] A. Stesmans, Physical Review B, "Dissociation kinetics of hydrogen passivated P_b defects at the (111) Si/SiO_2 interface," vol. 61 (12), (2000).

[70] E. Cartier, J. H. Stathis and D. A. Buchanan, Appl. Phys. Lett. "Passivation and depassivation of silicon dangling bonds at the Si/SiO_2 interface by atomic hydrogen," vol. 63 (11), (1993).

[71] N. M. Johnson, D. K. Biegelsen and M. D. Moyer, Appl. Phys. Lett., "Deuterium at the Si-SiO_2 interface detected by Secondary-Ion-Mass-spectroscopy," vol. 38 (12), (1981).

[72] T. Sakurai and T. Sugano, Appl. Phys. Lett., "Theory of continuously distributed trap states at Si-SiO_2 interfaces," 52 (4), pp. 2889-2897, (1981).

[73] N. M. Johnson, D. K. Biegelsen and M. D. Moyer, Appl. Phys. Lett., "Deuterium passivation of grain boundary dangling bonds in silicon thin films," vol. 40 (10), (1982).

[74] S. Ashok, IEEE, "Hydrogen in silicon: defect interactions and applications," (1998).

[75] J. I. Pankove, R. O. Wance and E. Berkeyheiser, Appl. Phys. Lett., " Neutralization of acceptor in silicon by atomic hydrogen," vol. 45, p. 1100, (1984).

[76] K. Srikanth and S. Ashok, J. Appl. Phys., "Trapping of atomic hydrogen by disordered regions," vol. 70 (9), (1991).

[77] D. E. Carson and C. W. Magee, Appl. Phys. Letter, "A SIMS analysis of deuterium diffusion in hydrogenated amorphous silicon," vol. 33, (1978).

[78] B. Sopori, M. I. Symko, R. Reedy, K. Jones and R. Matson, 26th IEEE Photovoltaic Specialists Conference, "Mechanism(s) of hydrogen diffusion in silicon solar cells during forming gas anneal," (1997).

[79] L. Darling and H. B. Schlegel, J. Phys. Chem., " Heats of formation of SiHnO and $SiHnO_2$ calculated by ab inito molecular orbital methods at the G2 level of theory," vol. 97, pp. 8207-8211, (1993).

[80] M. Jariaz, G. H. Gilmer, J. M. Poete and T. D. de la Rubia, Appl. Phys. Lett., " Atomistic calculations of ion implanted in Si: Point defect and transient enhanced diffusion phenomenon," vol. 68, (1996).

[81] G. Carter and W. A. Grant, *Ion implantation of semiconductors,* John Wiley and sons, New York, (1976).

[82] E. Kapetanakis, D. Skarlatos, C. Tsamis and P. Normand, Appl. Phys. Lett., " Influence of ion implantation energy on the electrical properties of ultrathin gate oxides grown on nitrogen implanted silicon", vol. 82 (26), pp. 4764-4766, (2003).

[83] C. Lin, A. I. Chou, P. Choudhury, J. C. Lee, K. Kumar, B. Doyle and H. R Soleimani, Appl. Phys. Lett., "Reliability of SiO_2 grown on nitrogen implanted silicon substrate," vol. 69, p. 3701, (1996).

[84] D. J. Maria and J.W. Stathis, J. Appl. Phys., "Trap creation in silicon dioxide produced by hot electrons," vol. 65, pp. 2342-2356, (1989).

[85] R. Moazzami and C. Hu, "Stress induced current in thin silicon dioxide films," IEEE, IEDM, pp. 139, (1992).

[86] Kumar Sinniah, Michael G. Sherman, B. Lisa, W. Henry, John T. Yates and Kenneth C. Janda, Journal of Chem. Phys., "Hydrogen desorption from monohydride phase on Si (100)," vol. 92 (8), 1990.

[87] E. Harari, J. Appl. Phys, "Dielectric breakdown in electrically stressed thin films of thermal SiO_2," vol. 49, p. 2478, (1978).

[88] R. Rodriguez, E. Miranda, R. Pa and J. Sune, Microelectronics Reliability, "Monitoring the degradation that causes the breakdown of ultra thin (<5nm) SiO_2 gate dielectrics", vol. 40 (4), May (2000).

[89] G. F. Ceroflini, L. Meda and C. Volpones, Physical Review B, "Structure and evolution of the displacement filed in hydrogen implanted silicon", vol. 41 (18), (1990).

[90] W. B. Jackson, P. V. Santos and C. C. Tsai, Physics Review B, "Role of clustering in hydrogen transport in silicon," vol. 47 (15), (1993).

[91] D. D. Skarlatos, C. Tsamis and D. Tsoulklas, J. Appl. Phys., "Oxidation of nitrogen-implanted silicon: Energy dependence of oxide growth and defect characterization of the silicon substrate," vol. 93 (3), (2003).

[92] D. D. Skarlatos, E. Kapetanikas, P. Normand, C. Tsamis and D. Tsoulklas, J. Appl. Physics, "Oxidation of nitrogen-implanted silicon: Comparison of nitrogen distribution and electrical properties of oxides formed by very low and medium energy nitrogen implantation," vol. 96, pp. 300-305 (2004).